European Space Research and Technology Centre
Keplerlaan 1, 2201 AZ Noordwijk, The Netherlands
Tel. (31) 71 5656565 www.esa.int

DOCUMENT

LightShip

Instrument Definition Team, Final Report

V1.0 – Release date **05/12/2024**

APPROVAL

Title: LightShip Instrument Definition Team, Final Report
Ref: ESA-E3P-LS1-RP-002 - v1.0

Issue: 1	**Revision 0**
Authors: IDT Team, C. Wilson	**Date 2024-12-05**
Approved by	**Date**

CHANGE LOG

Reason for change	Issue	Revision	Date

CHANGE RECORD

Issue 0	**Revision**		
Reason for change	**Date**	**Pages**	**Paragraph(s)**

Table of Contents

Executive summary

ESA is studying a new Mars mission concept providing essential infrastructure to support its future programme of Mars exploration. The concept includes a series of electric propulsion-powered tugs named LightShips to transport space elements to Mars orbit and establish a high-altitude communications and navigation network. To optimise the communications and navigation functions, the LightShips will be placed in near-equatorial (20° inclination), high altitude (5720 km) orbits. ESA's proposal is that further LightShips would be launched with a regular cadence after the first, delivering ever more spacecraft to Mars in similar orbits, building up a fleet of LightShips distributed around the equator to provide constant communications capability for low-latitude surface stations.

The LightShips have the capacity to carry a small (30 kg) scientific payload. Consistent with the vision outlined in its Explore 2040 strategy documents, ESA has specified that an overarching theme of atmospheric monitoring was suitable for these high-altitude LightShip platforms. An Instrument Definition Team (IDT) was formed to define science and measurement objectives for this payload, and to define a strawman payload capable of addressing them. The team were asked to give particular consideration to *exploration-focussed* science objectives, i.e. those which provide datasets needed for development of future missions. Key *exploration-focussed* objectives to be addressed by this mission are specifically described in Theme D "Enabling Mars Exploration".

The IDT has defined a number of key science questions, categorised in four themes:

- Atmospheric circulation and dynamics
- Dust cycle and storms
- Water cycle, clouds and chemistry
- Enabling Mars exploration (safe arrival & operation)

To address these themes, key meteorological variables to be measured were identified:

- Wind speeds
- Atmospheric and surface temperatures
- Dust and cloud abundances
- Water vapour and other volatiles
- Surface pressure

To measure these variables, a strawman payload was identified consisting of the following:

- Thermal infrared mapper
- Sub-mm sounder

- Multiband imaging suite
- Near-infrared spectral imager
- Radio occultation, both spacecraft-to-spacecraft and spacecraft-to-Earth.

Further to the above, ESA has noted that radiation monitoring and *in situ* micrometeoroid/dust monitoring have also been identified as potential exploration-focussed measurements, however they were not discussed by the IDT.

In addition to payload and measurement objectives, recommendations for the ground segment have also been made by the IDT: if the LightShips are to provide operational weather monitoring and forecasting capabilities, then this will require downlink availability and speeds, plus ground processing, that are able to provide near-real-time delivery of meteorological data products. Furthermore, development of atmospheric data assimilation and numerical weather prediction for Mars will be needed. These considerations are further detailed in Appendix A.

The LightShip science payloads will deliver the first ever direct orbital measurements of winds, and simultaneous measurements of temperatures, aerosols and trace gases on hourly to multi-year timescales and at horizontal resolutions down to a few kilometres.

The LightShips will be transformational for Mars atmospheric science, moving ESA towards operational global atmospheric monitoring and forecasting at Mars.

Scope and Acknowledgments

This document describes the case for the proposed LightShip science payload and provides the strawman instrumentation description, required resources, interface requirements, operational requirements, and any other system level impacts on the orbiter. The information contained in this report has been collected and discussed by the Instrument Definition Team (IDT) during a workshop at ESTEC on 6-8 May 2024 and subsequent on-line meetings, through which the IDT has collaboratively written this report.

The IDT has been formed through a competitive call to provide inputs to ESA regarding the science case and strawman payload. This call was open from 5th February until 28th March 2024. In parallel to this call, ESA issued a Request For Information (RFI) to provide inputs for potential scientific instruments to be considered for the strawman payload.

The IDT was tasked with the following:

- Describe the exploration and science case for this mission study.
- Provide trade-offs related to the performance and impact of different payload options.
- Propose the strawman science instrumentation within the provided mass allocation of approximately 30 kg, and constraints imposed by the predefined LightShip orbit requirements.
- Provide the strawman instrumentation description, required resources, interface requirements, operational requirements, and any other system level impacts on the orbiter.
- Provide inputs for a preliminary Payload Definition Document (PDD), including the requirements on these instruments and the requirements that these instruments imply on the spacecraft and the mission overall.

The objective is both to enable a well-defined specification to be written for the Invitation To Tender (ITT) for a spacecraft Phase A/B1 study and to provide scientific guidelines to inform a Call for Payloads.

In parallel to the IDT, a Measurement Definition Team was formed to define the requirements on the measurements on the passenger spacecraft carried to Mars by the first Lightship mission.

The members of the IDT team, listed in alphabetical order, are:

- Paul Hartogh, Max Planck Institute for Solar System Research (MPS), GE
- Jorge Hernández Bernal, LMD Sorbonne Université, FR
- Giuliano Liuzzi, University of Basilicata, IT
- Luca Montabone, Paneureka, FR
- Lori Neary, Royal Belgian Institute for Space Aeronomy, BE
- Claire Newman, Aeolis Research, UK
- Manish Patel, The Open University, UK

- Ian Thomas, Royal Belgian Institute for Space Aeronomy, BE
- Colin Wilson, ESA, Noordwijk, NL

Assistance to the team has been provided by several experts at ESA, especially by Daniel Paardekooper, Andrew Ball, Håkan Svedhem, Claire Parfitt and Alejandro Cardesin-Moinelo

The LightShip Project Team and the IDT members would like to thank everyone who submitted a response to ESA's Request For Information for LightShip payloads, as these were invaluable in assessing the most recent advances in instrument development, and also the following scientists for their expertise, in alphabetical order: Apostolos Christou, François Forget, Scott Guzewich, Akira Kazama, Tim McConnochie, Aymeric Spiga, Anthony Toigo, Michael Wolff, and Roland Young.

1. Introduction

ESA is studying a new Mars mission concept providing essential infrastructure to support the future Mars exploration programme. It includes a series of electric propulsion-powered tugs, called LightShips, to transport future payloads to Mars orbit. Each LightShip will be capable of transporting an orbital spacecraft to Mars as a 'passenger'. Once passengers are delivered, the tugs will ascend and then remain in a high orbit (5720 km altitude and 20° inclination) where they will serve as part of a communication network, to provide data relay and navigation support to landers and rovers on the surface, and to other orbiters. As an infrastructure-based platform, the objectives of the EP Tug are not science driven and so the choice of orbit and other such mission parameters will be tailored for the service provision, with science as an additional opportunity. The first LightShip mission ('LightShip-1') is being developed with a launch readiness date of late 2032, with the idea that future LightShip missions could follow at every second launch window (i.e. in 2036, 2040 and beyond) in order to build up continuous data relay and navigation capability.

Each LightShip will, in addition to its communication and navigation payload, carry a scientific instrument payload focussing on measurements of the Martian atmosphere. When further LightShips are sent to Mars they will form the backbone of a global atmospheric monitoring network which could eventually be supplemented by meteorological measurements from low orbiters and surface stations.

This focus on atmospheric monitoring has its origin in the Terrae Novae 2030+ Strategy Roadmap (2022), with the SciSpacE Strategy Roadmap (2023), and the Explore 2040 Exploration Strategy (2024), all of which specified weather & climate monitoring capability. *Climate and weather* has been identified as a distinct European scientific identity for Mars, evidenced by the world-leading atmospheric research being undertaken across Europe and accelerated through pioneering missions such as the ExoMars Trace Gas Orbiter. This past and present investment has led to European leadership in Mars atmospheric research, and the LightShip programme now offers the opportunity for achieving ESA's strategic ambition for a distinct and world-leading scientific identity in Mars exploration.

The scientific payload is *exploration-focussed,* in that it provides crucial data for future exploration missions. Safe and precise entry and descent of exploration craft is supported by collecting data about atmospheric density, temperature, winds and their variability. Safe and effective surface operations of exploration vehicles is supported by collecting data on Mars climate and weather, particularly on the dust storms which govern the availability of sunlight and affect solar panel effectiveness, and on the water cycle which determines the availability of both atmospheric water vapour and near-surface accessible water ice deposits.

At the same time, there is an *exploration-enabled* element to the science payload: this addresses scientific questions which are not directly related to enabling future missions but rather are enabled by this mission. For example, how is water transported around Mars and lost to space,

and how has this varied though the history of Mars? How is dust transported through the atmosphere of Mars, and what governs the onset and dissipation of large-scale dust storms?

The LightShip-1 mission will carry one passenger named SpotLight. The SpotLight payload comprises a high-resolution imager and a context imager, and if additional mass becomes available an imaging spectrometer and/or a Lidar. The science case and instrumentation proposed for SpotLight is presented in the report of the SpotLight Measurement Definition Team[1].

Certain aspects of the mission and payloads were already defined by the mission concept; these were specified by the LightShip project team to the Instrument Definition Team:

- The orbit of the LightShips will be 5720 km altitude with an inclination of 20°. The orbital period at this altitude is 7.34 hours. From this altitude, Mars appears as a disk about 45° across (see Figure 1). One lightship has visibility of some 136° of longitude at once, so a set of three LightShips equally spaced around the equator would have visibility of all equatorial longitudes (albeit at sometimes high emission angles).
- The mass allocation for the science payload of a LightShip spacecraft is approximately 30 kg.
- There will be a nadir-pointing face on the spacecraft, on which the science payload can be mounted.
- The rotation around the nadir axis of the spacecraft may be determined by power or communications needs rather than for science purposes, so science payloads must not assume that they can determine this rotation.
- The design lifetime of each Lightship mission should be 12 years; this implies careful consideration of components like Stirling coolers which may have shorter design lifetimes.

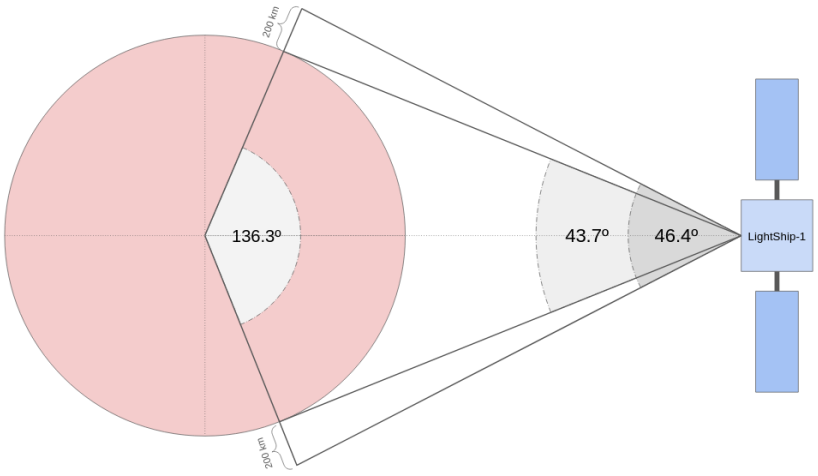

Figure 1: The 5720 km altitude LightShip orbit allows to survey a very large area of the planetary disk at once. This is ideal for providing the large-scale atmospheric monitoring which is, on Earth, essential for weather observation and prediction.

[1] SpotLight Measurement Definition Team Report, ESA-E3P-LS1-RP-001 v 1.1 Nov 2024

2. Science themes & objectives

Several strategic knowledge gaps have been identified that could endanger future human missions to Mars, particularly those related to weather (especially dust storms), the radiation environment, and the use of Mars' water for human life support (MEPAG, 2020). Regarding weather, data from orbiters, landers, rovers and numerical models have been used to study the Martian atmosphere extensively. This research has provided a general understanding of its current climate processes and allowed us to infer some aspects of past climate conditions (see Haberle et al., 2017, and references therein). However, we still lack a deep understanding of its weather phenomena, which is crucial to ensure astronaut safety during landing and while operating on the Martian surface.

Past and present orbiters, such as Mars Global Surveyor, Mars Odyssey, Mars Express, Mars Reconnaissance Orbiter, and the ExoMars Trace Gas Orbiter, have provided a comprehensive picture of Mars' climate and valuable insights into its meteorology. Other missions, such as the Mars Atmosphere and Volatile Evolution (MAVEN) mission (Jakosky et al., 2015), Mars Orbiter Mission "Mangalyaan," and Tianwen-1, have also contributed sporadic observations of meteorological phenomena. However, most of these orbiters are in low-altitude polar orbits, which offer point observations at close distance but lack global coverage. Additionally, some of these orbiters are in sun-synchronous orbits, optimised for repeating observations with consistent solar illumination and thermal conditions, but leaving significant gaps in temporal coverage with respect to local solar time. The ongoing Emirates Mars Mission (EMM) 'Hope' orbiter (Almatroushi et al., 2021) operates in a high-altitude, elliptical, 25° inclined orbit, allowing for regular observations of large portions of the Martian disk at different distances. Its unique orbit has significantly improved the spatio-temporal coverage of previous observations by enabling the current monitoring of atmospheric temperature and aerosols over sub-diurnal to seasonal timescales (Atwood et al., 2022; Smith et al., 2022).

Despite this recent addition, the spatial and temporal coverage of EMM atmospheric observations do not yet provide sufficient resolution and cadence to enable continuous, simultaneous, global monitoring of synoptic weather systems. Weather observations by any single spacecraft are more or less discontinuous and asynchronous, whereas the dynamics of meteorological phenomena such as dust storms (particularly the most extreme ones), fronts, waves, and water/CO_2 ice clouds are characterised by rapid temporal variability (sub-hourly) and multi-scale spatial extension (local, regional, planetary), see for example Liuzzi et al., 2020; Montabone et al., 2020. Furthermore, key dynamical measurements such as global winds and surface pressure anomalies are still conspicuously missing.

Current state-of-the-art Mars Global Climate Models (GCMs) are reasonably good at modelling diurnal and seasonal dynamical patterns across a large parameter space, but they mostly rely on prescribed dust distributions. Models are not yet sophisticated enough to explicitly simulate this distribution physically, partly because simulated winds are not accurate, partly because parameterizations of surface (e.g., dust lifting) and boundary layer phenomena are not fully

validated, and partly because the physical properties of the dust particles are not well characterised under all conditions. The likely stochastic nature of dust storm initiation processes, combined with the inherent chaos in Martian weather patterns, makes it challenging to predict these events solely based on models.

The use of data assimilation techniques, coupled with GCMs, can help fill the gaps to reconstruct the dynamical state of the atmosphere at any given time (including those variables that are not directly observed), self-consistent with the available observations, and to allow weather prediction. However, the uncertainties in the current Mars GCMs are still too large, and the validation of non-directly observed variables is too poor to allow data assimilation to work accurately. As a result, observations with a sub-hourly cadence, covering the largest possible portion of the planet simultaneously, and incorporating novel data such as wind speeds and surface pressure anomalies, are needed to enable comprehensive monitoring, understanding, and forecasting of Martian weather phenomena, including the initiation and evolution of dust storms.

Atmospheric and surface temperatures, three-dimensional aerosol and water vapour distributions can be included in a list of recommended variables to be retrieved from orbital observations. Surface pressure observations from orbit have been previously attempted, but the precision of the measurements would need to increase significantly to detect weather systems using surface pressure anomalies of the order of a few tens of Pascal. Global wind measurements in the lower atmosphere -from near ground to about 100 km altitude - would be groundbreaking and highly beneficial for advancing our understanding of atmospheric dynamics.

ESA's LightShip program aims to address these challenges by focusing on atmospheric circulation and dynamics, the dust cycle and storms, the water cycle and related volatiles, and enabling safe Mars exploration, including safe landing and surface operations. The orbit of each LightShip provides a full-disk view of Mars, making it ideal for monitoring the weather over sub-diurnal to seasonal timescales, including inter-annual and long-term variability. When only one LightShip is in orbit, it will already be observing weather systems all-round the planet, as it circumnavigates the planet just over three times per day, providing the ability to monitor low- and mid-latitude regions for developing storms and other weather features, crucial for preparing for future human and robotic exploration.

The current document describes the payload for a single LightShip, however, this payload is designed with a view to being deployed on multiple LightShips operating simultaneously. Multiple LightShips, in their near-equatorial orbits, could provide continuous coverage of low latitudes around the globe (albeit at varying emission angles; this will be discussed further in Section 4.6 below). Additional atmospheric measurements from a polar orbiter such as the proposed SpotLight orbiter could be used to fill in coverage gaps at polar regions. The low altitude of the proposed SpotLight orbiter offers opportunities to bridge the gap between global-scale atmospheric processes and small-scale surface features such as dust devils, dune movement, recurrent slope lineae. Lidar and spectrometric measurements could provide vertical profiling of winds, aerosols, and atmospheric water vapor within the boundary layer, hence delivering critical

data to link surface dust-lifting events with atmospheric dynamics. High-resolution imaging would enable precise tracking of surface changes caused by weather events, offering valuable insights into how Martian weather influences and reshapes the landscape over time. A Doppler wind-measuring LIDAR on the SpotLight orbiter would be particularly complementary to the observations from LightShip, as will be discussed further below (see Section 3). In the remainder of this section, we provide a description of the science themes and objectives of the LightShip mission's science payload.

Table 1: Science themes and objectives.

Level 0 (Themes)		Level 1 (Objectives)
Atmospheric circulation and dynamics	**OBJ-SCI-01**	a. How are **temperatures, winds and surface weather systems connected** in all seasons and dust conditions?
	OBJ-SCI-02	b. How **variable is the martian circulation and wave activity** on sub-diurnal to decadal timescales, and what drives this?
	OBJ-SCI-03	c. Does the spatial and temporal variation of quasi-passive **trace gases** agree with expectations from our understanding of transport and the CO_2 cycle?
Dust cycle and storms	**OBJ-SCI-04**	a. What is the **radiative impact of dust** and how does this affect the **circulation**?
	OBJ-SCI-05	b. How **variable is the martian dust cycle** on sub-diurnal to decadal timescales, and what drives this?
	OBJ-SCI-06	c. How do **dust storms grow** from local through regional up to global, and how is this related to tides, waves, and the diurnal cycle of solar insolation?
	OBJ-SCI-07	d. Do **global dust storms decay** due to changes in the circulation, changes in surface dust availability, or something else?
Water cycle, clouds, and chemistry	**OBJ-SCI-08**	a. What is the **radiative impact of water ice clouds** and how does this affect the **circulation**?
	OBJ-SCI-09	b. How **variable is the martian water cycle** on sub-diurnal to decadal timescales, and what drives this?
	OBJ-SCI-10	c. What are the **interactions between the water and dust cycles**?
	OBJ-SCI-11	d. What chemical, dynamical and dust processes affect **transport of water** towards the **upper atmosphere**?
	OBJ-SCI-12	e. How **variable is martian atmospheric chemistry** on sub-diurnal to decadal timescales, and what drives this?
Enable Mars exploration (safe arrival & operations)	**OBJ-SCI-13**	a. How accurately are **density and wind profiles**, and their variability, represented in atmospheric models?
	OBJ-SCI-14	b. How well can **weather be predicted** by assimilating temperature, dust, winds, and surface pressure?
	OBJ-SCI-15	c. How much **warning can be given of dust storms** headed for landing sites?
	OBJ-SCI-16	*d. What is the **radiation environment** during cruise and in Mars orbit?*
	OBJ-SCI-17	*e. How many **potential impactors** (dust / micrometeoroids) are present during cruise and in Mars orbit?*

2.1 Theme A: Atmospheric circulation and dynamics

Mars has an axial tilt of 25°, and an eccentric orbit from 1.4 to 1.7 AU, leading to pronounced seasonal changes over the course of the Martian year. It is also a desert planet with low surface thermal inertia, low atmospheric density and small amounts of water vapour, which means the magnitude of seasonal changes in atmospheric circulation is much larger than what is observed on Earth. The amount of atmospheric dust varies greatly between the northern spring/summer and autumn/winter seasons, with the latter being the seasons when the planet experiences the largest and most intense dust storms. Dust particles absorb solar radiation and heat the atmosphere locally, altering temperature gradients, which in turn drive changes in surface pressure and generate winds as the atmosphere moves to balance these pressure differences. Thus, the interconnection between temperatures, pressures, winds, and weather systems on Mars varies across seasons and is significantly influenced by dust conditions. Atmospheric trace gases like carbon monoxide, ozone, and water vapor provide valuable insights into the dynamics of Mars' atmosphere, including transport mechanisms and the carbon dioxide cycle.

OBJ-SCI-01 How are temperatures, winds and surface weather systems connected in all seasons and dust conditions?

The atmospheric thermal structure through seasons and dust conditions is currently the most characterized parameter, thanks to the significant increase in observations over the past 25 years (see Vlasov et al., 2022, Smith et al., 2022, Lopez-Valverde et al., 2023, for some of the latest observations). This contrasts sharply with the scarcity of direct wind and high-precision surface pressure observations, only available at few locations. The local time coverage of global temperature observations has recently improved thanks to missions like ESA's Mars Express and Trace Gas Orbiter, as well as UAESA's Emirates Mars Mission. However, the lack of direct global wind and surface pressure anomaly measurements means our understanding of Mars' global circulation relies on theoretical relationships among temperature, pressure, and winds, or indirect atmospheric observations of the transport of atmospheric species.

Indirect observations and simulations by advanced numerical models, such as Global Climate Models (GCMs) and mesoscale models, allow inference of phenomena like jet streams, extratropical cyclones/fronts, polar vortices, orographic spiral circulations, Lee-waves, crater circulations, mesoscale convective systems, etc. Despite these successes, the fundamental relationships between temperature and winds (e.g., geostrophic and thermal wind) remain untested due to the lack of direct wind observations at different altitudes. Additionally, surface weather systems, including dust storms, and their link to atmospheric waves (e.g., baroclinic waves and thermal tides), are poorly understood without simultaneous wind and surface pressure measurements at the synoptic scale, which could be provided by LightShip.

Data assimilation experiments suggest that equatorial atmospheric super-rotation increases during large-scale dust storms, potentially contributing to their growth from regional to planetary

scale (Rajendran et al., 2021). Similarly, such experiments indicate that transient teleconnection events, driven by strong local heating from dust storms, can modify surface pressure and wind patterns, triggering responses far from the storm (Montabone et al., 2008Montabone et al., 2008Montabone et a., , Martinez-Alvarado et al., 2009). These events may influence the initiation of secondary dust lifting centres and the disruption of northern polar vortex shape and intensity (Montabone et al., 2013, 2014, Mitchell et al., 2015, Guzewich et al., 2016, Streeter et al., 2024). However, no direct dynamical data are available to test these hypotheses. Verification requires direct wind measurements, as shown in Figure 2 below and planned for LightShip.

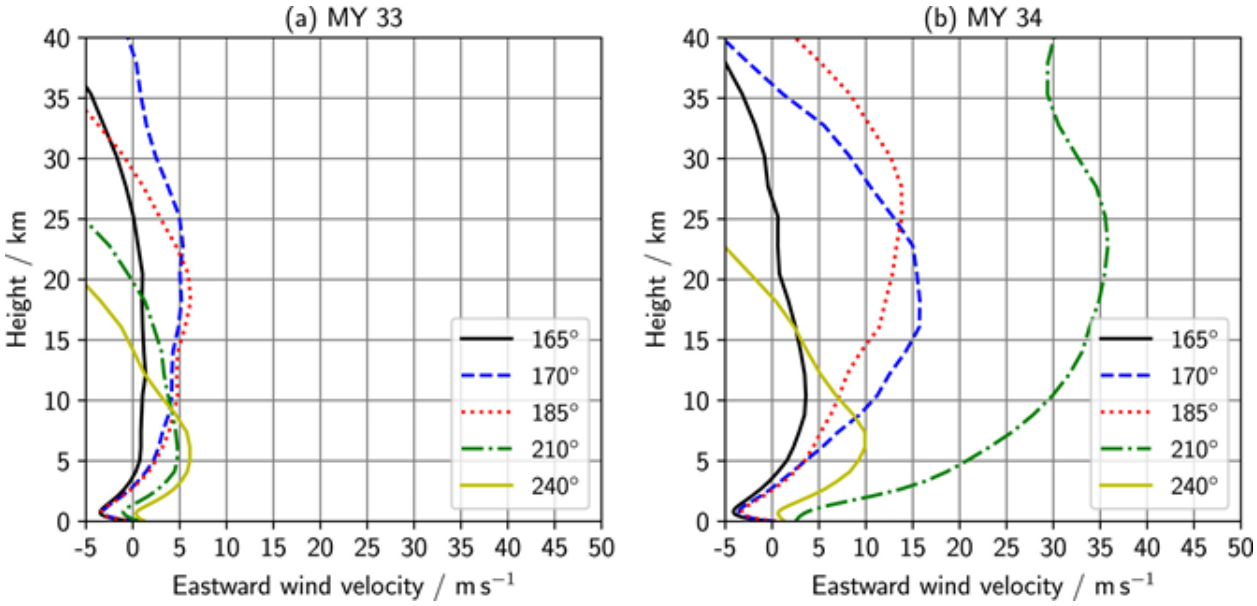

Figure 2: Profiles of tropical zonal-mean zonal winds (averaged diurnally and across 30°S–30°N) for different times between LS=165° and LS=240° in MY 33 (left) and MY 34 (right). The figure is from Rajendran et al., 2021, Figure 3. In MY 34 an extreme dust event ("global dust storm") occurred. The eastward wind appears stronger in MY 34 even before the storm onset at LS~186°. Profiles are extracted from an atmospheric reanalysis which has assimilated MRO/MCS thermal and dust profiles as well as TGO/ACS thermal profiles into the Mars PCM-UK-spectral. There is no assimilated wind data, emphasizing the need for future validation of this potential precursor scenario to an extreme dust event through wind observations, such as those that LightShip could provide in the equatorial region.

OBJ-SCI-02 How variable is the Martian circulation and wave activity on sub-diurnal to decadal timescales, and what drives this?

The Martian atmospheric circulation and wave activity vary significantly across a wide range of timescales from sub-diurnal to decadal. On shorter timescales, rapid changes driven by the planet's thin atmosphere and day-night temperature variations produce strong thermal tides—global-scale waves caused by solar heating. These tides modulate atmospheric temperature, pressure, and wind patterns daily, creating a dynamic weather system. Small-scale dust events, such as dust devils and local dust storms, also contribute to short-term variability by altering local conditions and triggering feedback loops that can amplify these effects. While observations have revealed the effects of tides on global temperature fields (see, e.g., recent measurements by the EMM mission, (Fan et al., 2022) and local surface pressure at specific landing sites, measurements

of their effects on winds at fixed locations are scarce. Moreover, no global measurements of surface pressure or winds exist, a gap LightShip seeks to address.

On seasonal to interannual timescales, Martian circulation variability is primarily driven by solar heating distribution, which changes significantly between seasons, altering temperature gradients, surface pressure, and wind patterns. Seasonal changes are particularly evident in the polar ice caps, which grow and recede with the seasons, influencing atmospheric pressure and circulation patterns. Latent heat released by CO_2 condensation during polar nights is believed to sustain the unstable shape of Martian polar vortices (Toigo et al., 2017, Ball et al., 2021), see an example in Figure 3. However, current knowledge of vortex dynamics and variability relies solely on indirect data from numerical simulations and data assimilation of temperature and dust, with no direct wind observations for validation. Large-scale dust storms, which can last for weeks and spread dust over the entire planet, are a critical factor on seasonal to interannual timescales.

On decadal timescales, Martian circulation and wave activity are shaped by long-term climatic shifts and possibly by variations in solar activity. Data from 14 continuous Martian years suggest periodic changes in dust storm frequency and intensity, potentially linked to cycles in atmospheric dust loading and surface conditions. Variations in solar output and Mars' orbital parameters, affecting the received insolation, may also drive these changes. Extreme dust events (also called "global dust storms" or "planet-encircling dust storms") occur irregularly and infrequently, requiring the accumulation of long-term statistics to characterize them properly. Understanding these patterns requires continuous monitoring, achievable through an uninterrupted series of LightShip missions focused on atmospheric observations.

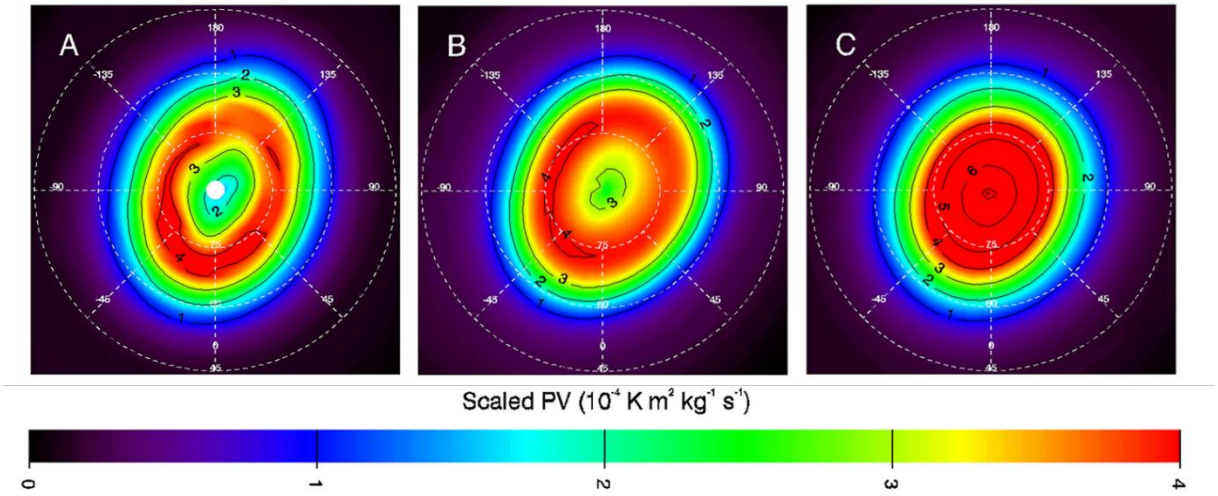

Figure 3: North polar stereographic projection maps of scaled PV (10−4 K m2 kg−1 s−1) on the ϑ = 300 K isentropic surface from (a) the Mars Analysis Correction Data Assimilation v1.0 (MACDA, Montabone et al., 2014) and the (b) standard and (c) no-CO_2-latent-heating MarsWRF simulations. PV is also shown in black contours. The outer latitude is 45°N and 0° longitude is at the bottom of the maps. This figure (adapted from Figure 1 of Toigo et al., 2017) illustrates that a GCM simulation without CO_2 condensation (and thus without latent heat release) cannot maintain an annular PV structure at the northern pole, unlike the standard GCM simulation and the MACDA data assimilation dataset. While this result has been obtained using a climate model

and observed in an assimilation of temperature and dust data, there are no direct measurements available to verify either the PV structure or the impact of CO_2 condensation—something that LightShip will be able to provide.

OBJ-SCI-03 Does the spatial and temporal variation of quasi-passive trace gases agree with expectations from our understanding of transport and the CO_2 cycle?

Quasi-passive trace gases, such as carbon monoxide (CO), ozone (O_3), and water vapour (H_2O) offer critical clues about the atmospheric processes, including transport mechanisms and CO_2 cycle. Understanding their spatial and temporal variations is crucial for developing a comprehensive model of Mars' atmosphere and climate. The current understanding of CO_2 cycle itself is generally robust (Titus et al., 2017) yet a full representation of thermal tides and their influence over CO_2 condensation occurrence and atmospheric temperatures is still not fully reflected in atmospheric models, particularly referring to the role of CO_2 ice clouds in the formation of polar vortex and their coupling with water ice (Määttänen et al., 2022).

Tracers such as CO can offer clues in this sense: CO is indeed produced primarily from the photodissociation of CO_2 and its atmospheric lifetime is long enough to make it a useful tracer of some atmospheric processes: Observations have shown that CO exhibits spatial and temporal variations that correspond with seasonal changes and atmospheric circulation patterns (Smith et al, 2022). Similarly, the cycle of O_3 has been explored recently (Figure 4), showing that O_3 concentrations increase during the night when the photodissociation rates are low, and decrease during the day. Seasonally, O_3 levels are higher during the colder months and lower during the warmer months, following the CO_2 cycle and atmospheric transport processes (). It has also been observed that O_3 can be efficiently depleted during global dust events by odd hydrogen species due to the photolysis of high altitude transported water (Daerden et al., 2022). Observations show a general correlation between O_3 and water vapour (Brown et al., 2022), the latter of which has a strong seasonal cycle which regulates very different phenomena, ranging from polar caps condensation/sublimation to hydrogen escape. The Hadley circulation and thermal tides also play essential roles in redistributing water vapour across the planet, which is well seen through observation of isotopic ratios of H in H_2O (Villanueva et al., 2022).

The synergy between novel measurement techniques as foreseen in the LightShip strawman payload will provide data useful to further constrain the vertical distribution of trace elements on a larger spatial scale than previously done by, e.g., MRO-MCS and TGO-NOMAD and ACS. Microwave soundings will enhance the availability of limb profiles of trace elements and provide wind measurements to predict transport. Nadir IR measurements would, at the same time, provide a quasi-hemispheric view of the thermal state of the atmosphere, which is useful to inform the CO_2 cycle description from the Equator to high latitudes (Toigo et al., 2017; Ball et al., 2021).

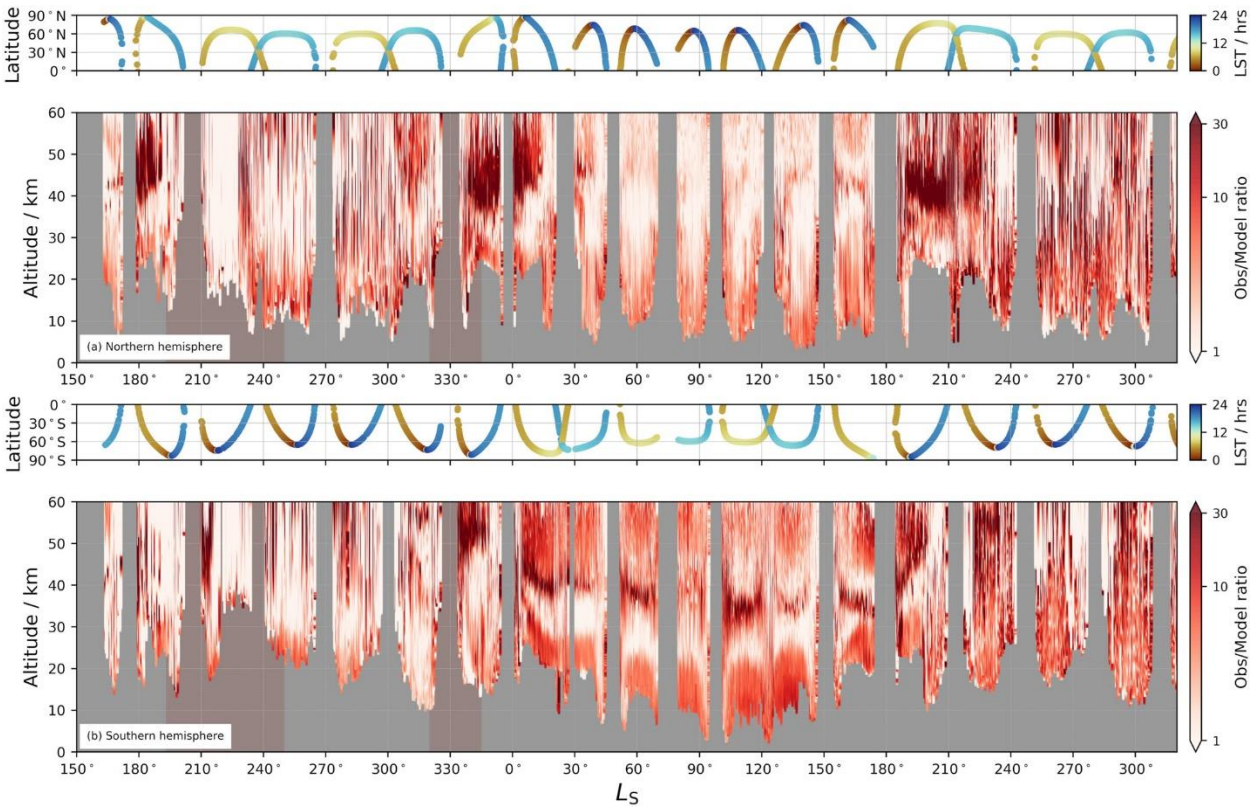

Figure 4: Ratio of ozone observations by Trace Gas Orbiter NOMAD-UVIS to modelled ozone abundance, from [Patel et al. (2021)](), showing how certain layers and features are not well-simulated in the GCM. The top row shows the northern hemisphere, and the bottom row is the southern hemisphere. Lighter (darker) shading indicates stronger (weaker) agreement between observation and model abundances; higher ratio values indicate that modelled values are lower than that observed by NOMAD-UVIS. The sub-mm sounder in Lightship's strawman payload would measure ozone and related trace species, and wind speeds, with a more regular sounding pattern than TGO, allowing to disentangle the circulation patterns causing ozone variability.

2.2 Theme B: Dust cycle and storms

Dust is the major climate driver on Mars, influencing the thermal structure and circulation of the atmosphere. Once lifted from the surface, airborne dust particles can absorb and scatter sunlight causing local thermal gradients which drive circulation patterns. As Mars lacks surface liquid or significant latent heating in the atmosphere, the variability of the dust cycle - and in particular, of large dust storms - is the main driver of both weather and climate, akin to phenomena such as thunderstorms, tropical cyclones, or ENSO on Earth (Read et al., 2015; Newman et al., 2022).

There are complex feedbacks between the radiative effects of dust and the dynamic impacts such as dust lifting from both straight-line surface winds and dust devils, buoyancy, thermal tides and the large-scale overturning of the atmosphere. These feedbacks and effects greatly impact the state of the thin Martian atmosphere, where airborne dust can lead to global-scale dust storms lasting many weeks (Kahre et al., 2017; Wolff et al., 2017). For the success of future missions and exploration, it is crucial to answer the open question of what causes local dust lifting to grow into local and sometimes regional dust storms, and what causes some regional storms to grow or merge to become global.

OBJ-SCI-04 What is the radiative impact of dust and how does this affect the circulation?

The amount of absorption and scattering of sunlight by dust particles in the atmosphere depends on the size, shape and composition of the particles. Both the dust distribution and its radiative properties are required to accurately simulate the heating rates and temperatures in a General Circulation Model (GCM) and hence the associated winds (Figure 5). The current observational datasets provide a general picture of the global column dust opacity and some information on the vertical distribution but are still quite limited in spatial and temporal coverage. Some information on dust particle size and radiative properties can be inferred from observations as well but suffer from the same limitations (e.g. Wolff et al., 2010; Smith, 2004; Clancy et al., 2019).

Due to its simultaneous measurements, with good spatial and temporal coverage including multiple times of sol, LightShip will provide a more complete picture of the vertical distribution of dust, temperatures and winds to directly relate the radiative impacts of dust to the thermal structure and to the circulation. In addition, LightShip instruments will measure at multiple wavelengths. The simultaneous measurements obtained of dust particle size and scattering properties will be incredibly valuable in the effort to constrain models and retrieval algorithms.

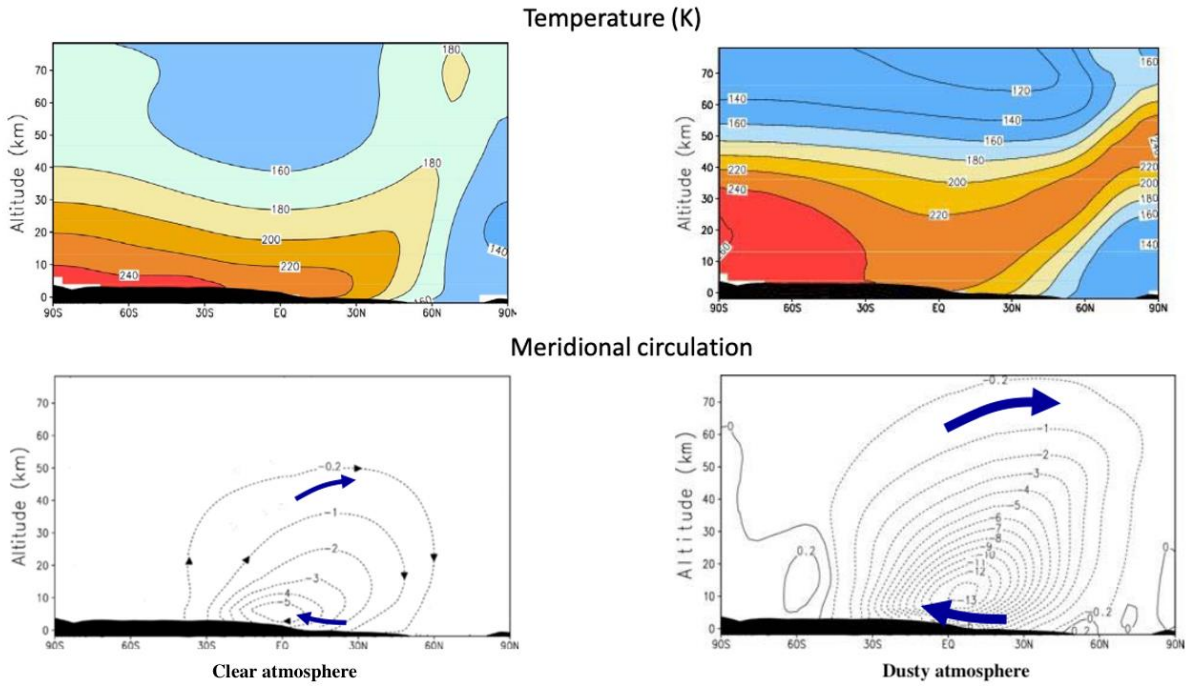

Figure 5: Impact of dust on temperature and winds in a GCM. These figures show a zonal mean average (over longitudes) from South to North pole of the profiles of temperature (top) and of the meridional (North-South) circulation (bottom) in a GCM simulation with clear (left) and dusty (right) conditions. Dust in the atmosphere produces warmer temperatures which increase the circulation. Stronger surface winds cause more lifting, adding more dust into the atmosphere. With more complete spatial and temporal coverage of dust, temperature and winds from LightShip, we can better constrain dust properties and models. (Figure credit F. Forget Mars V Workshop)

OBJ-SCI-05 How variable is the Martian dust cycle on sub-diurnal to decadal timescales, and what drives this?

Understanding *how* the atmospheric dust distribution varies on a range of timescales - from hourly all the way up to interannual variability over multiple decades - requires observing such changes. Further, understanding *why* the dust varies as observed requires additional measurements to constrain the forcing, processes and feedbacks responsible. LightShip will simultaneously do both, providing the most valuable orbital dataset to date for understanding the Martian dust cycle, as described below.

LightShip will image dust clouds in the visible and UV, as well as retrieving variations in column dust opacities and aerosol properties, and vertical dust profiles, over most latitudes and covering all longitudes and times of sol over a period of ~3 sols. This will hugely improve temporal monitoring of the evolution of dust storms, high-altitude dust maxima, and other dusty phenomena. In addition, LightShip will measure atmospheric temperature profiles and line-of-sight winds at the same times and locations and times as the dust measurements. Although LightShip wind measurements may be limited to above ~15km, the lower altitude SpotLight orbiter could provide line-of-sight winds down to nearly the surface. LightShip also aims to measure surface pressure anomalies from orbit, which reveal details of weather systems that

control significant dust lifting and regional storm development (e.g., Wang et al., 2003; Battalio and Lora, 2021).

These observations will extend the existing time-series of orbital measurements of the 3D dust distribution and thermal forcing on Mars, which go back more than 13 Mars years almost continuously as of 2024, thus enabling inter-decadal investigations (e.g., Figure 6). The existing time series has already revealed patterns in local and regional dust storms that were not appreciated before (e.g., Wang and Richardson, 2015; Kass et al., 2016; Montabone et al., 2020), although we still cannot even predict the onset time and location of most of these smaller storms. Further, the infrequent global storms continue to surprise us with new onset times and patterns of growth and decay, with even their appearance (or not) in a given year potentially linked to anything from the distribution of surface dust (Newman and Richardson, 2015) to solar system dynamics (Shirley and Mischna, 2017; Newman et al., 2019). Hence this continued - and improved - monitoring is imperative.

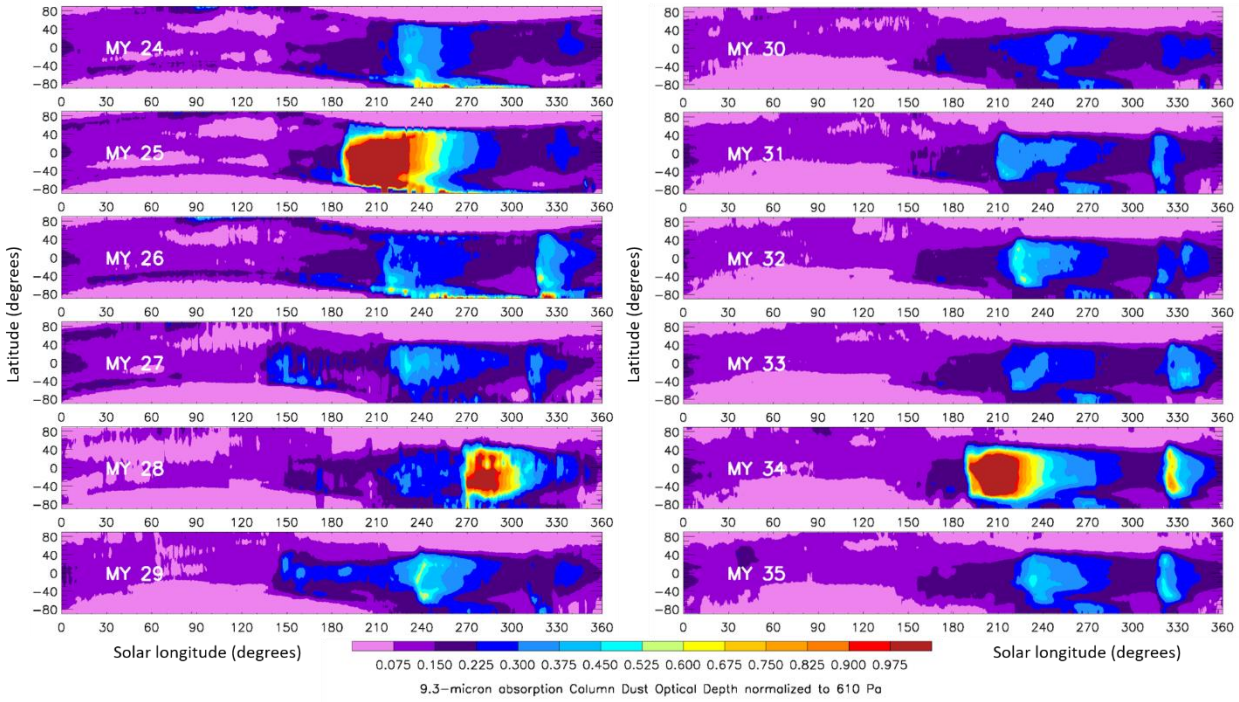

Figure 6: Zonal means of the daily regularly kriged maps of 9.3 µm absorption column dust optical depth normalized to the reference 610 Pa pressure level for the different Martian Years, using observations of the Martian atmosphere from April 1999 to December 2022 made by the Thermal Emission Spectrometer (TES) aboard Mars Global Surveyor, the Thermal Emission Imaging System (THEMIS) aboard Mars Odyssey, and the Mars Climate Sounder (MCS) aboard Mars Reconnaissance Orbiter (MRO). Using data described in Montabone et al., 2015, 2020, and available on the Mars Climate Database webpage at https://www-mars.lmd.jussieu.fr/mars/dust_climatology/. LightShip will expand this vital dust climatology by extending it to more Mars years, observing dust at all times of sol, and crucially by providing simultaneous data on dust properties, the water cycle and winds, enabling better understanding of the causes of these dust variations. In particular, long-term monitoring of the dust climatology is essential to gather sufficient statistics for understanding infrequent phenomena such as extreme dust events (also called "global dust storms"), which have been observed in only three Martian years—MY 25, 28, and 34—since the early 2000s, as shown in this figure.

OBJ-SCI-06 How do dust storms grow from local through regional up to global, and how is this related to tides, waves, and the diurnal cycle of solar insolation?

By its very nature, answering this question requires measurements at a range of spatial scales, over periods ranging from hours (the timescale for local dust lifting to develop into a local dust storm) to several sols (the timescale for regional storms to grow or merge into a global storm) (Cantor et al., 2001; Wang et al., 2023; Guha et al., 2024). The full-disc, all-local-times coverage of dust cloud imaging, dust column abundances, and vertical profiles of aerosol abundance and properties, provided by LightShip, will enable the growth of storms over all such scales except the very smallest to be tracked and studied. The addition of further LightShip orbiters would allow such tracking to be continuous over all local times and longitudes, up to mid-latitudes, providing an unprecedented dataset on the onset, growth, and decay of dust storms.

At the same time, the LightShip suite of measurements will enable many hypotheses about what *causes* this growth to be tested, as partially shown in Figure 7. Line-of-sight wind profiles, temperature profiles, and surface pressure will provide information on the polar circulation and baroclinic wave activity on and around the seasonal cap, which are critical to dust lifting, the production of high-latitude dust storms, and the latter's subsequent motion/expansion. These datasets, as well as dust imaging, will be used to identify the combination of tides and other planetary waves associated with both increased dust lifting and the equatorward motion of frontal dust storms which develop around the polar cap edge, many of which then grow into the opposite hemisphere and sometimes combine with other storms to become global. Links to the placement of the seasonal cap edge will also be enabled by surface CO_2 and water ice observations. At lower latitudes, sub-diurnal imaging and temperature profiles will be able to confirm the role of large-scale slope winds and/or convection in generating strong dust lifting and storm onset or growth, such as around the Tharsis volcanoes or on the slopes of the Hellas basin.

While dust heating and cooling strongly modify the temperature and circulation, such changes also feed back on the dust distribution via changes to the water and CO_2 cycles (affecting dust sedimentation rates if dust particles act as condensation nuclei) and transport (mixing and advection). Another major feedback involves the relationship between atmospheric dust, the circulation and dust lifting from the surface. The simultaneous or contemporaneous measurement of all relevant fields from orbit will enable the presence of such feedbacks to be identified and studied.

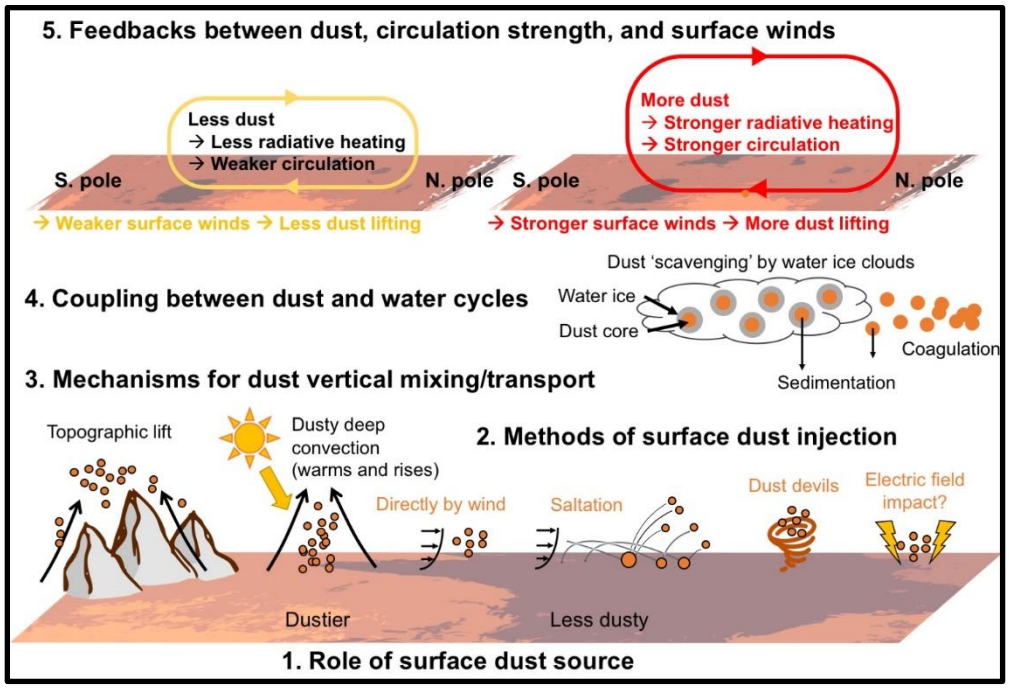

Figure 7: Diagram showing some of the most important processes and feedbacks involved in dust lifting and the onset and growth of dust storms on Mars. From Newman et al., 2022. LightShip will enable many of these processes and feedbacks to be investigated, in particular coupling between the dust and water cycles, the role of surface dust availability, and feedbacks between storm growth and circulation strength (with the latter measured directly for the first time).

OBJ-SCI-07 Do global dust storms decay due to changes in the circulation, changes in surface dust availability, or something else?

Real global dust storms are observed to decay far more rapidly than they do in free-running model simulations, even when limited surface dust availability is imposed. Potential causes in the real atmosphere include changes to the near-surface circulation (likely linked to greater atmospheric stability or a decoupling of the circulation aloft from that at the lowest levels), reduced surface dust availability (due to actual surface dust exhaustion or simply dust being harder to lift once the top layers are removed), or even interactions with the water and CO_2 cycles (via radiative feedbacks and/or dust acting as cloud condensation nuclei).

By observing the evolution of the circulation and thermal state during the mature phase of a global dust storm, and linking this to changes in weather patterns, clouds and the water cycle, and surface albedo changes, many of these hypotheses can be tested. Of particular value would be measurements of winds and temperatures down to the surface during very dusty conditions, to study near-surface wind and stability changes during the peak of a major storm. This may only be possible from the SpotLight lower-altitude orbiter, i.e. if it carries Wind Lidar instrument. However, observed changes to the circulation, temperatures, and aerosol abundances and properties at higher altitudes, made possible by the LightShip instrument suite, can also be used to validate atmospheric model simulations at these levels (providing support for model

predictions closer to the surface), and to test other mechanisms for global storm decay such as radiative and microphysical feedbacks. Similarly, imaging of surface albedo changes produced by the storm – both by LightShip's camera at lower resolution, and potentially by SpotLight imagers at high resolution – will shed light on how changes to surface dust availability may have resulted in reduced dust lifting as the storm progressed (Figure 8).

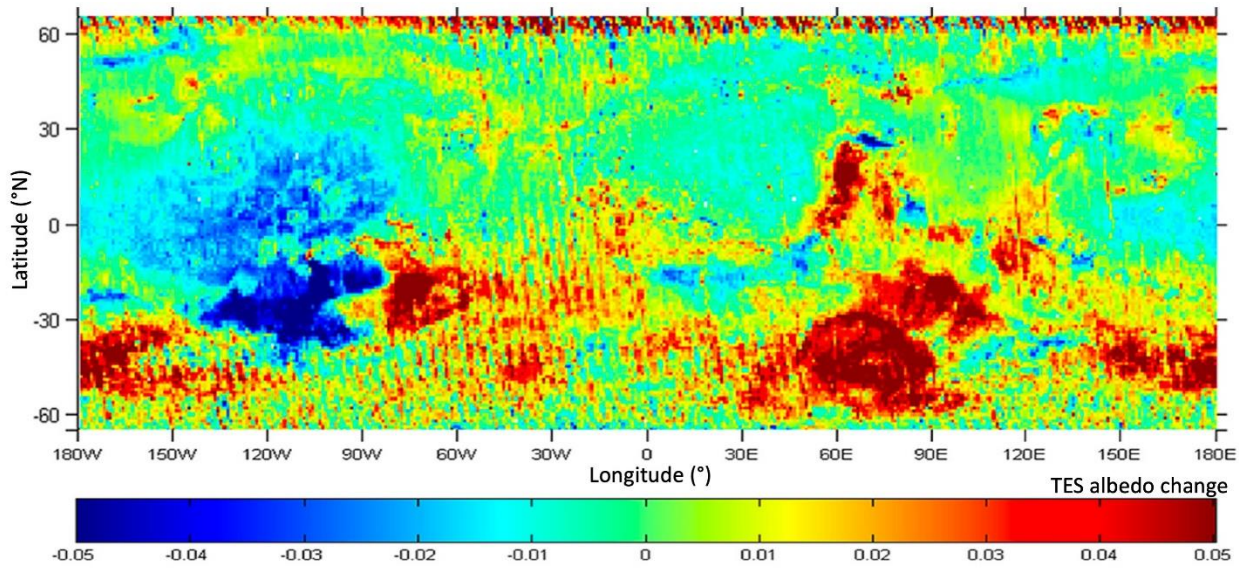

Figure 8: Mars surface albedo changes due to the 2001 (Mars Year 25) global dust storm. Shown is the TES albedo averaged over Ls=0-90° in the year following the storm minus the same for the year of the storm, which began shortly after Ls 181° in that year. Changes in surface albedo associated with dust storms, as monitored by LightShip's imager, will provide insight into the role of surface dust availability in causing both the onset and decay of storms, while LightShip observations of how the thermal state and circulation change aloft will be used to validate models that also simulate the near-surface changes most relevant to the decay of global storms.

2.3 Theme C: Water cycle, clouds, and chemistry

Despite the scarce availability of water vapor in the atmosphere and the fact that water has only two significant reservoirs on the surface (the two polar caps), water cycle on Mars is still dynamic and follows seasonal patterns on a global scale. The formation of the equatorial Aphelion Cloud Belt and the polar hoods are some of the most apparent atmospheric features related to the water cycle and have a measurable impact on radiation reaching the surface (Steele et al., 2014). Besides that, water circulation is the result of a complex relation between dust, its transport, winds, and temperature variability. In this sense, obtaining a more global view of water transport on the synoptic scale is important to gain insights into large scale atmospheric circulation, which ultimately informs models.

Water vapor and ice, together with odd hydrogen species (OH, HO_2) are thought to play also a role in the chemistry, production and destruction of other atmospheric trace constituents (such as HCl and O_3), whose characterization and mapping have been key questions for current and past missions. The continued quantification and detection of trace species is one possible pathway to infer more information about the atmospheric chemistry and, ultimately, about the interaction between trace and bulk, abundant atmospheric species.

OBJ-SCI-08 What is the radiative impact of water ice clouds and how does this affect the circulation?

The radiative impact of water ice clouds in the tropics is stronger (10-15 K at 10 Pa) compared to polar hood clouds which have only a small impact due to low density-scaled opacities (Steele et. al, 2014). Clouds also have an indirect effect on the atmosphere, with the strengthening overturning circulation increasing polar warming temperatures by ~6–8 K. Jet speeds are also modified by changes to the meridional temperature gradient. The cores of the winter westerly jets increase by ~10–20ms^{-1}, while the equatorial easterly jet weakens by ~60ms^{-1} (compared to a cloud-free atmosphere). The changing circulation also leads to the redistribution of atmospheric constituents, with increases in tropical dust amounts raising temperatures by ~2 K between 1 and 10 Pa. Understanding these impacts in a global sense is required to determine the sensitivity of circulation to the presence of water ice clouds at sub-diurnal to seasonal scales and quantify the impact on radiative processes and the coupling to atmospheric transport. (Figure 9)

Through limb observations with the instruments described in the strawman payload of LightShip, we can obtain vertical profiles of water ice and particle size distributions to better constrain models and help to answer this question.

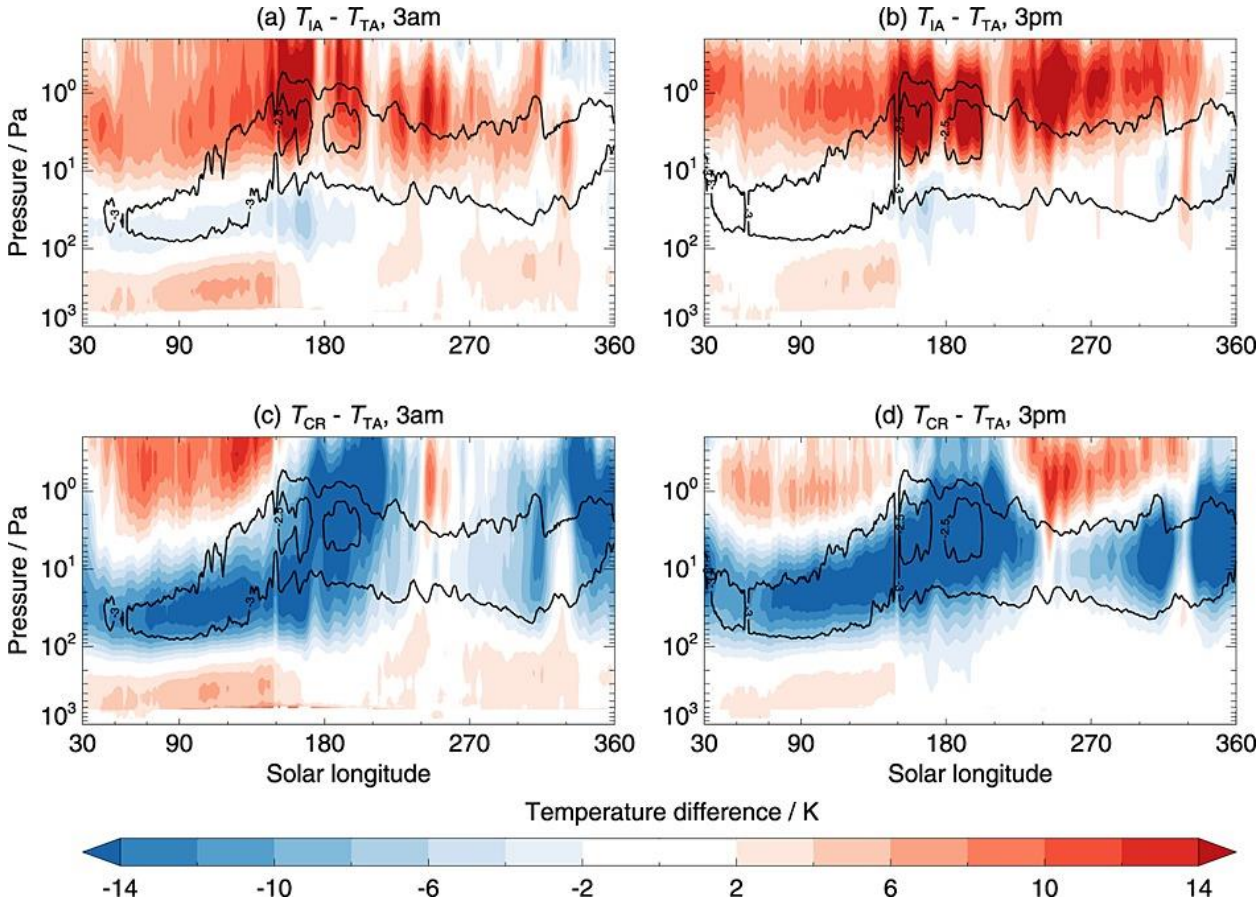

Figure 9: Zonal mean temperature differences at the equator at 3am (a + c) and 3pm (b + d) local time for different GCM assimilation runs of MCS data from Steele et al. (2014), showing that water ice cloud assimilation with radiatively active clouds is essential for correctly simulating temperatures. Top row: temperature difference between ice assimilation (IA) and temperature assimilation (TA) runs; bottom row: temperature difference between the control run (CR) and temperature assimilation (TA) run. Black contours show log10 (infrared density-scaled water ice opacity) at −3.5 and −2.5 log units. LightShip instruments will provide simultaneous measurements of temperature, dust, water vapour, water ice, and aerosol properties, at vertical resolution of ~1 scale height, hence will enable more accurate understanding of cloud radiative effects, better representation of them in models, and better simulation of the thermal state of the atmosphere.

OBJ-SCI-09 How variable is the Martian water cycle on sub-diurnal to decadal timescales, and what drives this?

On sub-diurnal timescales, the daytime water vapour column is fairly stable over a given location (Crismani et al., 2021). Water ice clouds in general are thicker during the nighttime compared to the daytime (Atwood et al., 2022). Atmospheric waves have a strong impact on water vapour structure near the edges of the polar vortex during the given hemispheric winter season and can induce strong sub-diurnal variation in water vapour and ice associated with changes in local temperature. On decadal timescales, the largest impacts to the water cycle come from global dust storm events, which potentially have an interannual impact on the global water cycle, shifting the water cycle out of equilibrium in years preceding a global dust event. For years in which no global dust events are present, the water cycle is largely similar from year-to-year with minimal interannual variation. LightShip will provide the opportunity to study the long-term (interannual) global response of the water cycle to such global-scale events, given the nominal mission lifetime that should include >1 global dust storm event. Figure 10 shows the changes in water vapour profiles due to dust activity measured by TGO/NOMAD through a large planet-encircling dust storm in MY34 and then in the relatively clearer dust season in MY35. Continuous monitoring of the water cycle by LightShip will be invaluable.

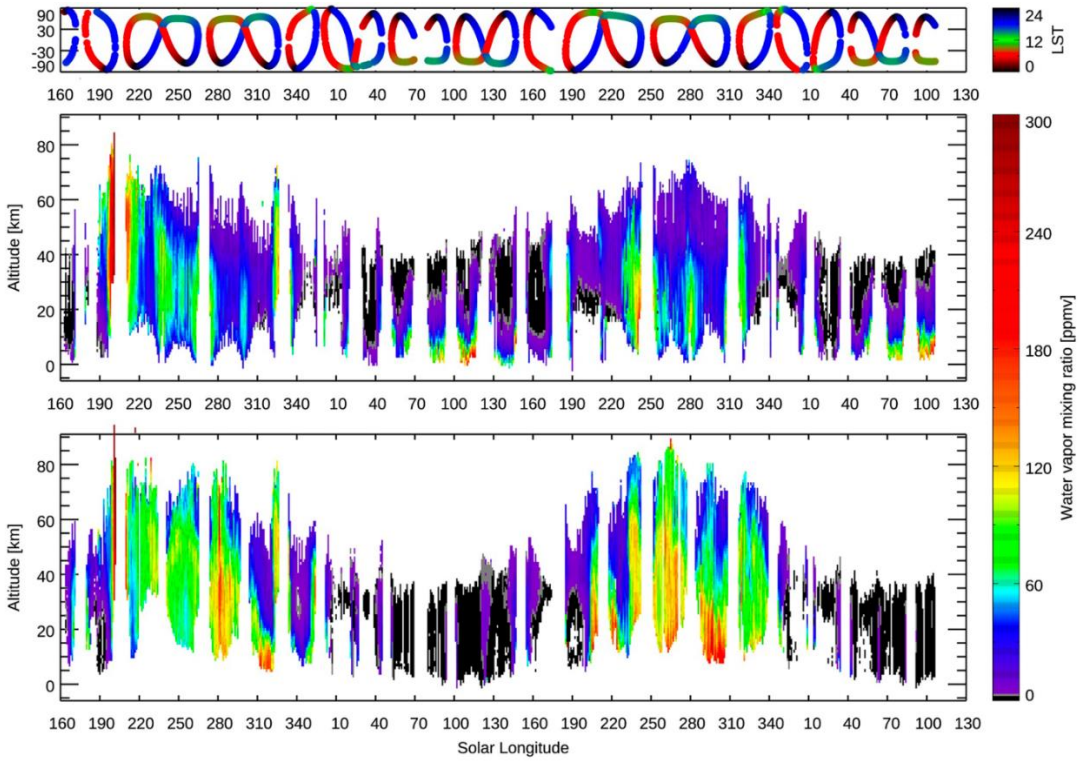

Figure 10: Seasonal variation of the water vapor vertical profiles from LS = 160° in MY 34 to LS = 130° in MY 36 from Aoki et al., 2022, retrieved from TGO/NOMAD-SO data in the northern hemisphere (the middle panel) and the southern hemisphere (the bottom panel); the top panel shows the latitudes and local solar time of the measurements. Solar occultation observations are constrained by Sun-Mars-orbiter geometry; whereas LightShip will provide vertical limb profiles of water vapor and water ice abundances – in addition to dust abundances - at a resolution of ~1 scale height at all local times over all low and mid latitudes every ~3 sols, enabling links between the water cycle and dust cycle on timescales from sub-diurnal to multi-annual to be identified.

OBJ-SCI-10 What are the interactions between the water and dust cycles?

The dust cycle is known to be one of the key regulators of the climate system of Mars. The link between dust and water cycles have been revealed in detail especially by recent observations by MAVEN and TGO (Chaffin et al., 2021; Villanueva et al., 2021; Aoki et al., 2019). Observing vertical profiles of dust and water vapor (and its isotopologue HDO) simultaneously at the same location during periods of high dust activity has demonstrated that dust-induced heating can raise the hygropause by several tens of kilometers in some cases, leading to the formation of water ice clouds at altitudes of up to 110 km. (Liuzzi et al., 2020). On the contrary, TGO observations have revealed that the altitude of the hygropause is as low as a few kilometers above ground level at aphelion with low to no dust activity at high southern latitudes (Villanueva et al., 2022).

In addition to dust modifying the water cycle as described above, changes to the distribution and nature of atmospheric and surface water can impact dust in return (e.g., Figure 11). For example, year-to-year variability in the onset timings and locations of dust storms could potentially be linked to interannual variability in the water (and/or CO_2) cycle, such as: differences in the size of polar surface reservoirs or the timing of their maximum extent; changes in the distribution of atmospheric volatiles and temperatures resulting in changes to the spatio-temporal distribution of dust scavenging via particle nucleation; and/or changes in radiative heating, temperatures, and transient eddy behaviour due to ice cloud radiative effects (e.g., Kahre et al., 2012)

To date, most simultaneous dust and water profiles are obtained via solar occultations and limb measurements, which are very localized without global spatial coverage on short timescales. Hence the main limitation of the aforementioned studies is that these data are not ideal to quantify the timescale on which water vapour vertical distribution changes due to dust lifting at various locations. Observations of the water vapour apparent column at the onset of a regional or global storm, and simultaneous observation of temperature vertical profile at high spatial resolution would provide the missing piece of information to answer this question. The observation geometry of LightShip would be ideal to obtain information that is global and continuous about temperature and water vapor.

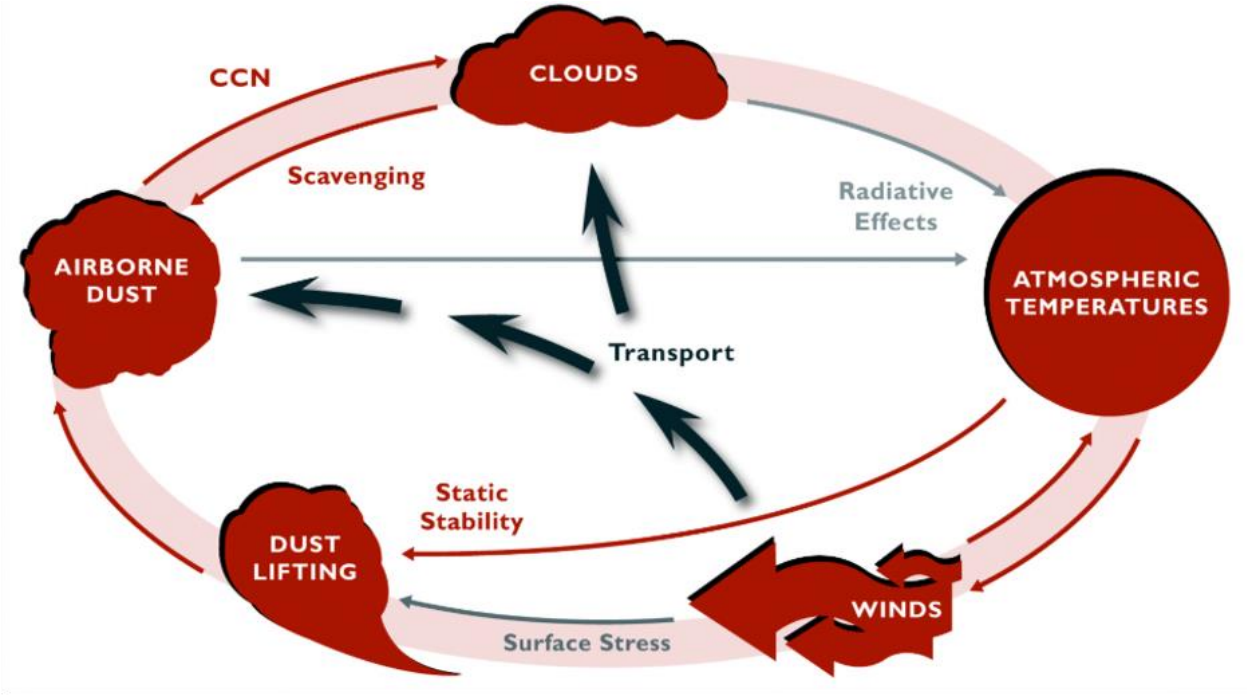

Figure 11: Schematic showing the many potential interactions between Mars's dust and water cycles (from Kahre et al., 2012). By making the first direct wind measurements from orbit, with co-located measurements of wind, temperature, aerosol and water vapour profiles, plus column aerosol properties, LightShip will provide insight into most of these processes and feedbacks (except for linking near-surface conditions to dust lifting), enabling better understanding of crucial dust-water interactions.

OBJ-SCI-11 What chemical, dynamical and dust processes affect transport of water towards the upper atmosphere?

Water is a minor component of the Martian atmosphere, which is largely confined within a few lower scale heights. Nevertheless, it is the main source of hydrogen in the upper atmosphere. Hydrogen is produced by photodissociation of H_2O molecules delivered to the upper atmosphere (above ~80 km) from below and, due to its low molecular mass, has the largest probability of escaping into space compared to other species. It was suggested that hydrogen escape was the main channel of atmospheric loss and dehydration of Mars in the past (McElroy, 1972). Escape of hydrogen atoms into space near the exobase varies by an order of magnitude seasonally, maximising around the southern summer solstice. Observed water in the lower atmosphere also experiences strong seasonal changes and depends on airborne dust load (Trokhimovskiy et al., 2015). Both hydrogen in the exosphere and water in the upper atmosphere increase significantly during major dust storms.

The Martian middle atmosphere is too cold to sustain water vapour, especially around the mesopause, while ice particles are sufficiently heavy and prone to sedimentation. This water behaviour is similar to that in the terrestrial middle atmosphere. The observed seasonal behaviour and the dependence on atmospheric dust has been explained by the water ``pump" mechanism (Shaposhnikov et al., 2019), according to which water is transported from the lower

to upper atmosphere by the meridional circulation. Similar results for the dust storm of MY34 have been produced in the simulation study of Neary et al. (2020), which showed that the water vapour distribution at higher altitudes is sensitive to the vertical distribution of dust. The simulations of Shaposhnikov et al. (2022) taking into account the influence of small-scale gravity waves further elucidated the mechanism of water transport to the upper atmosphere during the major dust storms of MY28 and MY34. (Figure 12)

It was shown that the main channels, through which water enters the upper atmosphere, are collocated with the regions of air updraft by the meridional circulation: in low latitudes during the northern autumn equinox and in high southern latitudes during perihelion. The influx of water to the upper atmosphere increases, whenever the meridional cell intensifies, for instance, during dust storms. In addition, dust storm-induced heating increases the amount of water vapour in the lower atmosphere. The water is transported above 80-100 km by the global circulation, while above ~120 km the molecular diffusion plays an increasingly larger role. These simulations and measurements from the ExoMars TGO and MAVEN spacecraft (Fedorova et al., 2020; Stone et al., 2020) solidified the concept of the water ``pump" mechanism of transporting vapour directly to the upper atmosphere. This mechanism has some similarities and differences with that on Earth. In the terrestrial stratosphere and mesosphere, there is also a strong water upwelling in the summer hemisphere that even compensates for photochemical destruction (Hartogh et al., 2010). Due to Earth's more circular orbit and unlike on Mars, it occurs during both solstices. However, water in the terrestrial atmosphere is rapidly destroyed by photolysis in the sun-lit summer hemisphere above ~70 km, whereas on Mars its significant portion can be transported across the globe.

Measurements of trace constituents up to the upper atmosphere, as would be achieved by the sub-mm instrument in LightShip strawman payload, would provide global mapping of such transport. The sub-mm instrument could provide sensitivity for mapping up to well above 100 km in altitude, providing thousands of measurements per day, at all times of day, rather than just ~20 profiles per day at the terminators as is the case with TGO solar occultation.

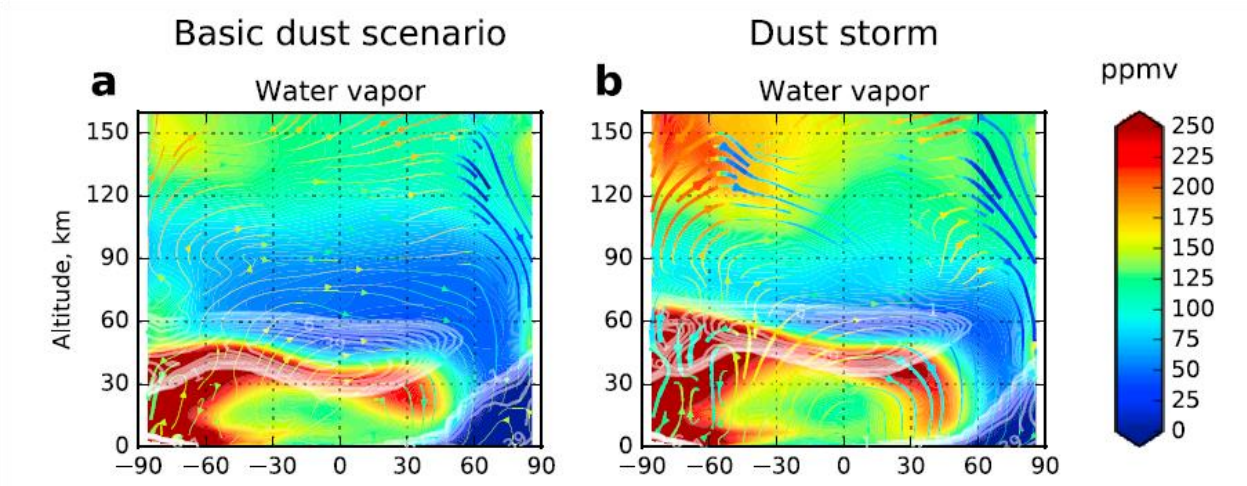

Figure 12: Latitude-altitude cross-sections of the quantities simulated for the "basic" dust scenario (left column) and the MY28 dust storm (right column): (a) water vapour (shaded), water ice (white contours), and the meridional flux of water vapour (the lines with arrows, the colour and thickness of which indicate the vertical direction and magnitude, correspondingly); (b) is the same as in panel (a), but for the dust storm of MY28 (from Shaposhnikov et al., 2019). However, overall fluxes of water are still poorly constrained by current observations. LightShip's strawman payload would observe profiles of water vapour and ice up to well above 100km, in addition to simultaneous dust vertical profiles, providing better constraints on vertical water transport and its link to the evolving dust distribution.

OBJ-SCI-12 How variable is Martian chemistry on sub-diurnal to decadal timescales, and what drives this?

The chemistry of the Martian atmosphere is driven by carbon dioxide (CO_2) and water vapour (H_2O) and the interactions of the products of their photolysis by sunlight. CO_2 is the main component of the atmosphere and varies seasonally due to its sublimation and condensation at the polar caps. As much as 30% of the atmosphere condenses during polar night, which in turn results in large global surface pressure variations. Another impact of this phenomenon is the enhancement relative to CO_2 of non-condensable species such as nitrogen, argon, oxygen, and carbon monoxide.

While H_2O vapour is not the most abundant species, it has a significant impact on diurnal and seasonal timescales through the formation of water ice clouds in the atmosphere (with radiative effects) and through sublimation/condensation on the surface. The products of H_2O photolysis have an impact on ozone (O_3) which also shows strong diurnal and seasonal variations. These products, collectively known as odd hydrogen species (H, OH, HO_2 referred to as HO_x radicals) have not been observed, but hydrogen peroxide (H_2O_2) which is a reservoir species for HO_x, has been measured in the infrared and sub-millimetre wavelength ranges. Once again, the data is sparse in time and space.

Despite the observations and modelling done to date, there are still aspects of the Martian atmospheric chemistry system that are not fully understood (Figure 13). The role of HO_x in the stability of the CO_2-rich atmosphere is an area of current research, where little is known about the impacts of heterogeneous processes in Martian atmospheric chemistry. Capturing the daily and seasonal variations of aerosols, H_2O vapour, O_3, HO_2 and H_2O_2 will advance this area of research and help to improve model simulations and our understanding of these processes.

As well as these relatively short-term variabilities, on a decadal scale, the atmospheric chemistry is impacted by dust storms which can modify the vertical profiles of water vapour and therefore ozone. It is important to continue to collect observations to have a long-term picture of the variability in the atmosphere.

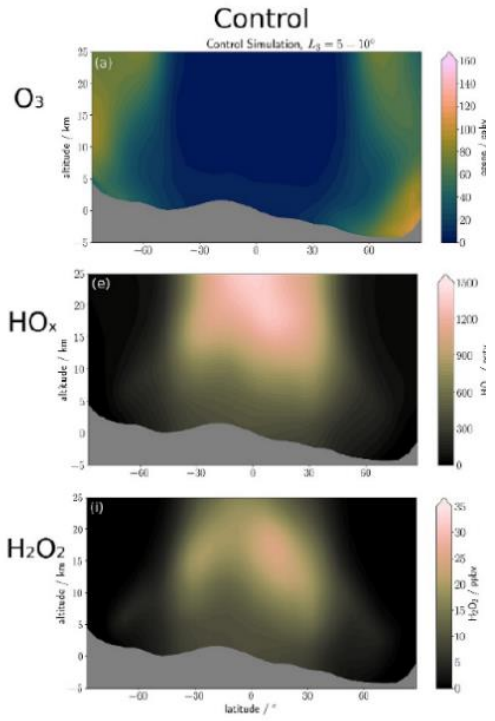

Figure 13: At present, TGO can measure vertical profiles of H_2O, HDO and O_3 but only at the terminator([Brown et al, 2022](#)); most other species are not directly measured and must be inferred from calculation. A sub-mm sounder as proposed on LightShip would be able to map more related species, including HO_2 and H_2O_2, at all times of day.

2.4 Theme D: Enabling Mars exploration (safe arrival & operations)

Accurate knowledge of density profiles is typically vital for the safe arrival of both orbital and surface Mars missions: aerobraking procedures, in which a spacecraft is 'dragged' through the upper atmosphere to convert to a circular orbit without requiring thrusters, rely on knowing the density of the upper atmosphere, while knowing the density from high altitudes down to close to the surface is also key for the entry-descent-landing (EDL) phase of surface missions. Accurate knowledge of wind profiles is also crucial for the EDL of surface missions, especially for the altitude range (typically below ~15km) corresponding to the descent under parachute. Large variations in atmospheric dust loading typically provide the largest perturbations in density, wind, and temperature from surface to upper atmosphere on Mars.

Accurate knowledge of densities, winds, and temperatures near the surface are also vital for the safe operation of aerial vehicles once they reach the surface. Post-landing, advance warning of the arrival of dust storms at the location of a surface asset on Mars is of great value to mission planners and engineers. For mission operations and safety, it provides notice to solar-powered spacecraft to save battery power and (if possible) move to a position that maximises energy production by the solar panels. And while Martian dust storms do not carry the force needed to blow over equipment or astronauts, a warning that one is imminent provides time to close dust covers and protect delicate equipment, and to cancel activities that require good visibility (e.g. long-distance imaging), quiescent winds, a certain temperature range, and/or more predictable near-surface conditions (e.g. the flight of an aerial vehicle).

OBJ-SCI-13 How accurately are density and wind profiles, and their variability, represented in atmospheric models?

When designing future missions entering the Martian atmosphere, whether these are probe/landers or aerobraking satellites, accurate knowledge of what atmospheric densities and winds will be encountered is essential.

General Circulation Models (GCMs) have made significant advancements in recent years and can generally reproduce the basic average state of the Mars atmosphere, but many important details are still not well constrained in simulations. Observational data is used as a metric for model performance, and with the current missions, we can compare model densities, temperatures, aerosol optical depths and trace gas abundances but we are limited in the times of day and regions when and where we observe. We cannot validate model winds as they have not been measured directly but must indirectly evaluate the circulation through the movement of dust and quasi-passive trace gases such as carbon monoxide (CO), ozone (O_3) and water vapour (H_2O).

The increase in spatial and temporal coverage of observations provided by LightShip will enable refinement of the physical models used in GCMs to represent processes such as dust lifting and cloud microphysics. High cadence measurements at all local times of surface temperature and pressure, and of vertical profiles of temperatures, aerosols and winds, will result in better knowledge of the true state of the Martian atmosphere against which models can be validated, and ultimately better prediction of the present Martian climate and weather.

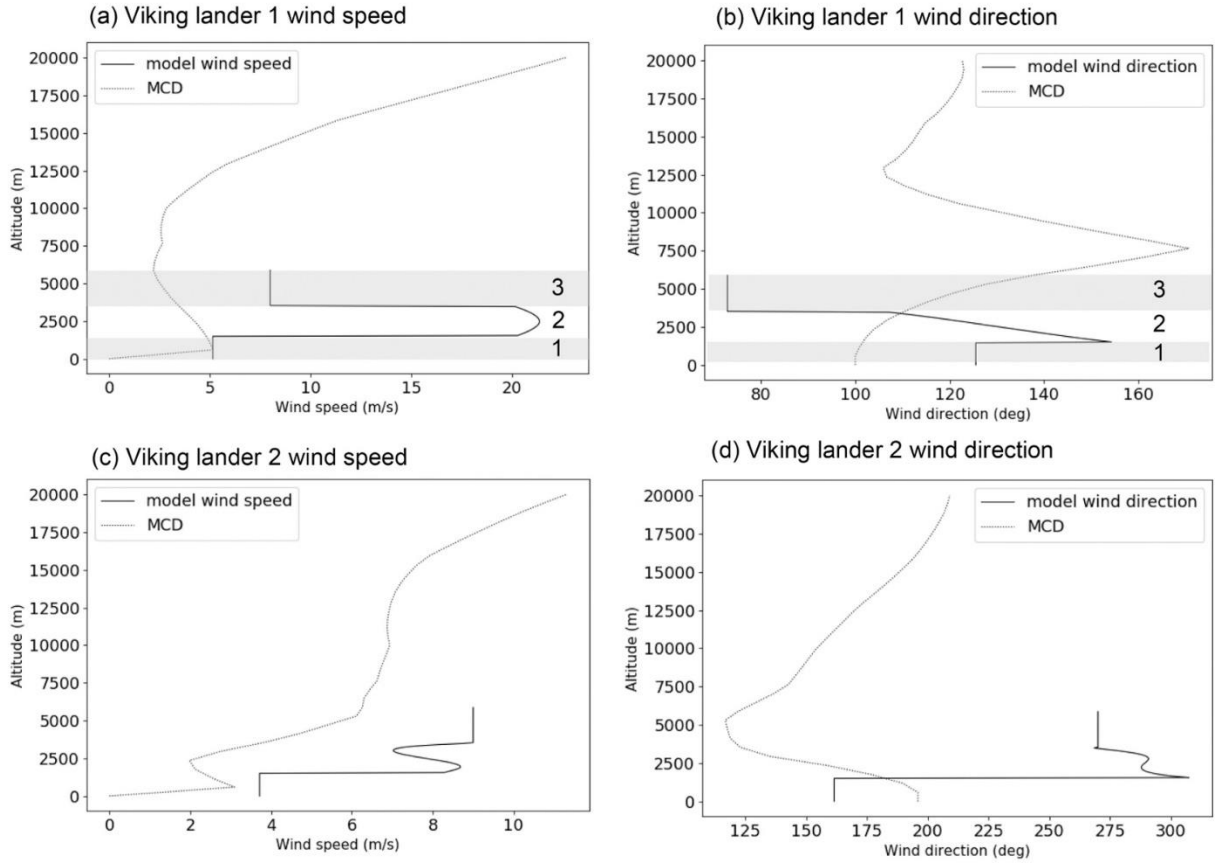

Figure 14: Wind speeds (left) and directions (right) for the descent of Viking landers 1 and 2 through the atmosphere, comparing inferred winds from trajectory and aerodynamical modelling with global atmospheric model-derived predictions from the Mars Climate Database (from Paton et al., 2021). This demonstrates the large mismatch between observed and predicted wind profiles at altitudes above the surface, but also the lack of wind measurements above the altitude of parachute deployment (here ~6km). Direct wind measurements at altitudes from ~10 to over 100km by LightShip's strawman payload would be revolutionary for understanding winds in that vertical region, while observations of temperature profiles at all times of sol would be a major advantage for engineers who require accurate density profiles for the local time of EDL.

OBJ-SCI-14 How well can weather be predicted by assimilating temperature, dust, winds, and surface pressure?

While the above Objective 13 is intended to capture the knowledge of the mean atmospheric state and variability, the present Objective 14 focusses on **atmospheric *prediction* over periods of hours, days or weeks**. When a new Mars lander is a few days away from arrival at Mars, an

atmospheric prediction updated using current observations may be used for adjustments to the entry trajectory, to enable safer or more accurate landing.

Temperature and dust assimilation has proven to be able to replicate weather identified in observational data through multiple publications (Wang & González Abad, 2021, Holmes et al., 2022, Hinson & Wilson, 2024). Human exploration efforts will require assimilation on a finer grid resolution (i.e. mesoscale or better) than is currently standard for Mars modelling studies, with such mesoscale simulations being informed by boundary conditions achieved through global-scale assimilation. Assimilation of winds is a challenging process – current assimilation approaches include methods to adjust wind velocities from thermal wind balance after the assimilation of temperature profiles, but a major unknown is whether this process results in wind fields that are better aligned with reality. LightShip will revolutionise our understanding of the thermal wind balance for Mars, by providing both temperature and wind fields for assimilation and study of the coupling between these parameters on Mars, driving the need for wind and temperature observations with good spatiotemporal cadence. Surface pressure assimilation on Earth has been shown to improve forecasting of mesoscale convective events and associated rainfall (Demortier et al., 2024). Surface pressure assimilation, although it has previously only been attempted as an "Observing System Simulation Experiment" (OSSE) for Mars (Lewis and Read, 1995, Lewis et al., 1996), should result in improvements to wave feature representation in models (see e.g. Figure 15).

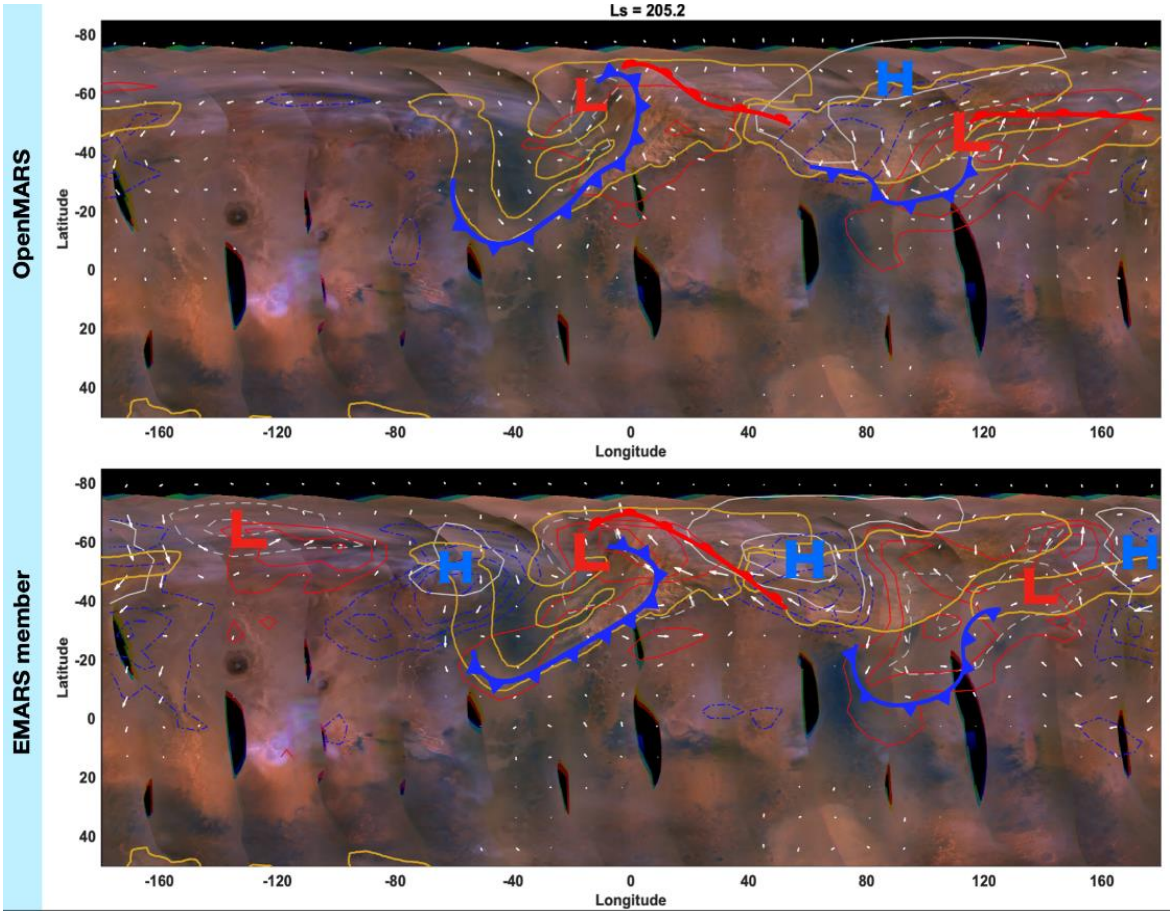

Figure 15: Near-surface wind (white arrows), surface pressure (red and blue contours), location of fronts and low (L) and high (H) pressure systems, and observed dust loading (yellow contours), for two reanalysis data products (i.e., simulations using data assimilation) for the exact same time. The upper and lower panel results are taken from the OpenMARS (Holmes et al., 2020) and EMARS (Greybush et al., 2019) reanalysis datasets, respectively, and both are overlaid on MARCI images of Mars at close to the same time. The figure is courtesy of J. Michael Battalio and demonstrates that, even when assimilating the same fields at the same time, two different GCMs and data assimilation systems provide different representations of surface weather systems (near-surface wind and surface pressure fields), which are crucial to determining future dust transport and lifting. By providing global measurements of surface pressure and winds at higher altitudes, LightShip should improve the ability of models to correctly represent reality and make accurate predictions.

OBJ-SCI-15 How much warning can be given of dust storms headed for landing sites?

Like Objective 14, this focusses on prediction; however, here the focus is on **weather prediction at the surface**, and in particular on dust storms.

At present, the earliest advance warnings of dust storms typically come from the rapid retrieval and analysis of thermal and imaging data from instruments on the Mars Reconnaissance Orbiter spacecraft: Mars Climate Sounder (MCS) and the Mars Color Imager (MARCI), respectively (Figure 16). Data from these instruments are produced very rapidly compared to those from other missions due to a combination of greater DSN access (so that the data are rapidly downlinked to

Earth) and fast data processing pipelines. Thanks to the strong temperature response to the presence of dust in the atmosphere, in addition to direct dust retrievals, MCS can warn speedily that a dust storm is underway and give a general sense of its location. Images from MARCI typically provide the earliest warnings of dust storm activity, such as cap edge 'frontal' storms building, then sometimes moving south into 'storm track' corridors, particularly when combined with knowledge of past decade dust activity at similar Ls. In both cases, there may be a sol's delay if the dust storm is on the opposite side of Mars, however.

LightShip's instruments will extend and expand this early warning ability by providing greater spatiotemporal orbital coverage of temperature and dust, and by adding wind and surface pressure observations from orbit, with continuous global coverage becoming available from multiple LightShip orbiters.

Further, LightShip data will both increase understanding of what drives dust storm onset, evolution and decay *(Objectives 4-7) and* provide better measurements of the current atmospheric state (more complete spatio-temporal coverage *and* more atmospheric quantities, i.e. winds and pressure) for improved weather prediction via Data Assimilation *(Objective 14).* These efforts will improve our ability to predict dust storm onset and evolution, and hence storm arrival at landing sites in the future.

In order to provide operational weather monitoring and forecasting, it is noted that the processing of the observational data to create usable data products is essential. The ground segment should be set up to allow delivery of meteorologically useful data in within a short period (e.g. 24 hrs) after acquisition. Corresponding investment in numerical weather prediction capability for Mars is also essential in order to allow operational dust storm prediction. Further information about these points is given in an Appendix to this document.

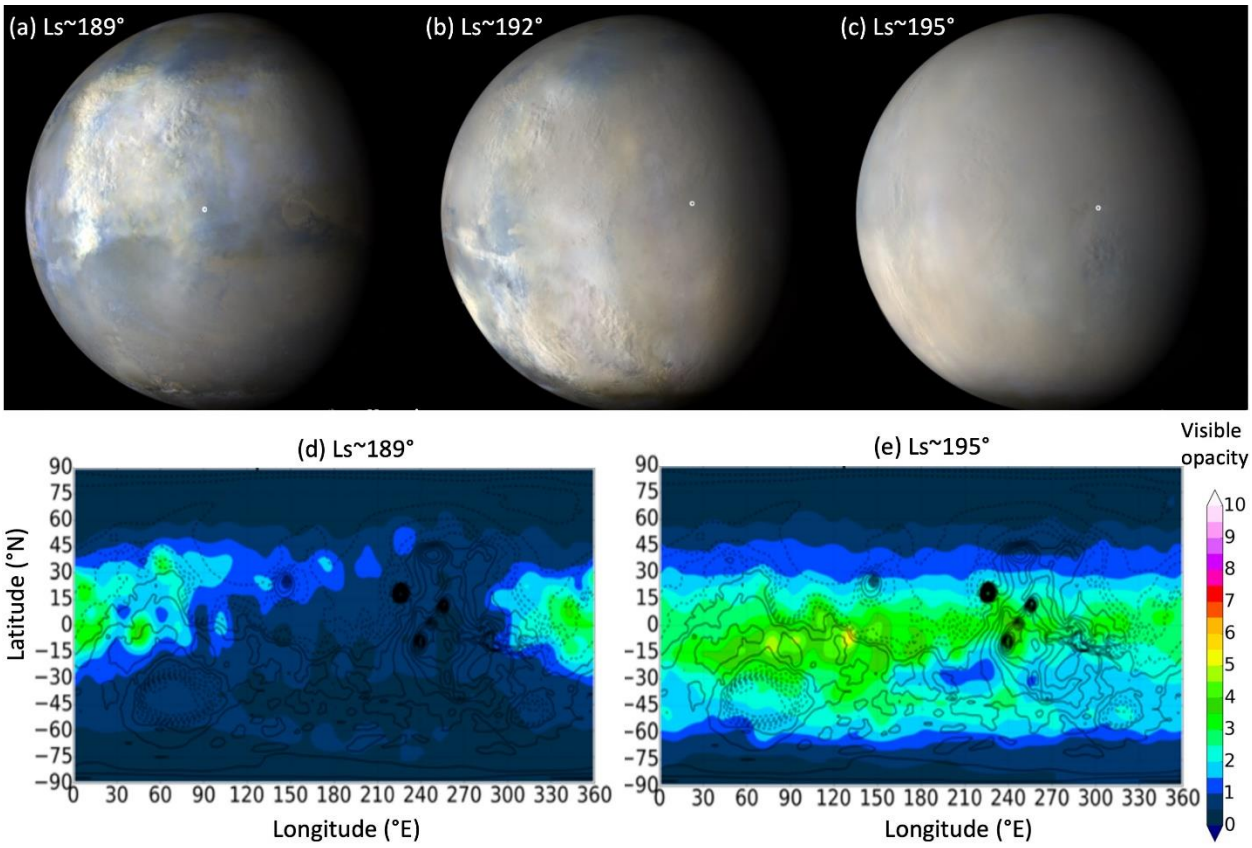

Figure 16: (top) MARCI images of the 2018 global dust storm from onset through global expansion (a-c); (bottom) re-gridded and interpolated dust maps from MCS retrievals during the same period (Montabone et al., 2020). LightShip will extend and expand this early warning ability by providing greater spatiotemporal orbital coverage of temperature and dust, and by adding wind and surface pressure observations from orbit, with continuous global coverage becoming available from four LightShip orbiters.

OBJ-SCI-16 How variable is the radiation environment in cruise and in Mars orbit?

Requirements for radiation monitoring were not discussed by the IDT. It is included here as a placeholder for future discussion.

OBJ-SCI-17 What is the micrometeoroid population in cruise and in Mars orbit?

Requirements for an instrument to perform this investigation were not discussed by the IDT. It is included here as a placeholder for future discussion.

The science themes and objectives

3. Investigation & Measurement Objectives

From the science themes and key questions as described in Table 1, Investigation and Measurement objectives were derived. There are shown in Table 2, and summarized in turn below.

Table 2: Lightship Investigations and Measurements, and traceability to the strawman payload instruments shown on the right. L and N denote Limb and Nadir measurement, respectively.

Level 2 (Investigation)	Level 2 (Measurement)	submm	TIR	MIS	NIRSI	Radio occ
Measure **winds**	Measure vertical profiles of line-of-sight wind speeds, accuracy < 10 m/s & vert. res. <8 km	L				
	Measure wind vectors by tracking moving dust & cloud features		N	N		
Measure **temperatures**	Measure vertical profiles of temperature, accuracy 1 K & vert. res. < 8 km	L	L			X
	Map thermal emission of atmosphere in spectral bands covering altitudes of 0-60 km, accuracy 1 K & spatial resolution < 10 km	N	N			
	Map surface radiometric temperature to accuracy 1 K, spatial resolution < 10 km	N	N			
Measure **airborne dust**	Measure vertical profiles of dust abundance at 0 - 60 km altitude, vertical resolution < 8 km		L	L		
	Map column abundances across disk of Mars, spatial resolution < 10 km		N	N	N	
	Constrain airborne dust size distribution		N,L	N,L	N,L	
Measure **ice cloud**	Measure vertical profiles of ice abundance at 0 - 60 km altitude, vertical resolution < 8 km		L	L		
	Map column abundances across disk of Mars, spatial resolution < 10 km		N	N	N	
	Constrain ice cloud size distribution & composition		N,L	N,L	N,L	
Measure **water vapour** and related volatiles	Measure profiles of key tracers [H_2O, HDO, HCl, CO(?), O_2, O_3, ...] at 0 - 100 km altitude, vert. resolution < 8 km	L	L			
	Map column abundances of key tracers [H_2O, CO, O_3, ...] across disk of Mars	N	N		N	
Map **surface-atmosphere exchange**	Map surface changes of dust, H_2O ice, CO_2 ice		N	N	N	
Map **surface pressure**	Map depth of CO_2 absorption features to map surface pressure to precision of <10 Pa				N	(X)

Measuring **air temperature profiles** is the foundation of satellite meteorological monitoring on Earth. Multichannel thermal infrared radiometry from a high-altitude vantage point (typically geostationary satellites, in the case of the Earth) is used to measure, for every pixel across the disk of the planet, a multi-point vertical temperature profile, providing in effect a 3-D map of air temperatures. (In practice, atmospheric reconstruction on Earth now directly assimilates the

thermal infrared radiances rather than first calculating air temperatures; this is not yet carried out at Mars but could be a goal of the LightShip missions).

The strawman payload addresses this investigation through:

- ***Thermal infrared radiometry*** *at several spectral bands in the wings of the 15 µm CO_2 feature. Further spectral bands will be included in order to characterise dust, water vapour and ice clouds. Ideally, the strawman instrument should have enough spatial resolution to allow measurement both at limb and at nadir.*
- ***Sub-mm spectrometry****; this is complementary to the thermal IR radiometry in that, despite its poorer spatial coverage, it will provide validation of temperature profiles in key locations*
- ***radio occultation:*** *radio occultation provides vertical profiles of density in the neutral atmosphere, from which temperature profiles are calculated through assumption of hydrostatic equilibrium. Radio occultation will be carried out using comms link between a Lightship and passenger spacecraft (and potentially with future orbital assets), and by using the comms link between a LightShip and Earth.*

Winds are central to atmospheric dynamics; the general circulation of the atmosphere and its short-term variability are vital for all atmospheric investigations but also for mission design. Wind velocities are not measured directly, with the exception of point measurements from landers; in general they are calculated from temperature (or thermal IR radiance) measurements from orbit, using fluid dynamics to calculate which wind field would be consistent with observed atmospheric temperature fields. However, this wind determination relies on several poorly constrained inputs; to name just one, gravity waves are known to transport momentum through the atmosphere in a way can change calculated winds by tens of metres per second. Accordingly, direct measurement of winds from orbit would provide a major leap forward in Mars atmospheric dynamics, reducing uncertainty in wind field and turbulence predictions and improving understanding of transport of volatiles, dust, heat and momentum.

The strawman payload addresses this investigation through:

- ***Sub-mm spectrometry****; the strawman sub-mm instrument has a high enough spectral resolution to allow measurement of line-of-sight winds to an estimated accuracy of < 10 m/s, at altitudes of 20 km - 80 km (carried out when looking at the limb).*
- ***Imaging suite****: wind vectors will also be calculated by tracking dust & cloud features in repeated imagery of the planet.*

It is noted that **Atmospheric Wind LIDAR** is another method of measuring line-of-sight winds from orbit. Doppler LIDAR measures the line-of-sight velocity of airborne dust particles, and therefore returns wind speeds to an estimated accuracy of < 1 m/s at altitudes of 1 – 20 km altitude. This altitude range is therefore very complementary to that probed by the sub-mm sounder. However, the power needed for wind LIDAR is only viable for a platform in low orbit, so it is not considered

further for the LightShip strawman payload. A wind LIDAR is included in the strawman payload not of the high-altitude LightShip, but of the low-altitude SpotLight passenger spacecraft (as described in SpotLight Measurement Definition Team report[2]). The altitude range covered by this would be very complementary to that covered by the sub-mm included in the LightShip strawman payload.

Dust is the most variable component of the Martian atmosphere. The presence of dust in the atmosphere changes the radiative balance of the atmosphere, governing the dynamics. The global dust storms which envelope the planet in some years are still enigmatic; focussing on how they arise, and how they decay.

The strawman payload addresses this investigation through:

- ***Thermal IR radiometry**; dust will be measured both in nadir mode, across the disk of the planet, and at the limb of the planet.*
- ***Imaging suite**: dust will be measured using multiband imaging. Use of different spectral channels will allow discrimination between dust and ice clouds.*
- ***Near-IR spectral imager**: this offers the chance for more robust measurements of dust including its vertical partition, through band depth measurement of spectral bands including the 1.44 and/or 2.06 µm CO_2 bands.*

Water and other minor constituents. Water is the most important atmospheric volatile from the point of view of understanding habitability through time, its role as an active tracer in the atmosphere and its potential for *in situ* resource utilisation. The sub-mm sounder allows measurement of many more volatile species, including CO, O_2, O_3 and HCl, shedding light on a wide range of atmospheric processes.

The strawman payload addresses this investigation through:

- ***Thermal IR radiometry**; will allow measurement of water vapour column abundance in nadir mode, across the disk of the planet, and water vapour profiles at the limb of the planet.*
- ***Sub-mm spectrometer**: will allow measurement of water vapour (in both H_2O and HDO isotopologues) both across the disk of the planet and at the limb. At the limb, it would have sensitivity to water vapour at altitudes up to 100 km (depending on integration time), allowing to trace how water and related species pass through the cryopause. Sub-mm spectrometer is also sensitive to a wide range of further species, shedding light on a wide variety of transport and chemistry processes.*
- ***Imaging suite**: water ice clouds will be detected using multiband imaging. Use of different spectral channels will allow discrimination between dust and ice clouds.*

[2] SpotLight Measurement Definition Team Report, ESA-E3P-LS1-RP-001 v 1.1 Nov 2024

- ***Near-IR spectral imager****: this offers a complementary measurement of water vapour and ice clouds, through band depth measurement of spectral bands including the 1.37 µm H_2O band.*

Measuring **Surface-atmosphere exchange** – of dust, water, heat and momentum - will be achieved primarily by monitoring all the constituents above, in order to identify sources and sinks. Furthermore, surface distribution of dust and ice will be monitored using the imaging suite and/or near-infrared spectrometer, in order to track seasonal/diurnal redistribution of these materials on seasonal or following dust storms.

Finally, the IDT recommend a goal to retrieve **surface pressure**. Maps of surface pressure serve as an indicator of a wide range of dynamical phenomena. Surface pressure can be measured spectroscopically from orbit by measuring the depth of CO_2 spectral lines (Forget et al., 2007; Spiga et al. 2007; Toigo et al. 2013; Kazama et al. 2023); some examples of using such data for studying meteorological phenomena are given by Spiga et al. (2007). The atmospheric science goals which can be addressed will depend on the precision to which the pressure can be determined. Table 3 below illustrates some of the atmospheric science topics which could be achieved at different surface pressure retrieval errors.

Table 3: Some examples of science topics addressable at different surface pressure determination precision levels.

Surface pressure retrieval error	2% (~ 20 Pa) [or ~4-24 Pa]	0.5% (~5 Pa) [or ~1-6 Pa]	0.2% (~2 Pa) [or ~0.4-2.4 Pa]
Benefits of achieving this error	- baroclinic waves at mid to high latitudes, - generation of frontal dust storms, and their expansion to regional or global storms - seasonal CO_2 cycle and - pressure variation due to large-scale topographic variation	- tidal modes and baroclinic waves at all latitudes - dust response and teleconnection	- diurnal pressure variations due to hydrostatic adjustment on slopes - smaller amplitude tidal modes and - gravity waves - dust response and momentum exchange / vertical stability & mixing

The strawman payload addresses this investigation through:

- ***Near-IR spectral imager****: this would measure CO_2 band depth at 1.4 & 2.0 µm bands. The achievable surface pressure precision would need to be demonstrated by instrument proposers.*

4. Strawman Instrument Descriptions

In this section, a strawman science payload is presented.

Certain aspects of the mission and payloads were already pre-defined by the mission concept; these were specified by the LightShip project team to the Instrument Definition Team:

- The orbit is already defined, optimised for communications and navigation, and is not to be chosen or modified by the Science Team.
- The mass allocation for the science payload of a LightShip spacecraft is approximately 30 kg.
- There will be a nadir-pointing face on the spacecraft, on which the science payload can be mounted.
- The rotation around the nadir axis of the spacecraft may be determined by power or communications needs rather than for science purposes, so science payloads must not assume that they can determine this rotation.
- The notional lifetime of each Lightship mission should be 12 years; this implies careful consideration of components like Stirling coolers which may have shorter design lifetimes.

4.1 Thermal Infrared Mapper

4.1.1 Measurement objectives and design considerations

A Thermal Infrared (TIR) instrument would be able to provide accurate information about the thermal structure of the lower atmosphere, together with the spatial distribution of two of the main drivers of Martian weather and climate: dust and water ice. This has been demonstrated by a long series of instruments orbiting around Mars (e.g. MRO/MCS [McCleese et al. 2007], MGS/TES [Christensen et al. 1992]), Venus (VEx/VIRTIS [Drossart et al. 2007]) and Earth (MSG/SEVIRI [Pasternak et al. 1994], MTG/FCI [Ouaknine et al. 2013]). Such an instrument, able to measure both in nadir and limb at similar spatial resolutions, would greatly improve our knowledge and ability to monitor the atmosphere of Mars.

Importantly, while information about aerosols can be efficiently derived by observations in several spectral intervals (e.g. from the UV [Wolff et al. 2010] or the NIR [Smith, 2004, Clancy et al., 2019]), TIR observations are the only ones that enable monitoring in both daytime and nighttime, provided that sufficient thermal contrast is present especially between the surface and the atmospheric layers where aerosols are present.

In general, there are two approaches to selecting a TIR instrument. One can have high spectral resolution, at the expense of spatial resolution; an example of this is the Emirates Mars Mission (EMM) Emirates Mars InfraRed Spectrometer (EMIRS); this achieves high-resolution spectra, but

has low spatial resolution (>> 100 km) and a poor temporal spatial resolution (>1hr between observations). The second approach is to image Mars at a few wavelength bands, selected to maximise the information content of the observation. Wavelength selection is performed using multiple infrared passband filters, operating in either push-broom mode, where filters are placed across an imaging microbolometer array, detector and the FOV is scanned across the planet - so that each part of the surface is observed at all desired wavelengths in a short timescale - or with a filter wheel, so that all wavelengths are measured consecutively. This approach of using filters is adopted for the Lightship strawman payload, allowing higher spatial resolution and lower mass than a full spectrometer like EMIRS.

This approach has extensive heritage from geostationary platforms on Earth, on which IR instruments such as SEVIRI and FCI provide full-disk observations that allow comprehensive monitoring of weather systems, surface temperature and emissivity, and high-altitude water vapour. On Mars, TIR observations - even only at carefully selected wavelengths - can achieve the same results, ranging from monitoring atmospheric thermal emission at altitudes up to 50 km via CO_2 absorption bands (at 4.3 and/or 15 µm) in nadir [Conrath al. 2000] and limb [Kleinböhl et al. 2009], to deriving surface temperature and emissivity, obtaining column abundances of dust (9.3 µm extinction) and ices in nadir, and ideally the top altitude of atmospheric dust masses. Limb observations allow these properties, such as dust and temperature [Kleinböhl et al. 2009], to be measured for different layers of the atmosphere giving crucial vertical information in addition to nadir mapping. TIR mappers have a long in-flight heritage both on Mars orbiters, such as MCS (MRO), and other missions such as Diviner (LRO), TIRI (HERA), and MERTIS (BepiColombo).

The TIR imager should have the following characteristics: a wide effective Field of View (FOV) of ~45 degrees or more, to image the full disk and limb; a detector array with many pixels, to provide high spatial resolution; and some form of wavelength selector, to take images in multiple thermal infrared spectral ranges. The spatial resolution requirement is driven by the need to resolve thermal structure in limb observations, so should be significantly less than the scale height of the atmosphere (8-10 km depending on altitude). From the LightShip altitude of 5720 km, the atmospheric limb is about 8000 km away, so in order to provide two pixels per scale height this suggests a target pixel size of 0.5 mrad. The apparent angular size of Mars from the Lightship altitude is ~45 degrees, or 0.8 radians, so this suggests at least 1600 pixels across the planet although these do not all need to be obtained simultaneously. In nadir geometry, such an instrument would provide imagery at 3-4 km spatial resolution; with an observing cadence of < 30 minutes, such an instrument would offer unprecedented ability to resolve mesoscale circulation processes.

4.1.2 Instrument Description

The strawman instrument is based on use of two units of the Thermal Infrared channel of Comet Interceptor's Modular InfraRed Molecules and Ices Sensor (MIRMIS) instrument. This unit has a 2-D microbolometer array, with 15 spectral bandpass filters arranged in parallel stripes. Each unit includes an independent scan mirror which is used to sweep the field of view across the visible

scene (with 1 DoF); the scan mirror also allows views of space and of an onboard blackbody target, in order to provide a two-point radiometric calibration.

Heritage of the strawman instrument is from the Comet Interceptor/MIRMIS and Lunar Trailblazer/Lunar Thermal Mapper (LTM) multispectral imaging radiometers, which themselves find heritage in the MRO/Mars Climate Sounder and LRO/Diviner instruments. Necessary modifications would be:

- An increased field of view to at least 23° width, to cover the full disc of Mars with the two telescopes, with an overlap of at least 1°. The width of the Mars disc (including atmosphere to 100 km altitude) as viewed from the spacecraft is 45.5°.
- Upgrade the detector from the current Lynred Pico640 Gen2 640 x 480 pixel bolometer to a Lynred Atto Gen2 1280 x 1024 pixel detector, in order to double spatial sampling.
- Achieve mass reduction by using a single electronics unit to drive the two Thermal IR telescope / focal plane array units

4.1.3 Concept of Operations

The baseline instrument has two telescopes, with field of view oriented as in Figure 17 below. The direction of the scan mirror direction is oriented to allow scanning in the across-track direction.

Each image acquisition starts with the scan mirror looking at its blackbody target, it then acquires a space view and the FOV is then moved across the planet at a constant rate. This rotation has a nominal duration of 10 minutes, after which the FOV is returned to the blackbody target. Time delay integration (TDI) is performed during the scan, greatly increasing the sensitivity of the measurement.

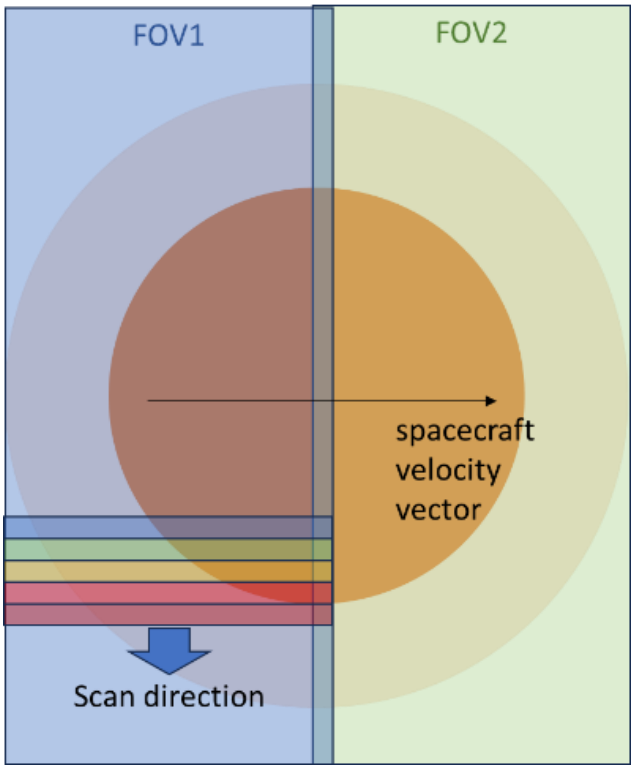

Figure 17: the baseline instrument has two telescopes, with their fields of regard (field visible with use of scan mechanism) as shown above. The central look direction of each instrument is therefore set to + 10° and 10° to the nadir direction. The direction of the scan mirror direction is oriented to allow scanning in the across-track direction.

Each scan returns a raw 2560 x 2560-superpixel image across 15 spectral channels at 2 bytes/pixel. Hence the scan returns an approximately 200MB raw image. Returning a lossless JPEG XL-encoded image provides an anticipated 8:1 compression ratio, yielding a 25MB image per scan. At 15-minute scan cadence, the instrument would produce approximately 2.4GB (19.2Gbit/sol) of data per day. Low-resource adaptive decimation schemes can be leveraged to further decrease data volumes in lieu of a JXL scheme and will be studied in Phase A. Decimation parameters will be fully telecommandable.

Calibration approach: the scan mirror also allows views of space and of an onboard blackbody target, in order to provide a two-point radiometric calibration. So, the scan mirror should allow view of space, i.e. a limb view with a tangent altitude at least 150 km above the planet.

Pointing requirements: Since the primary objective is full-disk atmospheric temperature measurements, but the total observable field-of-view includes the atmospheric limb, any errors in nadir pointing will result in a partial loss of the limb observations and not compromise the primary objective. The limb coverage is estimated at about 30-40 pixels, accounting for 70-90 km in tangent height. 1° error in nadir pointing will shift the field-of-view by 40 pixels, cutting off the limb from one side of Mars, but leaving the full disk in view. This should be the maximum expected nadir pointing error.

4.1.4 Interface and Physical Resources

Dimensions:

- Telescope 1 - 260 x 225 x 105 mm, 4.2 kg
- Telescope 2 - 260 x 225 x 105 mm, 4.2 kg
- Common electronics unit – included in size and mass constraints of telescope 1 and 2.
- Two telescopes: 8.4 kg with 20% margin = 10.08 kg

Power (at instrument level):

- 8.8 (4.4 x 2) W (average)
- 22 (11 x 2) W (peak)
    - 4.4 W average and 11 W peak are the measured values from the completed LTM instrument.

Thermal interface:

- Thermally coupled to spacecraft (radiator not required). Detectors do not require active cooling.

Data interface:

- Spacewire (TBC)

4.1.5 Environment, Cleanliness and Ground Operations

Currently assumed design temperatures /°C are listed in Table 4:

Table 4: design temperature of the instrument units.

Min. non-op	Min. op.	Max. op.	Max. non-op.
-40°C	-40°C	+60°C	+60°C

Other environmental considerations: instruments to be stored under nitrogen purge on ground.

4.2 Sub-mm Sounder

4.2.1 Measurement objectives and design considerations

The main measurement objectives for the sub-mm sounder are to measure the vertical and horizontal distribution of temperature, trace gas species, and direct measurement of line-of sight winds. A sub-mm sounder can characterise the structure, dynamics, composition (including isotopic) and chemistry of the Martian atmosphere from the near-surface up to altitudes of 100-130 km. One key advantage of a sub-mm instrument is that the long wavelengths of these observations can be carried out at all times of day, and are not affected by the dust or cloud in the Martian atmosphere.

The instrument would observe Mars in nadir and limb mode. Due to LightShip's high-altitude orbit of 5720 km (and ~8000 km distance to the limb), and due to likely spacecraft mass and volume constraints that allow only limited telescope diameters, combining observations in two sub-mm wave bands are preferred. A lower frequency band covering the range of ~ 500 to 650 GHz with better receiver noise temperature, and a higher band of ~ 1050 to 1280 GHz with reduced diffraction-limited beam size (by a factor of two) and a larger number of molecules for retrieval dynamic range optimization, is recommended. This is the case especially for limb observations. Simultaneous retrievals including these low- and high frequency bands will be able to achieve high horizontal and vertical wind resolutions, plus many molecules: the sub-mm wave range is rich in rotational transitions of molecules important for Martian atmospheric chemistry, e.g. H_2O, HO_2, H_2O_2, CO, O_2, O_3, HCl, KCl, NaCl, CH_4. Additionally, simultaneous observation of hydrogen isotopologues can be used to constrain atmospheric escape processes. Furthermore, radiometric observations in the two bands and potentially in two polarizations provide useful inputs for characterising regolith and surface / subsurface thermo-physical properties.

The sensitivity of wind measurements in the sub-mm range depends on the brightness temperature gradient and opacity of the observed line. For lower altitudes, the pressure broadening reduces the brightness temperature gradient and as a result the sensitivity of wind measurement is reduced. Figure 18 shows winds retrieved from CO limb spectra simulated for a 5720 km orbit.

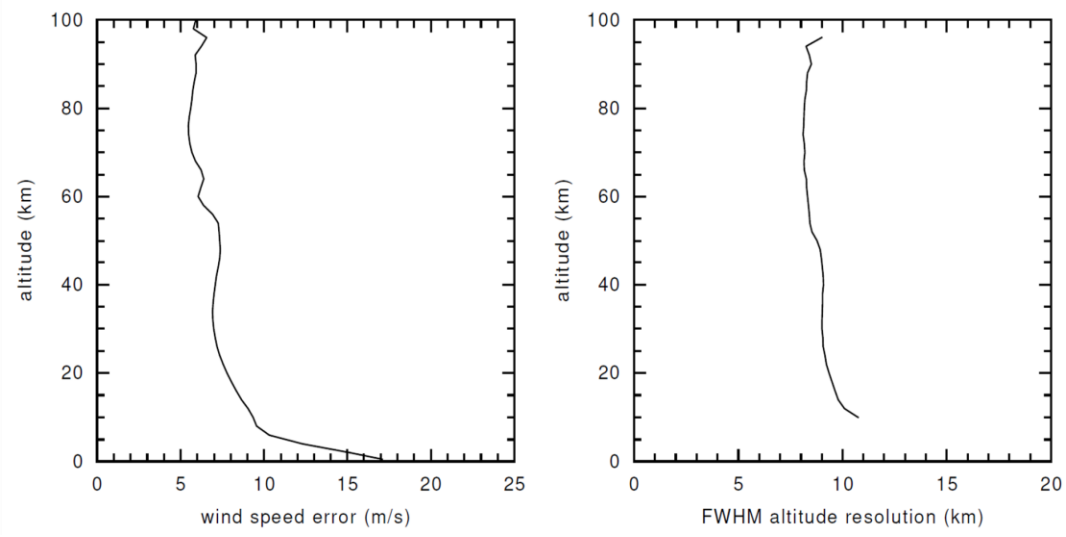

Figure 18: Estimate of the measurement uncertainty to which wind speed can be retrieved from CO limb spectra, simulated for a high altitude 5720 km orbit. Actual performance will depend on factors including detector efficiency and integration time.

For wind velocity measurement in particular, the passive Doppler measurements made by the sub-mm instrument give most sensitivity above 10 km altitude; they are therefore highly complementary to active Doppler measurements made by Doppler LIDAR, which therefore give the highest sensitivity in the 0 – 20 km altitude range. An aerosol LIDAR (MARLI) (Cremons et al., 2020) was proposed to detect wind speeds from the backscattered light of aerosols in the Martian atmosphere, showing high sensitivity in the lower 10-20 km altitudes with wind speed accuracies of 2 to 6 m/s. The combination of a LIDAR in low Mars orbit and the sub-mm wave instrument on the high-flying orbiter would provide high quality wind measurements from ground to more than 100 km altitude.

4.2.2 Strawman Instrument Description

The strawman sub-mm sounder is based on the Sub-mm Wave Instrument (SWI) developed for JUpiter ICy moons Explorer (JUICE), launched in April 2023. It consists of two passively cooled, tuneable heterodyne receivers covering the frequency ranges of 530 to 630 GHz and 1066 to 1275 GHz and two types of spectrometer backends per band: high resolution Chirp Transform Spectrometers (CTS with 1 GHz bandwidth and 100 kHz spectral resolution) and broadband Autocorrelation Spectrometers (ACS with 4 GHz bandwidth and 4 MHz spectral resolution). The receivers are locked against an ultrastable oscillator (USO) that is calibrated vs the ground station via the S/C USO/PPS (Pulse Per Seconds), required for wind measurements. The primary mirror of the telescope has a diameter of 29 cm and can be moved in azimuth (±72°) and elevation (±4.3°) by specially designed pointing mechanisms. The rocker element of this pointing mechanism would need to be adjusted to allow an increased ±22° of travel for the orbit of LightShip. The diffraction limited spatial resolution is about 1 mrad (1200 GHz channel) respectively 2 mrad (600 GHz channel). For limb scanning of the Martian atmosphere from 5720 km distance these parameters result in geometrical vertical resolutions of about 8 and 16 km, respectively. The resolution can be improved by taking advantage of the fact that the line shapes can be exactly measured. With the additional information of the pressure broadening the vertical resolution of the 600 GHz channel will be around 10 km.

Current TRL assessment: JUICE/SWI is TRL 9, but the following modifications are proposed:

- Modify rocker mechanism to allow an increased ±22° of travel (increase from the current ±4.3° of travel). This modification is so that the full disk of Mars would be in the field of regard without requiring spacecraft attitude changes.
- Reduce radiation shielding, due to lower radiation at Mars w.r.t. Jupiter.
- Possibly adjust the radiator / thermal arrangement depending on thermal accommodation.
- Possibly shorten the harness, depending on accommodation, to achieve mass saving.

4.2.3 Concept of Operations

The sub-mm instrument is capable of both limb and nadir observation. The limb observation mode allows measurement of Doppler line-of-sight wind velocity, and allows retrieval of temperature and trace gas abundances. The nadir view allows measurement of temperature and composition, although with reduced sensitivity compared to the limb viewing mode.

This instrument is non-imaging: its field of view is pointed at the desired scene of interest using the instrument's own 2-degree-of-freedom scanning capability; no attitude changes by the spacecraft are required.

- The following pattern of observations is repeated every hour:20x Vertical profiles at the limb (40 minutes duration).
- Each profile consists of 10x individual views, at tangent altitudes of 10, 20, 30, 40, 50, 60, 70, 80, 100, 120 km, each with an integration time of 10 seconds, followed by a space view (tangent altitude of 150 km).
- The 20x profiles are assumed to be evenly spaced around the visible limb of Mars.
- 10x10 grid of (off-)nadir observations across the visible disk of Mars (20 minutes duration).
- Each individual observation has an integration time of 10 seconds.
- A space view is performed after every set of 10 observations by rotating the scan mirror such that it views space (tangent altitude at least 150 km).

This pattern is illustrated in Figure 19.

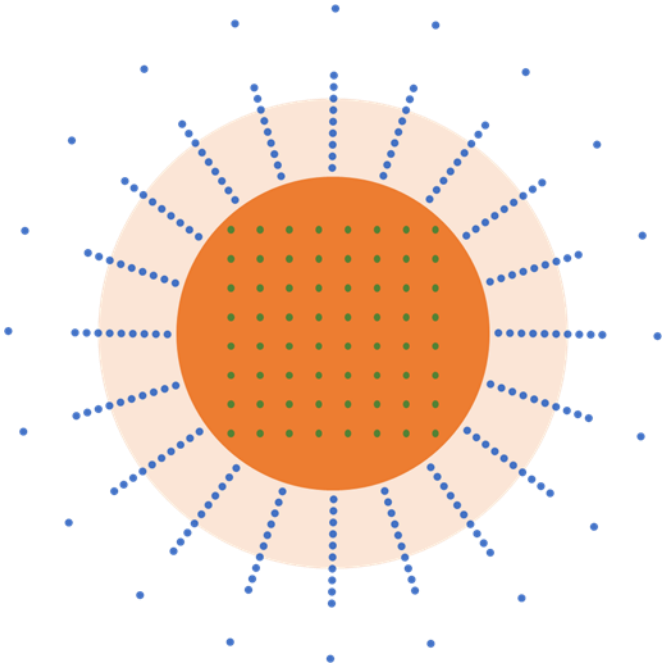

Figure 19. Notional sub-mm instrumentation scan pattern, as described in text. Dark and orange circles represent the disk of Mars and its atmosphere, respectively, as viewed from spacecraft (not to scale). Scan pattern consists of 20x profiles of 10 points, shown in blue, followed by a 10x10 grid of points on the disk of Mars (green points). Every 10 points are followed by a space view for calibration.

The orbit is near-equatorial, with an orbital inclination of only 20 degrees, and the sub-mm instrument will produce useful line-of-sight wind vector at the limb. Atmospheric limbs at the equator will only be viewed in a nearly E-W or W-E direction, so will enable measurement only of the zonal (E-W) component of wind vectors (we are neglecting here the vertical component of wind vectors). Similarly, high latitudes will always be observed in a N-S or S-N direction so here, only the meridional (N-S) component of wind vectors will be measured. In between, there is a broad latitude range in which the combination of SE-NW and SW-NE observing geometries, obtained within a few hours of each other, will enable both meridional and zonal components of the wind vector to be retrieved. This is illustrated in **Error! Reference source not found.**.

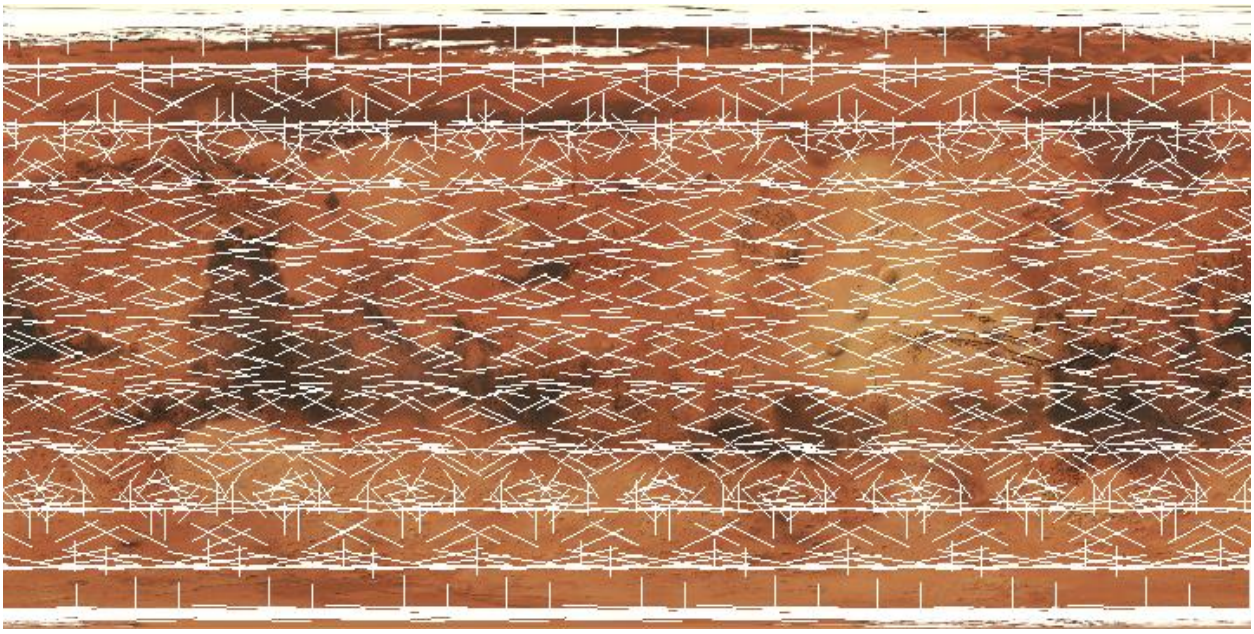

Figure 20: Map of Mars with white lines representing the direction of observed wind vectors in the limb after 10 orbits of LightShip. There is a broad range of latitudes in which both N-S and E-W components of winds can be determined.

4.2.4 Interface and Physical Resources

Dimensions (for each instrument unit):

- Telescope and Receiver Unit (TRU): 450 mm H x 390 mm W x 550 mm L.
- Electronics Unit (EU): 380 mm L x 185 mm W x 110 H.
- Distance between units on JUICE ~ 100 cm. Limit ~ 300 cm

Mass (for each instrument unit):

- Telescope and Receiver Unit (TRU): 7.265 kg
- Electronics Unit (EU): 7.046 kg

- Harness etc: 1.770 kg (for 100cm harness length as on JUICE; can be reduced for shorter harness)
- Radiator including Multi-Layer Insulation (MLI) and thermal strap: 1.221 kg

Power (at instrument level):

- 55 W average (60 W peak).
- 3 W standby power (USO, heaters, standby electronics). (Standby mode for JUICE is ~ 18 W. This is, because all power supplies and the Data Processing Unit (DPU) are on. Required is that the USO (1.5 W) and the DDLs (Dispersive Delay Lines) of the spectrometers (0.8 W) stay powered. In case they can be also controlled, powered by the spacecraft we are at 2.3 W.

Data interface protocol:

- Spacewire

Data: the full native datarate produced by the instrument is 320 kbits/sec (2 spectrometers * 10,000 channels per spectrometer * 16 bits). The baseline datarate of the instrument is 10 kbits/sec; this onboard reduction is obtained by fitting peaks, amplitudes & widths to each identified peak in the spectra. This can be further reduced through compression or windowing if needed.

Table 5: data rates of the instrument.

	Data rate	Duty cycle	Data per sol
Uncompressed	320 kbits/sec	100%	28.5 Gbit/sol
Nominal	10 kbits/sec	100%	900 Mbit/sol
Low rate	5 kbits/sec	100%	450 Mbit/sol

The heritage example SWI has no built-in memory storage.

4.2.5 Environment, Cleanliness and Ground Operations

Currently assumed design temperatures /°C are listed in Table 6.

Table 6: design temperature of the instrument units.

	Min. non-op.	Min. op	Max. op.	Max. non-op.
Telescope and Receiver Unit	-150°C	-50°C	+50°C	+100°C
Electronic Unit	-30°C	-20°C	+60°C	+60°C

Thermal interface:

Cooling is required for high frequency doublers (300/600 GHz) and mixers, in order to provide high Signal to Noise Ratio (SNR) and to preserve lifetime of components. Cooling to 140 K is desired, cooling to < 220 K required. On JUICE, SWI has a dedicated radiator (~ 40 cm x 40 cm). This requires a permanently cold face of the spacecraft. The cooling power needed is modest (<2 W), perhaps a radiator of at least 20 x 20 cm is needed (< 220 K), with compromises on SNR.

4.3 Multiband Imaging Suite

4.3.1 Measurement objectives and design considerations

The multiband imaging suite provides full-disk synoptic images including the limb using various filters in the visible and the near-middle ultraviolet, these images provide a big picture of the global atmosphere, useful as context and for the detailed investigation of aerosol morphology and dynamics. The various filters provide information on characteristics of aerosols that facilitates the interpretation of images and is complementary to that provided by other instruments in the strawman payload.

Full-disk and synoptic visible and ultraviolet images are acquired on Earth for example by Meteosat satellites and by the EPIC instrument on the DSCOVR mission. On Mars such images used to be uncommon, but are now routinely acquired by a few instruments: MEX/VMC, MEX/HRSC, MAVEN/IUVS, EMM/EXI, and MOM/MCC (no longer operating since 2022). The multiband imaging suite on Lightship would provide significantly improved spatial and temporal resolution, and a more continuous coverage that would enable tracking meteorological phenomena with unprecedented detail.

In addition to the standard RGB filters, spectral filters should be selected to provide information about dust and cloud abundances and properties. Previous analyses show that a UV filter at 220 nm is useful for retrieving dust (Connour et al., 2022); a filter at 320 nm is useful for retrieving water ice (e.g. Wolff et al., 2019; 2022); and an additional filter at 250nm could enable retrieving column abundances of ozone (Clancy et al., 2016). Further filters across the UV-VIS-NIR range should be selected to maximise the information content of the retrieval with regards to ice and dust properties. The inclusion of polarisation filters would increase the ability to discriminate aerosol properties, but detailed assessment of this was not carried out in the present study. The strawman payload has assumed that imagery will be acquired at six spectral (or polarising) filters.

Desirable spatial resolutions range from 1 to 5 km in nadir, this represents an improvement from current imagers and is enough to resolve meteorological phenomena in high detail. In addition to that, this would translate to a limb vertical resolution in the order of 2 to 7 km, enough conduct observations of the limb with a spatial resolution of less than one scale height. The angular extent of the full disk of Mars from Lightship (including its atmosphere up to 50 km altitude) will be approximately 45º, and so the field of view should be at least this large in order to allow observation of Mars and its atmospheric limb, with allowance for pointing uncertainty margin.

The acquisition of images showing the same areas from various angles would enable the estimation of aerosol altitudes, and the study of the Emission Phase Function to retrieve aerosol properties (e.g. Clancy, 2003), the most promising outcome of this would be the optical depth of dust, which would complement the retrievals with the 220 nm filter.

The nominal observation interval should be approximately 1 hour to provide continuous monitoring from the Lightship orbit. Some studies would benefit from a more continuous

coverage with observations every 10-15 minutes, to capture dynamics in high detail. Even higher temporal resolutions could be convenient for specific science cases (e.g. Hernández-Bernal et al., 2022 show cloud dynamics in timescales of 5 minutes). It would be necessary to apply binning schemes to reduce the effective resolution of images when the highest resolution is not necessary. The colour depth of acquired data should ideally be at least 11-14 bits to account for the large variations in the brightness of the disc of Mars, depending on the observation geometry. An onboard compression scheme would be required to reduce the data volume.

There are various possibilities for the architecture of this imaging suite, with one or various full-frame sensors (e.g. VIS and UV) and one or multiple telescopes. Filter wheels would be preferred over Bayer filters, because the latter impose gaps in the spatial coverage for each spectral band. While a pushbroom architecture could also work, it seems too complex for our purposes, given the low number of desired wavelengths and the interest of obtaining occasional observations with high-temporal resolution. The rotation of the spacecraft around its nadir axis may be changed for power or communications considerations rather than kept oriented as needed for pushbroom observations; this provides an additional reason to prefer a framing camera(s) over a pushbroom instrument. Other configurations may be possible as long as the full disk of Mars can be observed at different wavelength bands within minutes, fulfilling the temporal and spatial requirements.

Beyond pure atmospheric science, full-frame imagers can serve a different and novel kind of science. It would be possible to use full-frame imagers to monitor the disintegration of meteors and fireballs in the Martian atmosphere by observing the night side of Mars from orbit (Christou et al., 2012). This would provide constraints on the density of interplanetary dust in the orbit of Mars, which would also be convenient for the long-term safety of space missions. A proposal for a dedicated imaging system was described by Christou et al. (2012), and some experimental tests were performed using MEX/VMC (Hernández-Bernal et al., 2021). The monitoring of meteors would require the use of full-frame sensors with high sensitivity and prepared for high imaging rate. Onboard processing would be necessary to keep only valuable data actually showing meteors. And it would benefit from having at least two separate sensors, to rule out false positives (e.g. cosmic rays; Christou et al., 2012)

4.3.2 Instrument description

The strawman instrument selected here is a nadir-facing framing camera using a filter wheel for spectral selection. The instrument, based on JUICE/JANUS heritage, uses the Teledyne CIS 120 sensor with UV coating, allowing imaging from the UV (250 nm) to NIR (900 nm); spectral filters in this range will be chosen to optimise discrimination and characterisation of airborne dust and cloud.

The instrument will be mounted on the nadir-pointing face of the platform, and by continuously monitoring Mars from its 5720 km orbit, the 45° field of view will allow imaging of a considerable fraction of the Martian surface and atmosphere with every exposure. Given the Field of View

(FoV) and the orbit drift, global coverage of the Martian surface is achieved every 3 days without slewing the S/C. A blank plate in the filter wheel acts as a shutter to avoid detector damage in the case of sun ingress; imaging is not possible while sun is close to the field of view.

4.3.3 Operational Requirements

Potential rotation of LightShip around the yaw axis can be compensated by the operational concept, e.g. by timing of taking images. Images will be taken at a cadence synchronized with the orbit to achieve global coverage every 3 days. For each scene, images shall be taken using multiple spectral bands (for datarate calculations, 6 spectral bands were assumed). Timing of the images will compensate the S/C rotation around the yaw axis. Image compression will be implemented in the instrument.

Data will be produced at 7.3 Mbyte per image at 14 bit dynamic range. For high datarate mode, every 10 minutes images of the scene are acquired. This results in 148 times 6 images that will be taken per day. Assuming a compression factor of 5, this amounts to 10.4 Gbit/sol.

At times of low datarate this could be scaled back to 2 (reducing the number of images per scene to 3), and imaging cadence can be reduced to 30 minutes. Assuming a compression factor of 5, this amounts to 1.2 Gbit/sol.

Optical calibration at instrument level prior to delivery. Alignment measurements after integration. Blank plate in filter wheel allows dark fields to be obtained. Occasional star pointing (e.g. during cruise for geometric calibration).

Pointing requirements:

- 100 arcsec (control)
- 8 arcsec over 10 ms (stability)
- 10 arcsec (knowledge)

4.3.4 Interface and Physical Resources

Dimensions:

- 220 mm (L) x 200 mm (W) x 150 mm (H)

Mass:

- 3.00 kg (with 20% margin = 3.6 kg)

Power (at instrument level): 14.6 W (average) and 22.3 W (peak)

Thermal interface: no active cooling required.

Data interface protocol: Spacewire (TBC).

4.3.5 Environment, Cleanliness and Ground Operations

Currently-assumed design temperatures /°C are listed in Table 7.

Table 7: design temperature of the instrument units.

Min. non-op	Min. op.	Max. op.	Max. non-op.
-55°C	-40°C	+55°C	+85°C

No EMC requirements. The imaging sensor is radiation hardened by design.

4.4. Near Infrared Spectral Imager

4.4.1 Measurement Objectives and design considerations

As has been outlined above, key measurement priorities for this mission include dust, ice clouds, and water vapour. These measurements are already addressed by the Thermal Infrared instrument, and – in the case of dust and cloud – by the multiband imaging suite.

However, in order to increase the robustness of these measurements, the strawman payload also includes a near-infrared imaging spectrometer. The goal of this instrument is to add information to the meteorological retrievals, in particular by resolving spectral bands of water and carbon dioxide. Speaking first of the nadir (and off-nadir) measurements, this serves several purposes. Firstly, it increases the robustness of the water vapour column abundance retrieval, compared to using thermal IR alone; for example, the thermal IR retrievals are not possible when there is little vertical gradient of temperature. Secondly, it gives information on vertical partitioning of water vapour when combined with thermal IR retrievals, due to the different vertical sensitivity of these two techniques (Montmessin et al. 2022, Knutsen et al., 2022). Thirdly, the carbon dioxide band depth can be used as an indicator of dust vertical distribution, as it gives a measure of the $\tau = 1$ level. When the dust loading is low ($\tau << 1$), the carbon dioxide band depth gives an indication of column-integrated carbon dioxide abundance and thus would allow to map surface pressure.

Such surface pressure measurement from orbit was demonstrated by Forget et al. (2007) using MEX/OMEGA data, and by Toigo et al. (2013) using MRO/CRISM data. These studies showed that surface pressure could be retrieved using existing instruments orbiting Mars, and that particular attention to temperature and dust effects was needed in order to achieve a meteorologically-

useful precision level of surface pressure determination. More recent work by Kazama et al. (2023), in preparation for the MMX/MIRS mission, suggests that surface pressure can be mapped to a precision of <20 Pa (using the 2 µm CO_2 line). Assessment of how this performance could be optimised in a future instrument, perhaps by measuring several spectral bands at once with higher spectral resolution, was beyond the scope of the present study but is a potential goal for the NIRSI strawman payload instrument. Direct assimilation of CO_2 band depth into a data assimilation scheme could provide valuable constraints on surface pressure, particular when dust abundances from limb measurements are also being assimilated.

As with the Thermal Infrared and Multiband Imager instruments, NIRSI observations can also be carried out in limb geometry. For this to be useful, the limb measurements should have a spatial resolution of significantly less than a scale height: given that a scale height at Mars is on the order of 8 km (altitude dependent), this leads to a spatial resolution requirement of < 8 km at the limb, or preferably <4 km for robust measurement.

There are many ways in which a hyperspectral imager can achieve the above measurement goals. The strawman instrument is a full-frame imager, viewing Mars through a Fabry-Perot Interferometer used as the frequency selective technique; this allows full-frame imaging, and makes the technique insensitive to rotation around the viewing direction (as would be the case, for example, for pushbroom imaging).

This technique has been demonstrated in-flight by instruments such as the ASPECT imager for the MILANI CubeSat for ESA's HERA mission, and the MIRMIS instrument on Comet Interceptor. The strawman instrument includes two imagers with different spectral ranges; 1330-1470 nm for covering the 1370 nm water and the 1430 nm CO_2 bands; and potentially 1960-2100 nm for covering the 2060 nm CO_2 band. The 2060 nm CO_2 band is a stronger band so is likely to be needed for surface pressure retrieval. It is estimated that a spectral resolution of 1 nm would be desirable to meet the measurement goals, but a trade-off of performance vs spectral resolution was beyond the scope of the present study.

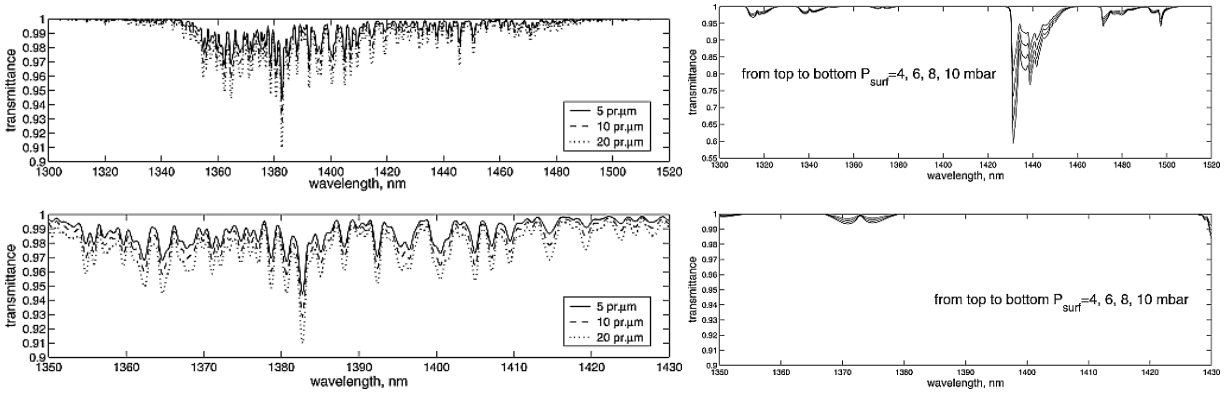

Figure 21: calculated absorption spectra of (left panels) H_2O and (right panels) CO_2 at 1300-1500 nm wavelengths. Such modelling informs the calculation of spectral and radiometric resolution requirements for the NIRSI instrument. Figures are from Fedorova et al 2006.

4.4.2 Instrument Description

The imager operation is based on a tuneable Fabry-Perot Interferometer, which is used as an adjustable bandpass filter. The filter is combined with an InGaAs Focal Plane Assembly (FPA).

Heritage: the design is based on refractive optics, based on design utilized in the ASPECT imager developed by VTT for the MILANI CubeSat for ESA's HERA mission. It has been selected as part of the MIRMIS module for Comet Interceptor.[3] The prototype has been flying in low Earth orbit since November 2018 on-board the Reaktor Hello World nanosatellite. The NIR module is a spectral imager capable of taking 2D images at freely selectable wavelengths at 0.9 – 1.7 µm region using an InGaAs detector. For the 2µm channel, qualification of an 'extended range' InGaAs sensor may be needed, in order to avoid the active cooling typically needed by HgCdTe detectors.

The spectral datacube is formed by taking a sequence of multiple images at different wavelengths. The Field of View of the heritage instrument is 6.7 x 5.4 degrees with 640 x 512 pixels, but it is anticipated that the Field of View (and pixel density) can be adjusted in future versions with minimal impact. If the required Field of View cannot be obtained by redesign of the optics, alternatively a scan mirror can be implemented that allow the instrument to cover the full Martian disk.

4.4.3 Operational Requirements

Images will be taken at a cadence synchronized with the orbit to achieve global coverage every 3 days. Timing of the images will compensate the S/C rotation around the yaw axis. Image compression will be implemented at instrument level.

4.4.4 Interface and Physical Resources

Dimensions (for each instrument unit):

- 262 mm x 282 mm x 127 mm

Mass (for each instrument unit):

- 3.0 kg

Power (at instrument level):

- 6.6 W (average)

[3] https://www.cosmos.esa.int/documents/3760686/3760706/Comet+Interceptor+Red+Book.pdf/dfa9634f-b15b-e918-17b5-5a8523149ea7?t=1664524062069

Thermal interface: no active cooling is needed.

Data interface protocol: Spacewire (TBC)

Data, processing algorithm assumed to be present at instrument level (TBC).

Data to platform: 10 Gbit/sol (average)

Data to ground: 5 Gbit/sol (average)

The values provided here are the average data to platform and data to ground. Initially, the amount of data that requires to be downlinked is higher. After optimization of the measurement scheme it is assumed that this will reduce to the values provided here.

4.4.5 Environment, Cleanliness and Ground Operations

Currently assumed design temperatures /°C are listed in Table 8.

Table 8: design temperature of the instrument units.

Min. non-op	Min. op.	Max. op.	Max. non-op.
-40°C	-30°C	+50°C	+60°C

No EMC requirements.

4.5 Radio occultation

Radio occultation is an important part of the LightShip measurement capabilities, and is highly complementary to the other strawman payload instruments.

However, the IDT was not instructed to define a strawman radio occultation investigation because the hardware configuration of the radios will be determined primarily by communications and navigation needs.

In the present document, a brief description of the envisaged radio occultation is given, without detailed strawman investigation specifications.

4.5.1 Measurement Objectives

Radio occultation is a well established technique which provides, with a vertical resolution often better than 1 km, vertical profiles of **density, pressure and temperature** in the neutral atmosphere, and **ionospheric electron densities** in the ionosphere. For LightShip's focus on the lower atmosphere, the neutral atmospheric profiles will be highly complementary to those returned by other the thermal IR and sub-mm sounder instruments.

4.5.2 Investigation design

Radio occultation (RO) can be carried out both in spacecraft-to-Earth and spacecraft-to-spacecraft modes.

Frequency bands below one 1 GHz, such as the UHF 400 MHz used by Electra & MELACOM radios for surface data relay, are relatively more sensitive to electron content in the ionosphere. Frequency bands above 1 GHz (e.g. S- X- and Ka- bands) are relatively more sensitive to the neutral atmosphere. Simultaneous radio occultation in more than one frequency band leads to more robust retrievals because it helps to eliminate some sources of error such as interplanetary plasma oscillations; also it may enable measurement of more variables (for example, robust separation of neutral atmosphere + ionosphere signals).

Radio occultation usually requires that the transmitting and receiving stations are both equipped with **ultra-stable oscillators (USOs)** as frequency references. If one spacecraft does not have an USO, then radio occultation can be performed in two-way mode, but this has disadvantages including complexity and should be adopted as the baseline for LightShip.

Configurations

- **Lightship-to-Earth RO**. This will be carried out using the main Lightship-to-Earth communications radio. The main link is expected to be in Ka-band; simultaneous transmission in X-band (referenced to the same onboard oscillator on LightShip) would be advantageous for robust error reduction. The number of occultations exploitable will be up to 3 ingress & 3 egress occultations per day, per LightShip, because of LightShip's ~8hr orbital period.

LightShip-to-LMO (or LMO-to-LightShip) RO. LMO means a Low Mars Orbiter such as SpotLight or other subsequent users of the Marconi communications & navigations service. This radio occultation could be carried out using either the data relay radio (in which case it would likely be an LMO-to-LightShip transmission); or using a navigation radio (in which case it would likely be a LightShip-to-LMO transmission; or a dedicated radio system. It would be advantageous to perform the occultation in multiple frequency bands, including UHF (for sensitivity to ionosphere) and S-band (sensitivity to neutral atmosphere). This potentially leads to the largest number of occultations, increasing rapidly as the number of LightShips and LMOs increase.

LightShip-to-LightShip RO. The number of occultations between LightShips is expected to be very small, as they are spaced out in similar near-equatorial orbits, so this is not considered to be a significant part of the investigation.

4.4.3 Operational Requirements

LightShip-to-Earth RO takes advantage of the LightShip-to-Earth communications passes which will take place routinely.

LightShip-to-orbiter RO requires that the radio antennas used for this RO be pointed at each other, as would be the case if they are in use for data relay or navigation.

Data volume required to support this would depend on whether various parameters which were beyond the remit of the IDT's discussions.

4.4.4 Interface and Physical Resources

It is assumed that Radio Occultation will be performed using radio systems which are already onboard the LightShips. The only requirement imposed by the Radio Occultation is an Ultra-Stable Oscillator frequency stability requirement (typically this would be expressed as Allen deviation < 10^{-13} over averaging times of 1-100 seconds) – but this was not among the topics discussed as part of the present study.

4.6 Coverage of Science Observations

In this section we analyse the aspects of the orbit of LightShip that are relevant for the coverage of science observations and the design of instruments and operational strategies.

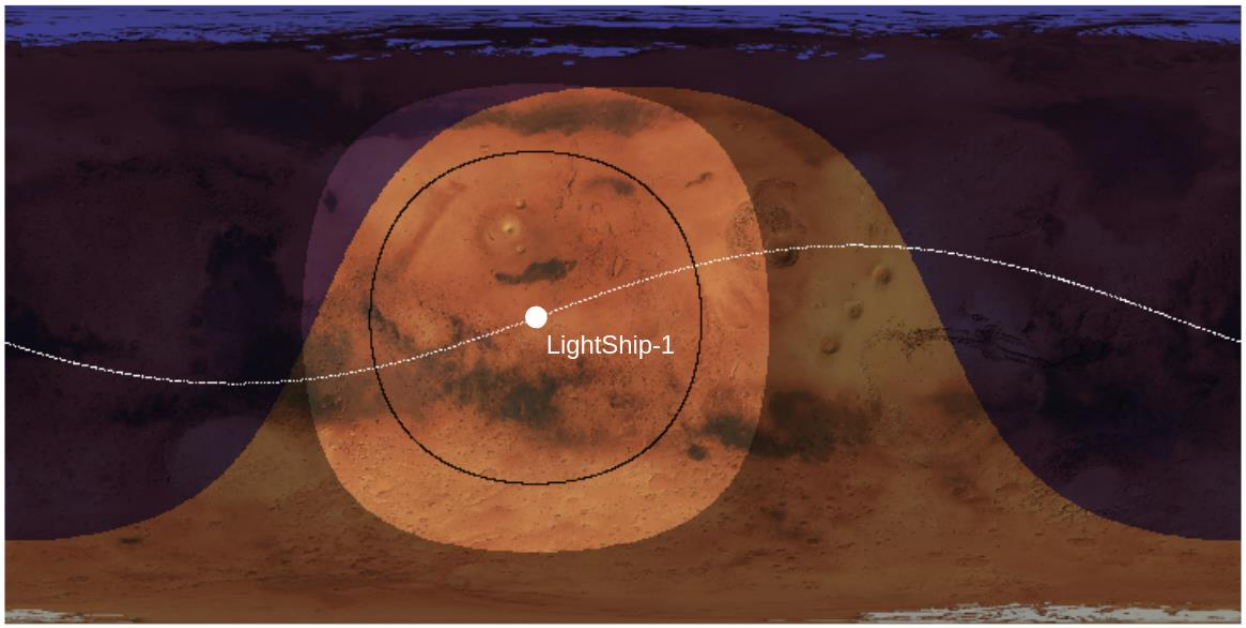

Figure 22: Map of Mars showing the night (dark blue), observed part of the disc (light shaded), area observed at emission angle <70º (black curve), and the orbital trajectory (white curve).

LightShip will orbit Mars in a circular orbit at an altitude of 5720 km over the surface, in an orbital plane tilted 20º with respect to the equator (Figure 22). These and other derived relevant parameters are given in Table 9. This orbit is quite favourable for the acquisition of a quasi-global coverage, and all local times and longitudes can be equally covered for low latitudes (see details below). The orbit is very close to a resonance of 3:10 with the mean solar day of Mars with a shift of around half an hour, meaning that every 3 Martian sols, LightShip covers almost exactly 10 orbits and almost the same local times and longitudes are revisited, with a slow evolution over time. This kind of resonance has been demonstrated useful in the case of Mars Express (whose orbit is in an equivalent resonance 2:7), because it is useful to observe sol-to-sol variability.

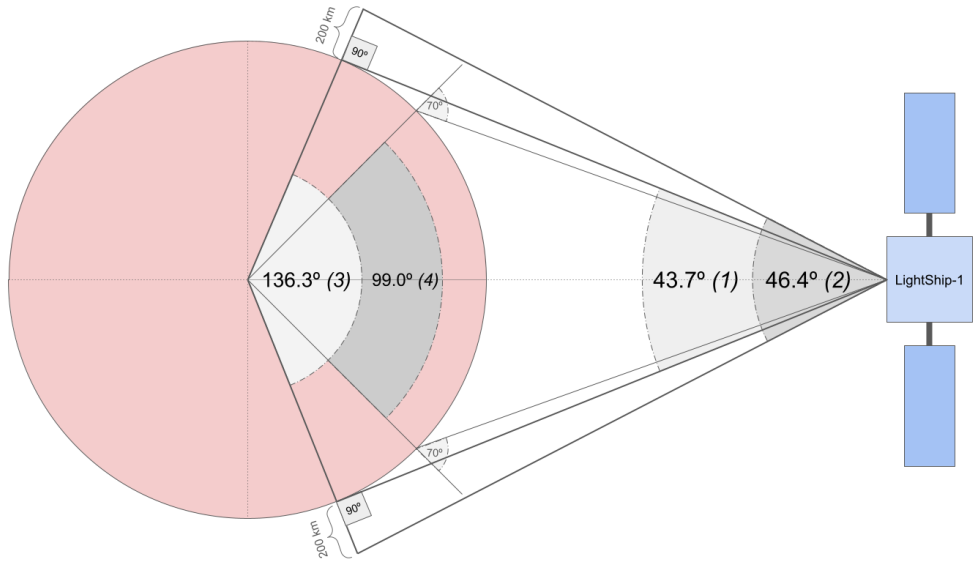

Figure 23: Scheme showing geometric parameters from table 8. Three LightShips equally spaced around Mars's equator would be able to see all longitudes at Mars' equator, although the emission angles at some points would be very high. A constellation of four equally spaced Lightships would be able to view all low-latitude longitudes with an emission angle below 70 degrees.

Table 9: Orbital parameters and derived quantities.

Orbital parameters	
Altitude (above mean surface elevation)	5720 km
Inclination of the orbital plane	20º
Period	7.34 h
Rate of nodal regression	-0.46º / Martian mean solar day
Geometric parameters *(See scheme in figure 7)*	
(1) Size of disc as seen from LightShip (limb)	43.7º
(2) Size of disc as seen from LightShip (limb+200 km)	46.4º
(3) Angular diameter of observed disc as measured from planet centre (limb to limb)	136.3º
(4) Angular diameter of observed disc as measured from planet centre (emission angle <70º)	99.0º

Observable latitudes *(Computed from geometric parameters 3 and 4 above and inclination of the orbital plane)*	
Maximum observed latitude (limb)	88.2º N/S
Maximum observed latitude (emission angle <70º)	69.5º N/S
Maximum latitude observed at all Local Times	48.2º N/S
Maximum latitude observed at all Local Times (Emission angle <70º)	29.5º N/S
Continuous and frequent monitoring	
Resonance with Mean Solar Day	~3:10
Time of permanence of a given point in the surface in the observed disc of the planet	~2h.

The coverage of latitude is not global, nor homogeneous with respect to Local Time. The maximum reachable latitude is 88° N/S but considering only reasonably low emission angles (below 70º), that maximum reachable latitude goes down to ~70° N/S for observations of the disc of the planet. Given the inclination of 20° of the orbital plane, the high latitudes are not always covered for all local times, but instead the local times that can be covered at those latitudes depend on the orientation of the orbital plane relative to the direction of the sun, which evolves due to orbital precession and translation of Mars around the Sun. As a result, the orbit imposes a Latitude - Local Time bias that evolves over time for latitudes over 50° N/S (30° N/S when excluding high emission angles. For lower latitudes, all local times are always equally covered. Right panel in figure 8 shows an example of this bias for a given moment, the pattern shown in this figure moves horizontally over time at an average rate of around 1h of local time every 8° of Ls, leading to a Latitude – Local Time - Solar Longitude bias that can compensate over the course of a few Martian Years.

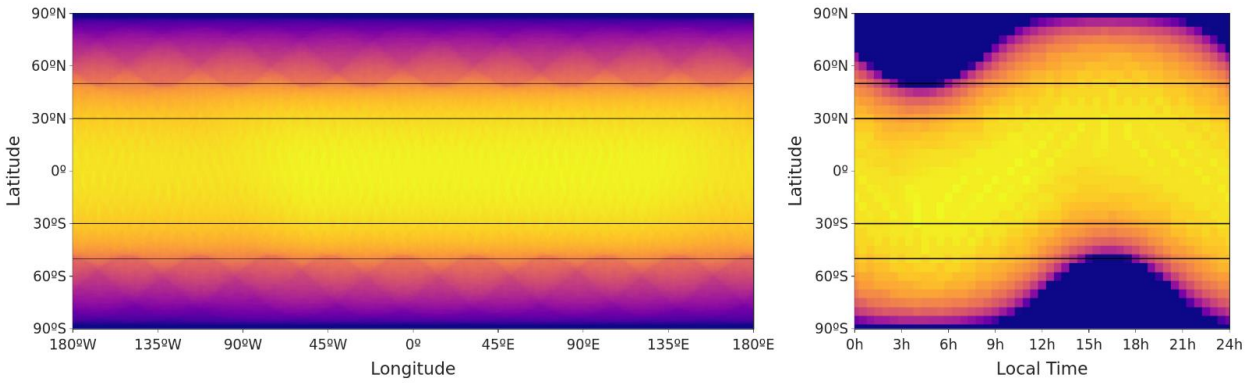

Figure 24: Coverage of Mars from LightShip after 10 orbits (3 sols). (Left) Coverage in Latitude-Longitude, which is basically uniform in Longitude. Horizontal lines indicate latitudes 30º and 50º N/S, which are at the limit where all local times are equally

sampled for low and high emission angles (see text). (Right) Coverage in Latitude-Local Time, the pattern shown in this figure moves horizontally over time at an average rate of around 1h every 8º of Solar Longitude (see text)

Instruments on LightShip observe in two main geometries: full-disc, and limb. In both cases, the biases just described are applicable.

Another relevant aspect of the orbit is how long a certain point of the planet can be monitored continuously, which is relevant for studies of the diurnal evolution of the atmosphere within a single sol and dynamics in general. Given the translation of the spacecraft and the rotation of the planet, a given point in the surface in low latitudes will be observable on average for around 2h[4]. This period of time reduces if we exclude geometries with high emission angles, and is limited by illumination around twilight hours.

4.7 Summary of the Strawman Payload

The LightShip payload overview block diagram is shown in Figure 25. Each of the payload requires an unobscured view of the full Martian disk including limb. Some payloads require views of deep space for calibration purposes. In Table 10 a summary of key resources for the strawman payload instruments is provided.

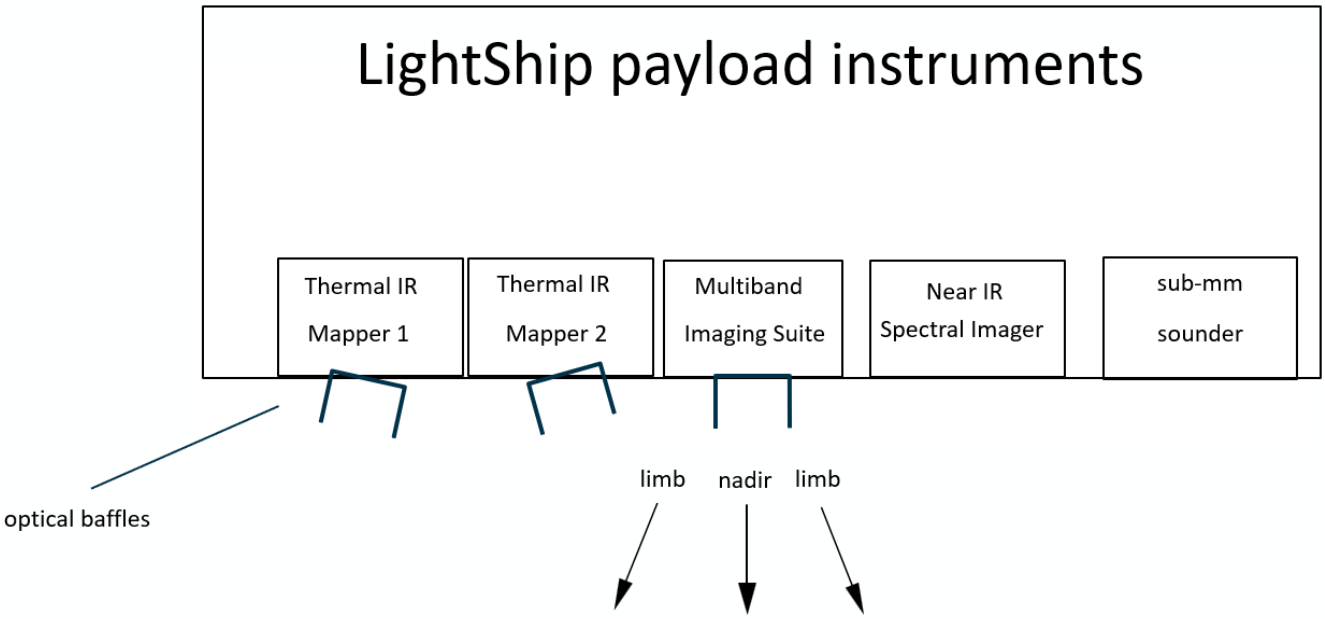

Figure 25: LightShip Payload Overview Block Diagram

[4] The angular velocity of the spacecraft is 49.0º/h (orbital period of 7.34h). The angular velocity of the rotation of Mars is 14.6º/h. And the area of the planet covered from the spacecraft is ~134º as measured from the center of the planet. 134º/(49.0º/h+14.6ºh)=2.1h.

Table 10: summary table of key resources for payload instruments.

Instrument	Mass incl. MMM /kg	Power before DMM /W	Dimensions /mm^3	Data to PDHU	Assumed data to downlink
Sub-mm Sounder (submm)	**18.7**	**55 W(average) 60 W (peak) 3 W (standby)**	**450x390x550 (TRU[5]) 380x185x110 (elec.)**	**3.15 Gbit/sol**	**900 Mbit/sol**
Thermal IR Mapper (TIR)	**10.08**	**8.8 W(average) 22 W (peak)**	**260x225x105 (telescope 1) 260x225x105 (telescope 2)**	**85.36 Gbit/sol**	**10.67 Gbit/sol**
Multiband Imaging Suite (Imager)	**3.6**	**14.6 W (average) 22.3 W (peak)**	**220x200x150**	**6.0 Gbit/sol (Low Datarate) 52 Gbit/sol (high Datarate)**	**1.2 Gbit/sol (Low datarate) 10.4 Gbit/sol (high Datarate)**
Near-IR Spectral Imager (NIR)	**3.6**	**6.6 W (average)**	**262x282x127**	**10 (TBC) Gbit/sol (average)**	**5 (TBC) Gbit/sol (average)**
Total	**35.98**	**85 W (average) 110.9 W (peak)**			

[5] **TRU: Telescope and Receiver Unit**

5. Conclusion

The Lightship IDT was convened in 2024 to assess the best scientific use for a small atmospheric science payload on the high-altitude LightShip platform currently being studied by ESA. It has defined a strawman payload of four scientific instruments which illustrate that a compelling set of measurements can be addressed within the boundary conditions of the mission.

The IDT is convinced that a scientifically exciting and technically viable mission can be conducted based on the LightShip concept. A focus on atmospheric monitoring would be entirely consistent with the vision spelled out in ESA's Terrae Novae and Explore 2040 strategic documents. The atmospheric measurements from LightShip as outlined in this document would be transformational for Mars atmospheric science because of their large coverage, simultaneous observation of multiple key meteorological variables using different spectral bands, and, for the first time, direct orbital measurements of wind speeds throughout the atmosphere. The first LightShip will already represent a great step forward in our atmospheric understanding, but also represents an important step towards a future in which multiple LightShips, working with observations from other orbiters and landers, would enable a level of scientific understanding and operational capability that until now has only been possible for Earth.

We invite ESA, the Member States, and the Associate Members, to consider how transformative the LightShip and Spotlight concept will be for the future exploration of Mars and European leadership.

References

Almatroushi, H., AlMazmi, H., AlMheiri, N., AlShamsi, M., AlTunaiji, E., Badri, K., Lillis, R.J., Lootah, F., Yousuf, M., Amiri, S., Brain, D.A., Chaffin, M., Deighan, J., Edwards, C.S., Forget, F., Smith, M.D., Wolff, M.J., Christensen, P.R., England, S., Fillingim, M., Holsclaw, G.M., Jain, S., Jones, A.R., Osterloo, M., Jakosky, B.M., Luhmann, J.G., Young, R.M.B., 2021. Emirates Mars Mission Characterization of Mars Atmosphere Dynamics and Processes. Space Sci. Rev. 217, 89. https://doi.org/10.1007/s11214-021-00851-6

Aoki, S., Vandaele, A.C., Daerden, F., Villanueva, G.L., Liuzzi, G., Clancy, R.T., Lopez-Valverde, M.A., Brines, A., Thomas, I.R., Trompet, L., Erwin, J.T., Neary, L., Robert, S., Piccialli, A., Holmes, J.A., Patel, M.R., Yoshida, N., Whiteway, J., Smith, M.D., Ristic, B., Bellucci, G., Lopez-Moreno, J.J., Fedorova, A.A., 2022. Global Vertical Distribution of Water Vapor on Mars: Results From 3.5 Years of ExoMars-TGO/NOMAD Science Operations. Journal of Geophysical Research: Planets 127, e2022JE007231. https://doi.org/10.1029/2022JE007231

Aoki, S., Vandaele, A.C., Daerden, F., Villanueva, G.L., Liuzzi, G., Thomas, I.R., Erwin, J.T., Trompet, L., Robert, S., Neary, L., Viscardy, S., Clancy, R.T., Smith, M.D., Lopez-Valverde, M.A., Hill, B., Ristic, B., Patel, M.R., Bellucci, G., Lopez-Moreno, J.-J., 2019. Water Vapor Vertical Profiles on Mars in Dust Storms Observed by TGO/NOMAD. Journal of Geophysical Research: Planets 124, 3482–3497. https://doi.org/10.1029/2019JE006109

Atwood, S.A., Smith, M.D., Badri, K., Edwards, C.S., Christensen, P.R., Wolff, M.J., Forget, F., Anwar, S., Smith, N., El-Maarry, M.R., 2022. Diurnal Variability in EMIRS Daytime Observations of Water Ice Clouds During Mars Aphelion-Season. Geophys. Res. Lett. 49, e2022GL099654. https://doi.org/10.1029/2022GL099654

Ball, E.R., Mitchell, D.M., Seviour, W.J.M., Thomson, S.I., Vallis, G.K., 2021. The Roles of Latent Heating and Dust in the Structure and Variability of the Northern Martian Polar Vortex. Planet. Sci. J. 2, 203. https://doi.org/10.3847/PSJ/ac1ba2

Battalio, J.M., Lora, J.M., 2021. Annular modes of variability in the atmospheres of Mars and Titan. Nat Astron 5, 1139–1147. https://doi.org/10.1038/s41550-021-01447-4

Brown, M. a. J., Patel, M.R., Lewis, S.R., Holmes, J.A., Sellers, G.J., Streeter, P.M., Bennaceur, A., Liuzzi, G., Villanueva, G.L., Vandaele, A.C., 2022. Impacts of Heterogeneous Chemistry on Vertical Profiles of Martian Ozone. Journal of Geophysical Research: Planets 127, e2022JE007346. https://doi.org/10.1029/2022JE007346

Cantor, B.A., James, P.B., Caplinger, M., Wolff, M.J., 2001. Martian dust storms: 1999 Mars Orbiter Camera observations. Journal of Geophysical Research: Planets 106, 23653–23687. https://doi.org/10.1029/2000JE001310

Chaffin, M.S., Kass, D.M., Aoki, S., Fedorova, A.A., Deighan, J., Connour, K., Heavens, N.G., Kleinböhl, A., Jain, S.K., Chaufray, J.-Y., Mayyasi, M., Clarke, J.T., Stewart, A.I.F., Evans, J.S., Stevens, M.H., McClintock, W.E., Crismani, M.M.J., Holsclaw, G.M., Lefevre, F., Lo, D.Y., Montmessin, F., Schneider, N.M., Jakosky, B., Villanueva, G., Liuzzi, G., Daerden, F., Thomas, I.R., Lopez-Moreno, J.-J., Patel, M.R., Bellucci, G., Ristic, B., Erwin, J.T., Vandaele, A.C., Trokhimovskiy, A., Korablev, O.I., 2021. Martian water loss to space enhanced by regional dust storms. Nat Astron 5, 1036–1042. https://doi.org/10.1038/s41550-021-01425-w

Christensen, P.R., Anderson, D.L., Chase, S.C., Clark, R.N., Kieffer, H.H., Malin, M.C., Pearl, J.C., Carpenter, J., Bandiera, N., Brown, F.G., Silverman, S., 1992. Thermal emission spectrometer experiment: Mars Observer mission. Journal of Geophysical Research: Planets 97, 7719–7734. https://doi.org/10.1029/92JE00453

Christou, A.A., Oberst, J., Elgner, S., Flohrer, J., Margonis, A., McAuliffe, J.P., Koschny, D., 2012. Orbital observations of meteors in the Martian atmosphere using the SPOSH camera. Planetary and Space Science 60, 229–235. https://doi.org/10.1016/j.pss.2011.09.002

Clancy, R.T., 2003. Mars aerosol studies with the MGS TES emission phase function observations: Optical depths, particle sizes, and ice cloud types versus latitude and solar longitude. Journal of Geophysical Research 108. https://doi.org/10.1029/2003JE002058

Clancy, R.T., Wolff, M.J., Lefèvre, F., Cantor, B.A., Malin, M.C., Smith, M.D., 2016. Daily global mapping of Mars ozone column abundances with MARCI UV band imaging. Icarus 266, 112–133. https://doi.org/10.1016/j.icarus.2015.11.016

Clancy, R.T., Wolff, M.J., Smith, M.D., Kleinböhl, A., Cantor, B.A., Murchie, S.L., Toigo, A.D., Seelos, K., Lefèvre, F., Montmessin, F., Daerden, F., Sandor, B.J., 2019. The distribution, composition, and particle properties of Mars mesospheric aerosols: An analysis of CRISM visible/near-IR limb spectra with context from near-coincident MCS and MARCI observations. Icarus 328, 246–273. https://doi.org/10.1016/j.icarus.2019.03.025

Connour, K., Wolff, M.J., Schneider, N.M., Deighan, J., Lefèvre, F., Jain, S.K., 2022. Another one derives the dust: Ultraviolet dust aerosol properties retrieved from MAVEN/IUVS data. Icarus 387, 115177. https://doi.org/10.1016/j.icarus.2022.115177

Conrath, B.J., Pearl, J.C., Smith, M.D., Maguire, W.C., Christensen, P.R., Dason, S., Kaelberer, M.S., 2000. Mars Global Surveyor Thermal Emission Spectrometer (TES) observations: Atmospheric temperatures during aerobraking and science phasing. Journal of Geophysical Research: Planets 105, 9509–9519. https://doi.org/10.1029/1999JE001095

Cremons, D.R., Abshire, J.B., Sun, X., Allan, G., Riris, H., Smith, M.D., Guzewich, S., Yu, A., Hovis, F., 2020. Design of a direct-detection wind and aerosol lidar for mars orbit. CEAS Space J 12, 149–162. https://doi.org/10.1007/s12567-020-00301-z

Crismani, M.M.J., Villanueva, G.L., Liuzzi, G., Smith, M.D., Knutsen, E.W., Daerden, F., Neary, L., Mumma, M.J., Aoki, S., Trompet, L., Thomas, I.R., Ristic, B., Bellucci, G., Piccialli, A., Robert, S., Mahieux, A., Lopez Moreno, J.-J., Sindoni, G., Giuranna, M., Patel, M.R., Vandaele, A.C., 2021. A Global and Seasonal Perspective of Martian Water Vapor From ExoMars/NOMAD. Journal of Geophysical Research: Planets 126, e2021JE006878. https://doi.org/10.1029/2021JE006878

Daerden, F., Neary, L., Wolff, M.J., Clancy, R.T., Lefèvre, F., Whiteway, J.A., Viscardy, S., Piccialli, A., Willame, Y., Depiesse, C., Aoki, S., Thomas, I.R., Ristic, B., Erwin, J., Gérard, J.-C., Sandor, B.J., Khayat, A., Smith, M.D., Mason, J.P., Patel, M.R., Villanueva, G.L., Liuzzi, G., Bellucci, G., Lopez-Moreno, J.-J., Vandaele, A.C., 2022. Planet-Wide Ozone Destruction in the Middle Atmosphere on Mars During Global Dust Storm. Geophysical Research Letters 49, e2022GL098821. https://doi.org/10.1029/2022GL098821

Demortier, A., Mandement, M., Pourret, V., Caumont, O., 2024. Assimilation of surface pressure observations from personal weather stations in AROME-France. Natural Hazards and Earth System Sciences 24, 907–927. https://doi.org/10.5194/nhess-24-907-2024

Drossart, P., Piccioni, G., Adriani, A., Angrilli, F., Arnold, G., Baines, K.H., Bellucci, G., Benkhoff, J., Bézard, B., Bibring, J.-P., Blanco, A., Blecka, M.I., Carlson, R.W., Coradini, A., Di Lellis, A., Encrenaz, T., Erard, S., Fonti, S., Formisano, V., Fouchet, T., Garcia, R., Haus, R., Helbert, J., Ignatiev, N.I., Irwin, P.G.J., Langevin, Y., Lebonnois, S., Lopez-Valverde, M.A., Luz, D., Marinangeli, L., Orofino, V., Rodin, A.V., Roos-Serote, M.C., Saggin, B., Sanchez-Lavega, A., Stam, D.M., Taylor, F.W., Titov, D., Visconti, G., Zambelli, M., Hueso, R., Tsang, C.C.C., Wilson, C.F., Afanasenko, T.Z., 2007. Scientific goals for the observation of Venus by VIRTIS on ESA/Venus express mission. Planetary and Space Science, The Planet Venus and the Venus Express Mission, Part 2 55, 1653–1672. https://doi.org/10.1016/j.pss.2007.01.003

Fan, S., Forget, F., Smith, M. D., Guerlet, S., Badri, K. M., Atwood, S. A., et al. (2022). Migrating thermal tides in the Martian atmosphere during aphelion season observed by EMM/EMIRS. *Geophysical Research Letters*, 49, e2022GL099494. https://doi.org/10.1029/2022GL099494

Fedorova, A., Korablev, O., Bertaux, J., Rodin, A., Kiselev, A., Perrier, S., 2006. Mars water vapor abundance from SPICAM IR spectrometer: Seasonal and geographic distributions. J. Geophys. Res. 111, 2006JE002695. https://doi.org/10.1029/2006JE002695

Fedorova, A., Montmessin, F., Korablev, O., Luginin, M., Trokhimovskiy, A., Belyaev, D.A., Ignatiev, N.I., Lefèvre, F., Alday, J., Irwin, P.G.J., Olsen, K.S., Bertaux, J.-L., Millour, E., Määttänen, A., Shakun, A., Grigoriev, A.V., Patrakeev, A., Korsa, S., Kokonkov, N., Baggio, L., Forget, F., Wilson, C.F., 2020. Stormy water on Mars: The distribution and saturation of atmospheric water during the dusty season. Science 367, 297–300. https://doi.org/10.1126/science.aay9522

Forget, F., Spiga, A., Dolla, B., Vinatier, S., Melchiorri, R., Drossart, P., Gendrin, A., Bibring, J., Langevin, Y., Gondet, B., 2007. Remote sensing of surface pressure on Mars with the Mars Express/OMEGA spectrometer: 1. Retrieval method. J. Geophys. Res. 112, 2006JE002871. https://doi.org/10.1029/2006JE002871

Greybush, S.J., H.E. Gillespie, R.J. Wilson, Transient eddies in the TES/MCS Ensemble Mars Atmosphere Reanalysis System (EMARS), Icarus, 317, 2019, 158-181, https://doi.org/10.1016/j.icarus.2018.07.001.

Guha, B.K., Gebhardt, C., Young, R.M.B., Wolff, M.J., Montabone, L., 2024. Seasonal and Diurnal Variations of Dust Storms in Martian Year 36 Based on the EMM-EXI Database. Journal of Geophysical Research: Planets 129, e2023JE008156. https://doi.org/10.1029/2023JE008156

Guzewich S.D., Toigo, A.D., Waugh, D.W., 2016. The effect of dust on the martian polar vortices, Icarus, Volume 278, Pages 100-118, ISSN 0019-1035, https://doi.org/10.1016/j.icarus.2016.06.009.

Haberle, R.M., Clancy, R.T., Forget, F., Smith, M.D., Zurek, R.W. (Eds.), 2017. The Atmosphere and Climate of Mars. Cambridge Planetary Science, Cambridge University Press. https://doi.org/10.1017/9781139060172

Hartogh, P., Sonnemann, G.R., Grygalashvyly, M., Song, L., Berger, U., Lübken, F. -J., 2010. Water vapor measurements at ALOMAR over a solar cycle compared with model calculations by LIMA. J. Geophys. Res. 115, 2009JD012364. https://doi.org/10.1029/2009JD012364

Hernández-Bernal, J., Sánchez-Lavega, A., Del Río-Gaztelurrutia, T., Hueso, R., Cardesín-Moinelo, A., de la Parra, J. M. Y., ... & Titov, D. (2021). *Looking for Meteors and Fireballs in the atmosphere of Mars from the Visual Monitoring Camera (VMC) on Mars Express* (No. EPSC2021-515). Copernicus Meetings.

Hernández-Bernal, J., Lavega, A. S., del Río Gaztelurrutia, T., Alonso, R. H., & Moinelo, A. C. (2022). *Cloud tracking and dynamics of Martian mesospheric clouds in twilight as seen by MEX/VMC* (No. EPSC2022-456). Copernicus Meetings.

Hinson, D., Wilson, J., 2024. Dust-storm forcing of Rossby waves on Mars. Icarus 412, 115998. https://doi.org/10.1016/j.icarus.2024.115998

Holmes, James A.; Lewis, Stephen R. and Patel, Manish R. (2020). OpenMARS: A global record of martian weather from 1999 2015. Planetary and Space Science, 188(1), article no. 104962.

Holmes, J.A., Lewis, S.R., Patel, M.R., Alday, J., Aoki, S., Liuzzi, G., Villanueva, G.L., Crismani, M.M.J., Fedorova, A.A., Olsen, K.S., Kass, D.M., Vandaele, A.C., Korablev, O., 2022. Global Variations in Water Vapor and Saturation State Throughout the Mars Year 34 Dusty Season. JGR Planets 127, e2022JE007203. https://doi.org/10.1029/2022JE007203

Jakosky, B.M., Lin, R.P., Grebowsky, J.M., Luhmann, J.G., Mitchell, D.F., Beutelschies, G., Priser, T., Acuna, M., Andersson, L., Baird, D., Baker, D., Bartlett, R., Benna, M., Bougher, S., Brain, D., Carson, D., Cauffman, S., Chamberlin,

P., Chaufray, J.-Y., Cheatom, O., Clarke, J., Connerney, J., Cravens, T., Curtis, D., Delory, G., Demcak, S., DeWolfe, A., Eparvier, F., Ergun, R., Eriksson, A., Espley, J., Fang, X., Folta, D., Fox, J., Gomez-Rosa, C., Habenicht, S., Halekas, J., Holsclaw, G., Houghton, M., Howard, R., Jarosz, M., Jedrich, N., Johnson, M., Kasprzak, W., Kelley, M., King, T., Lankton, M., Larson, D., Leblanc, F., Lefevre, F., Lillis, R., Mahaffy, P., Mazelle, C., McClintock, W., McFadden, J., Mitchell, D.L., Montmessin, F., Morrissey, J., Peterson, W., Possel, W., Sauvaud, J.-A., Schneider, N., Sidney, W., Sparacino, S., Stewart, A.I.F., Tolson, R., Toublanc, D., Waters, C., Woods, T., Yelle, R., Zurek, R., 2015. The Mars Atmosphere and Volatile Evolution (MAVEN) Mission. Space Sci. Rev. 195, 3–48. https://doi.org/10.1007/s11214-015-0139-x

Kahre, M. A., Murphy, J. R., Newman, C. E., Wilson, R. J., Cantor, B. A., Lemmon, M. T., & Wolff, M. J. (2017). The Mars Dust Cycle. In R. M. Haberle, R. T. Clancy, F. Forget, M. D. Smith, & R. W. Zurek (Eds.), *The Atmosphere and Climate of Mars* (pp. 295–337). chapter, Cambridge: Cambridge University Press. https://doi.org/10.1017/9781139060172.010

Kahre, M.A., J.L. Hollingsworth and R.M. Haberle, Simulating Mars' Dust Cycle with a Mars General Circulation Model: Effects of Water Ice Cloud Formation on Dust Lifting Strength and Seasonality, *Comparative Climatology of Terrestrial Planets meeting*, LPI Contribution No. 1675, id.8062, 2012. https://ntrs.nasa.gov/citations/20120016027

Kass, D.M., Kleinböhl, A., McCleese, D.J., Schofield, J.T., Smith, M.D., 2016. Interannual similarity in the Martian atmosphere during the dust storm season. Geophysical Research Letters 43, 6111–6118. https://doi.org/10.1002/2016GL068978

Kazama A., Kasaba, Y., Aoki, S., Nakagawa, H., Sato, T.M., Satoh, S., Yoshida, N., 2023. Analysis of surface pressure distribution on Mars by CO_2 μm absorption band observed by OMEGA/Mars Express, Japan Geoscience Union Meeting, 2023. PCG19-02. https://confit.atlas.jp/guide/event/jpgu2023/subject/PCG19-02/detail

Kleinböhl, A., Schofield, J.T., Kass, D.M., Abdou, W.A., Backus, C.R., Sen, B., Shirley, J.H., Lawson, W.G., Richardson, M.I., Taylor, F.W., Teanby, N.A., McCleese, D.J., 2009. Mars Climate Sounder limb profile retrieval of atmospheric temperature, pressure, and dust and water ice opacity. Journal of Geophysical Research 114. https://doi.org/10.1029/2009JE003358

Knutsen, E.W., Montmessin, F., Verdier, L., Lacombe, G., Lefèvre, F., Ferron, S., Giuranna, M., Wolkenberg, P., Fedorova, A., Trokhimovskiy, A., Korablev, O., 2022. Water Vapor on Mars: A Refined Climatology and Constraints on the Near-Surface Concentration Enabled by Synergistic Retrievals. Journal of Geophysical Research: Planets 127, e2022JE007252. https://doi.org/10.1029/2022JE007252

Lee, C., Richardson, M.I., Newman, C.E., Mischna, M.A., 2018. The sensitivity of solsticial pauses to atmospheric ice and dust in the MarsWRF General Circulation Model. Icarus 311, 23–34. https://doi.org/10.1016/j.icarus.2018.03.019

Leseigneur, Y., Vincendon, M., 2023. OMEGA/Mars Express: A new martian atmospheric dust hunter. Icarus 392, 115366. https://doi.org/10.1016/j.icarus.2022.115366

Lewis, S.R., Read, P.L., 1995. An operational data assimilation scheme for the martian atmosphere. Advances in Space Research, The Atmospheres of Venus and Mars 16, 9–13. https://doi.org/10.1016/0273-1177(95)00244-9

Lewis, S.R., Read, P.L., Collins, M., 1996. Martian atmospheric data assimilation with a simplified general circulation model: orbiter and lander networks. Planetary and Space Science, Intermarsnet 44, 1395–1409. https://doi.org/10.1016/S0032-0633(96)00058-X

Liuzzi, G., Villanueva, G.L., Crismani, M.M.J., Smith, M.D., Mumma, M.J., Daerden, F., Aoki, S., Vandaele, A.C., Clancy, R.T., Erwin, J., Thomas, I., Ristic, B., Lopez-Moreno, J.-J., Bellucci, G., Patel, M.R., 2020. Strong Variability of Martian

Water Ice Clouds During Dust Storms Revealed From ExoMars Trace Gas Orbiter/NOMAD. J. Geophys. Res. Planets 125, e2019JE006250. https://doi.org/10.1029/2019JE006250

López-Valverde, M. A., Funke, B., Brines, A., Stolzenbach, A., Modak, A., Hill, B., et al. (2023). Martian atmospheric temperature and density profiles during the first year of NOMAD/TGO solar occultation measurements. *Journal of Geophysical Research: Planets*, 128, e2022JE007278. https://doi.org/10.1029/2022JE007278

Määttänen, A., Mathé, C., Audouard, J., Listowski, C., Millour, E., Forget, F., González-Galindo, F., Falletti, L., Bardet, D., Teinturier, L., Vals, M., Spiga, A., Montmessin, F., 2022. Troposphere-to-mesosphere microphysics of carbon dioxide ice clouds in a Mars Global Climate Model. Icarus 385, 115098. https://doi.org/10.1016/j.icarus.2022.115098

Martínez-Alvarado, O., Montabone, L., Lewis, S.R., Moroz, I.M., Read, P.L., 2009. Transient teleconnection event at the onset of a planet-encircling dust storm on Mars. Annales Geophysicae 27, 3663–3676. https://doi.org/10.5194/angeo-27-3663-2009

McCleese, D.J., Schofield, J.T., Taylor, F.W., Calcutt, S.B., Foote, M.C., Kass, D.M., Leovy, C.B., Paige, D.A., Read, P.L., Zurek, R.W., 2007. Mars Climate Sounder: An investigation of thermal and water vapor structure, dust and condensate distributions in the atmosphere, and energy balance of the polar regions. Journal of Geophysical Research 112. https://doi.org/10.1029/2006JE002790

McElroy, M. B., 1972. Mars: An Evolving Atmosphere. *Science* **175**, 443 -445. https://doi.org/10.1126/science.175.4020.443

MEPAG, 2020. Mars Scientific Goals, Objectives, Investigations and Priorities: 2020. D. Banfield, ed., 89p white paper posted March, 2020 by the Mars Exploration Program Analysis Group (MEPAG) at https://mepag.jpl.nasa.gov/reports.cfm.

Mitchell, D.M., Montabone, L., Thomson, S. and Read, P.L. (2015), Polar vortices on Earth and Mars: A comparative study of the climatology and variability from reanalyses. Q.J.R. Meteorol. Soc., 141: 550-562. https://doi.org/10.1002/qj.2376

Montabone, L., Forget, F., Millour, E., Wilson, R.J., Lewis, S.R., Cantor, B., Kass, D., Kleinböhl, A., Lemmon, M.T., Smith, M.D., Wolff, M.J., 2015. Eight-year climatology of dust optical depth on Mars. Icarus 251, 65–95. https://doi.org/10.1016/j.icarus.2014.12.034

Montabone, L., Mitchell, D.M., Thomson, S.I., Read, P.L., McConnochie, T.H., 2014. The Martian Polar Vortices in the 'MACDA' Reanalysis: Climatology and Variability, 5th International Workshop on Mars Atmosphere: Modelling and Observations, Oxford (UK), January 2014, https://www-mars.lmd.jussieu.fr/oxford2014/abstracts/montabone_vortices_oxford2014.pdf

Montabone, L., Spiga, A., Kass, D.M., Kleinböhl, A., Forget, F., Millour, E., 2020. Martian Year 34 Column Dust Climatology from Mars Climate Sounder Observations: Reconstructed Maps and Model Simulations. J. Geophys. Res. Planets 125, e2019JE006111. https://doi.org/10.1029/2019JE006111

Montabone, L., Thomson, S.I., Wilson, R.J., Forget F., Lewis S.R., Millour, E., 2013. Using Reconstructed Dust Climatology to Study the Impacts of Martian Dust Storms on Dynamics, European Planetary Science Congress, London (UK), September 2013, https://meetingorganizer.copernicus.org/EPSC2013/EPSC2013-963.pdf

Montabone, L.; Martinez-Alvarado, O.; Lewis, S. R.; Read, P. L. and Wilson, R. J. (2008). Teleconnection in the martian atmosphere during the 2001 planet-encircling dust storm. In: Third International Workshop on The Mars Atmosphere: Modeling and Observations, 10-13 Nov 2008, Williamsburg, Virginia, https://oro.open.ac.uk/16963/

Montmessin, F., Belyaev, D.A., Lefèvre, F., Alday, J., Vals, M., Fedorova, A.A., Korablev, O.I., Trokhimovskiy, A.V., Chaffin, M.S., Schneider, N.M., 2022. Reappraising the Production and Transfer of Hydrogen Atoms From the Middle to the Upper Atmosphere of Mars at Times of Elevated Water Vapor. Journal of Geophysical Research: Planets 127, e2022JE007217. https://doi.org/10.1029/2022JE007217

Mulholland, D.P., Lewis, S.R., Read, P.L., Madeleine, J.-B., Forget, F., 2016. The solsticial pause on Mars: 2 modelling and investigation of causes. Icarus 264, 465–477. https://doi.org/10.1016/j.icarus.2015.08.038

Neary, L., Daerden, F., Aoki, S., Whiteway, J., Clancy, R.T., Smith, M., Viscardy, S., Erwin, J.T., Thomas, I.R., Villanueva, G., Liuzzi, G., Crismani, M., Wolff, M., Lewis, S.R., Holmes, J.A., Patel, M.R., Giuranna, M., Depiesse, C., Piccialli, A., Robert, S., Trompet, L., Willame, Y., Ristic, B., Vandaele, A.C., 2020. Explanation for the Increase in High-Altitude Water on Mars Observed by NOMAD During the 2018 Global Dust Storm. Geophysical Research Letters 47, e2019GL084354. https://doi.org/10.1029/2019GL084354

Newman, C.E., Richardson, M.I., 2015. The impact of surface dust source exhaustion on the martian dust cycle, dust storms and interannual variability, as simulated by the MarsWRF General Circulation Model. Icarus 257, 47–87. https://doi.org/10.1016/j.icarus.2015.03.030

Newman, C.E., Lee, C., Mischna, M.A., Richardson, M.I., Shirley, J.H., 2019. An initial assessment of the impact of postulated orbit-spin coupling on Mars dust storm variability in fully interactive dust simulations. Icarus 317, 649–668. https://doi.org/10.1016/j.icarus.2018.07.023

Newman, C.E., Bertrand, T., Fenton, L.K., Guzewich, S.D., Jackson, B., Lewis, S.R., Mischna, M.A., Montabone, L., Wellington, D.F., 2022. 7.24 - Martian Dust, in: Shroder, J. (Jack) F. (Ed.), Treatise on Geomorphology (Second Edition). Academic Press, Oxford, pp. 637–666. https://doi.org/10.1016/B978-0-12-818234-5.00143-7

Ouaknine, J., Gode, S., Napierala, B., Viard, T., Foerster, U., Fray, S., Peacoke, P., Hartl, M., Hallibert, P., and Durand, Y., 2013. MTG Flexible Combined Imager optical design and performances, Proc. SPIE 8866, Earth Observing Systems XVIII, 88661A (23 September 2013); https://doi.org/10.1117/12.2023078

Pasternak F., Lorsignol J., and Wolff L, 1994. Spinning enhanced visible and infrared imager (SEVIRI): the new imager for Meteosat Second Generation, Proc. SPIE 2209, Space Optics 1994: Earth Observation and Astronomy, (13 September 1994); https://doi.org/10.1117/12.185247

Patel, M.R., Sellers, G., Mason, J.P., Holmes, J.A., Brown, M. a. J., Lewis, S.R., Rajendran, K., Streeter, P.M., Marriner, C., Hathi, B.G., Slade, D.J., Leese, M.R., Wolff, M.J., Khayat, A.S.J., Smith, M.D., Aoki, S., Piccialli, A., Vandaele, A.C., Robert, S., Daerden, F., Thomas, I.R., Ristic, B., Willame, Y., Depiesse, C., Bellucci, G., Lopez-Moreno, J.-J., 2021. ExoMars TGO/NOMAD-UVIS Vertical Profiles of Ozone: 1. Seasonal Variation and Comparison to Water. Journal of Geophysical Research: Planets 126, e2021JE006837. https://doi.org/10.1029/2021JE006837

Paton, M.D., J. Leino, A.-M. Harri, H. Savijärvi, Martian boundary layer wind profiles during the landings of Viking and InSight, Icarus, 367, 2021, https://doi.org/10.1016/j.icarus.2021.114581.
Rajendran, K., Lewis, S. R., Holmes, J. A., Streeter, P. M., Fedorova, A. A., & Patel, M. R. (2021). Enhanced super-rotation before and during the 2018 martian global dust storm. *Geophysical Research Letters*, 48, e2021GL094634. https://doi.org/10.1029/2021GL094634

Read, P.L., Lewis, S.R., Mulholland, D.P., 2015. The physics of Martian weather and climate: a review. Rep. Prog. Phys. 78, 125901. https://doi.org/10.1088/0034-4885/78/12/125901

Shaposhnikov, D.S., Medvedev, A.S., Rodin, A.V., Hartogh, P., 2019. Seasonal Water "Pump" in the Atmosphere of Mars: Vertical Transport to the Thermosphere. Geophys. Res. Lett. 46, 4161–4169. https://doi.org/10.1029/2019GL082839

Shaposhnikov, D.S., Medvedev, A.S., Rodin, A.V., Yiğit, E., Hartogh, P., 2022. Martian Dust Storms and Gravity Waves: Disentangling Water Transport to the Upper Atmosphere. Journal of Geophysical Research: Planets 127, e2021JE007102. https://doi.org/10.1029/2021JE007102

Shirley, J.H., Mischna, M.A., 2017. Orbit-spin coupling and the interannual variability of global-scale dust storm occurrence on Mars. Planetary and Space Science 139, 37–50. https://doi.org/10.1016/j.pss.2017.01.001

Smith, M.D., 2004. Interannual variability in TES atmospheric observations of Mars during 1999–2003. Icarus 167, 148–165. https://doi.org/10.1016/j.icarus.2003.09.010

Smith, M.D., Badri, K., Atwood, S.A., Edwards, C.S., Christensen, P.R., Wolff, M.J., Bertrand, T., Forget, F., Al Tunaiji, E., Wolfe, C., Smith, N., Anwar, S., 2022. EMIRS Observations of the Aphelion-Season Mars Atmosphere. Geophys. Res. Lett. 49, e2022GL099636. https://doi.org/10.1029/2022GL099636

Spiga, A., Forget, F., Dolla, B., Vinatier, S., Melchiorri, R., Drossart, P., Gendrin, A., Bibring, J.-P., Langevin, Y., Gondet, B., 2007. Remote sensing of surface pressure on Mars with the Mars Express/OMEGA spectrometer: 2. Meteorological maps. Journal of Geophysical Research 112. https://doi.org/10.1029/2006JE002870

Steele, L. J., Lewis, S. R., & Patel, M. R. (2014). The radiative impact of water ice clouds from a reanalysis of Mars Climate Sounder data. Geophysical Research Letters, 41(13), 4471–4478. https://doi.org/10.1002/2014gl060235

Stone, S.W., Yelle, R.V., Benna, M., Lo, D.Y., Elrod, M.K., Mahaffy, P.R., 2020. Hydrogen escape from Mars is driven by seasonal and dust storm transport of water. Science 370, 824–831. https://doi.org/10.1126/science.aba5229

Streeter, P.M., Lewis, S.R., Patel, M.R., Holmes, J.A., Rajendran, K., 2024. An eight-year climatology of the martian northern polar vortex. Icarus 409, 115864. https://doi.org/10.1016/j.icarus.2023.115864

Titus, T. N., Byrne, S., Colaprete, A., Forget, F., Michaels, T. I., & Prettyman, T. H. (2017). The CO_2 Cycle. In R. M. Haberle, R. T. Clancy, F. Forget, M. D. Smith, & R. W. Zurek (Eds.), *The Atmosphere and Climate of Mars* (pp. 374–404). chapter, Cambridge: Cambridge University Press. https://doi.org/10.1017/9781139060172.012

Toigo, A. D., Waugh, D.W., and Guzewich, S.D., 2017. What causes Mars' annular polar vortices?, *Geophys. Res. Lett.*, 44, 71–78, doi:10.1002/2016GL071857.

Toigo, A.D., Smith, M.D., Seelos, F.P., Murchie, S.L., 2013. High spatial and temporal resolution sampling of Martian gas abundances from CRISM spectra. Journal of Geophysical Research: Planets 118, 89–104. https://doi.org/10.1029/2012JE004147

Trainer, M.G., Wong, M.H., McConnochie, T.H., Franz, H.B., Atreya, S.K., Conrad, P.G., Lefèvre, F., Mahaffy, P.R., Malespin, C.A., Manning, H.L.K., Martín-Torres, J., Martínez, G.M., McKay, C.P., Navarro-González, R., Vicente-Retortillo, Á., Webster, C.R., Zorzano, M.-P., 2019. Seasonal Variations in Atmospheric Composition as Measured in Gale Crater, Mars. Journal of Geophysical Research: Planets 124, 3000–3024. https://doi.org/10.1029/2019JE006175

Trokhimovskiy, A., Fedorova, A., Korablev, O., Montmessin, F., Bertaux, J.-L., Rodin, A., Smith, M.D., 2015. Mars' water vapor mapping by the SPICAM IR spectrometer: Five martian years of observations. Icarus 251, 50–64. https://doi.org/10.1016/j.icarus.2014.10.007

Villanueva, G.L., Liuzzi, G., Aoki, S., Stone, S.W., Brines, A., Thomas, I.R., Lopez-Valverde, M.A., Trompet, L., Erwin, J., Daerden, F., Ristic, B., Smith, M.D., Mumma, M.J., Faggi, S., Kofman, V., Robert, S., Neary, L., Patel, M., Bellucci, G., Lopez-Moreno, J.J., Vandaele, A.C., 2022. The Deuterium Isotopic Ratio of Water Released From the Martian Caps as Measured With TGO/NOMAD. Geophysical Research Letters 49. https://doi.org/10.1029/2022GL098161

Villanueva, G.L., Liuzzi, G., Crismani, M.M.J., Aoki, S., Vandaele, A.C., Daerden, F., Smith, M.D., Mumma, M.J., Knutsen, E.W., Neary, L., Viscardy, S., Thomas, I.R., Lopez-Valverde, M.A., Ristic, B., Patel, M.R., Holmes, J.A., Bellucci, G., Lopez-Moreno, J.J., NOMAD team, 2021. Water heavily fractionated as it ascends on Mars as revealed by ExoMars/NOMAD. Sci. Adv. 7, eabc8843. https://doi.org/10.1126/sciadv.abc8843

Vlasov, P., Ignatiev, N., Guerlet, S., Grassi, D., Korablev, O., Grigoriev, A., Shakun, A., Patsaev, D., Maslov, I., Zasova, L., Luginin, M., Trokhimovskiy, A., Millour, E., Forget, F., Haus, R., Arnold, G., Montmessin, F., 2022. Martian Atmospheric Thermal Structure and Dust Distribution During the MY 34 Global Dust Storm From ACS TIRVIM Nadir Observations. JGR Planets 127, e2022JE007272. https://doi.org/10.1029/2022JE007272

Wang, H., González Abad, G., 2021. Cloud Masks Derived from the Mars Daily Global Maps and an Application to the Tropical Cloud Belt on Mars. Geosciences 11, 324. https://doi.org/10.3390/geosciences11080324

Wang, H., Richardson, M.I., 2015. The origin, evolution, and trajectory of large dust storms on Mars during Mars years 24–30 (1999–2011). Icarus, Dynamic Mars 251, 112–127. https://doi.org/10.1016/j.icarus.2013.10.033

Wang, H., Richardson, M.I., Wilson, R.J., Ingersoll, A.P., Toigo, A.D., Zurek, R.W., 2003. Cyclones, tides, and the origin of a cross-equatorial dust storm on Mars. Geophysical Research Letters 30. https://doi.org/10.1029/2002GL016828

Wang, H., Saidel, M., Richardson, M.I., Toigo, A.D., Battalio, J.M., 2023. Martian dust storm distribution and annual cycle from Mars daily global map observations. Icarus 394, 115416. https://doi.org/10.1016/j.icarus.2022.115416

Wilson, R.J., Neumann, G.A., Smith, M.D., 2007. Diurnal variation and radiative influence of Martian water ice clouds. Geophysical Research Letters 34. https://doi.org/10.1029/2006GL027976

Wolff, M. J., Lopéz-Valverde, M., Madeleine, J.-B., Wilson, R. J., Smith, M. D., Fouchet, T., & Delory, G. T. (2017). Radiative Process: Techniques and Applications. In R. M. Haberle, R. T. Clancy, F. Forget, M. D. Smith, & R. W. Zurek (Eds.), *The Atmosphere and Climate of Mars* (pp. 106–171). chapter, Cambridge: Cambridge University Press. https://doi.org/10.1017/9781139060172.006

Wolff, M.J., Clancy, R.T., Kahre, M.A., Haberle, R.M., Forget, F., Cantor, B.A., Malin, M.C., 2019. Mapping water ice clouds on Mars with MRO/MARCI. Icarus 332, 24–49. https://doi.org/10.1016/j.icarus.2019.05.041

Wolff, M.J., Fernando, A., Smith, M.D., Forget, F., Millour, E., Atwood, S.A., Jones, A.R., Osterloo, M.M., Shuping, R., Al Shamsi, M., Jeppesen, C., Fisher, C., 2022. Diurnal Variations in the Aphelion Cloud Belt as Observed by the Emirates Exploration Imager (EXI). Geophysical Research Letters 49, e2022GL100477. https://doi.org/10.1029/2022GL100477

Wolff, M.J., Clancy, R.T., Goguen, J.D., Malin, M.C., Cantor, B.A., 2010. Ultraviolet dust aerosol properties as observed by MARCI. Icarus 208, 143–155. https://doi.org/10.1016/j.icarus.2010.01.010

Zurita-Zurita, S., De La Torre Juárez, M., Newman, C.E., Viúdez-Moreiras, D., Kahanpää, H.T., Harri, A. -M., Lemmon, M.T., Pla-García, J., Rodríguez-Manfredi, J.A., 2022. Mars Surface Pressure Oscillations as Precursors of Large Dust Storms Reaching Gale. JGR Planets 127, e2021JE007005. https://doi.org/10.1029/2021JE007005

Appendix A. Work to prepare for operational weather monitoring and forecasting

Near real-time data processing

In order to fulfil the exploration-focussed objective of operational atmospheric monitoring and weather forecasting, it is crucial that the atmospheric observables are made publicly available with a minimum of delay (ideally < 24 hours).

This implies:

- **Data latency requirement**: key meteorological data must be downlinked from the spacecraft to Earth within less than 24 hours. Datasets essential for forecasting (such as radiances) could be prioritised over others not needed for operational forecasting (such as trace gas measurements).
- Sufficient **data downlink bandwidth availability** for rapid download of key meteorological data.
- **Near real-time data pipelines** for processing data **from Raw to Calibrated data levels** need to be set up. This may suggest following models more typical for Earth Observation operational missions, rather than typical planetary missions. Further implications for ground segment design are beyond the remit of the present team's study.
- It should be a goal to set up near real-time data processing **from Calibrated level** (e.g. radiances in physical units) **to Derived level** (e.g. temperature profiles, dust & water abundances). This may not be necessary if Calibrated data (radiances etc) are used for data assimilation rather than Derived data. This is now common practice on Earth, and should be feasible on Mars although not yet demonstrated; this is discussed further in the section below.
- **Data processing pipelines need to be developed earlier** than is typical for planetary missions. A preliminary version of the data pipeline should be operational at the beginning of the mission; this can then be adjusted as needed during a data commissioning phase during which calibration and validation activities are conducted.

Mars data assimilation & forecasting

In order to move towards an operational weather monitoring and forecasting for Mars, significant investment will be needed in developing data assimilation and weather prediction schemes. The impact of atmospheric observations not yet available for Mars can be simulated using an **"Observing System Simulation Experiment" (OSSE)** framework. This approach, employed for over 30 years to evaluate the benefit of future orbital instruments for the observation of the Earth's climate system (see e.g. Atlas et al., 1985; Arnold and Dey, 1986), requires a rigorous setup to avoid unrealistic assessments (Reale et al., 2020). While Earth OSSEs

are computationally intensive, Mars' simpler observing system allows for exploratory but rigorous studies addressing basic questions.

An OSSE framework has three components: the nature run (NR), synthetic data, and the data assimilation (DA) scheme. The NR is a four-dimensional simulation of the Martian atmosphere at higher-than-standard resolution, produced by using a state-of-the-art Global Climate Model (GCM). It is considered to represent the true atmospheric state. Synthetic data simulate observations by extracting information from the NR using an observation simulator, mimicking data that would be collected by specific instruments aboard a platform orbiting Mars. The DA scheme combines these observations with the model to produce an "analysis," the best estimate of the atmospheric state, correcting model forecasts with observations while accounting for uncertainties. The analysis can then be compared to the NR.

In Earth weather forecasting, the analysis serves as the initial condition for generating forecasts, which are compared to the NR in OSSEs to assess the benefit of new observations for the forecasting skills of the observing system. In other words, to assess whether the new observations help to produce better initial conditions and better forecasts. For Mars, however, testing forecasting skills using OSSEs is currently impractical due to unvalidated GCM physical parameterizations, such as dust lifting schemes. It is currently impossible to separate the impact of new observations from the impact of numerical parameterizations in the GCM that produces the analysis. Failures in forecasting dust storms, for instance, cannot reliably be attributed to specific observations (or the lack of specific observations) if model parameterizations are inaccurate, limiting OSSE experiments' scope for forecasting.

Despite this, OSSEs can already be used to quantify the improvement in Martian weather characterization when new observations are integrated with a DA scheme. Synthetic observations can be evaluated against the NR to assess their impact. A key advantage of the DA-produced "reanalysis" (i.e., a “retrospective analysis” over a past period of time) is its complete, gridded, dynamically consistent four-dimensional meteorological fields, including variables like winds or near-surface fields not directly observed yet.

An Observing Simulation System Experiment commissioned by ESA analysed the case of four Mars spacecraft with orbital characteristics similar to those of the LightShip platforms. It demonstrated that, at least for temperature and dust retrievals using thermal IR observations, the weather monitoring potential of such a constellation, when combined with data assimilation, is equivalent to that of three areostationary satellites and far superior to that of a single polar orbiter (Montabone et al., 2023).

Building on what has been discussed, advancing toward operational weather forecasting for Mars would require **continued improvements in GCM parameterizations**, particularly those related to the dust cycle and boundary layer processes. Enhancing these aspects would ensure more accurate modelling of Martian atmospheric dynamics and dust transport—an essential step toward using models to produce reliable forecasts from initial conditions created by OSSEs and data assimilation schemes in general.

Additionally, incorporating **direct radiance assimilation** into the data assimilation framework would represent a critical step forward. Assimilating radiances directly, rather than relying on derived retrievals, would reduce the latency between acquiring measurements at Mars and generating forecasts. By eliminating the intermediate step of producing retrievals, this approach would streamline the data processing workflow and improve the timeliness of forecast production. Radiance assimilation is now standard for Earth weather forecasting; only a preliminary study of its application to Mars has been conducted to date (Lee et al., 2011).

Assimilation of line-of-sight wind vectors from Aeolus has proved to have a large impact on Earth weather forecasts. A similar study about the impact of orbital direct wind measurements at Mars, whether from the sub-mm instrument on LightShip, or from a wind LIDAR on SpotLight, would be important in order to prepare for this investigation and optimise the observation pattern.

Finally, advancing toward operational weather forecasting for Mars requires **further development of data assimilation schemes** and their adaptation to incorporate novel observations, such as winds. Currently, Martian data assimilation relies primarily on the Analysis Correction scheme (a type of "nudging" scheme) or the Ensemble Kalman Filter (Lewis et al., 2007, Hoffman et al., 2010). However, it remains unclear which approach is better suited for operational forecasting. Hybrid methods, such as those based on "ensemble nudging," may offer a promising alternative and warrant further exploration (Lei et al., 2012). Emerging weather forecasting approaches based on machine learning, which are beginning to show potential in Earth weather forecasting, could be valuable to test for Martian applications (Lam et al., 2023). These methods might complement or enhance traditional schemes, providing new avenues for improving the accuracy and efficiency of Martian weather predictions.

Appendix references

Arnold, C.P., and Dey, C.H., 1986. Observing-systems simulation experiments: Past, present, and future. Bull. Amer. Meteor. Soc., 67, 687–695.

Atlas, R., Kalnay, E., and Halem, M., 1985. Impact of satellite temperature soundings and wind data on numerical weather prediction. Opt. Eng., 24, 341-346. https://doi.org/10.1117/12.7973481

Hoffman, M.J., Greybush, S.J., John Wilson, R., Gyarmati, G., Hoffman, R.N., Kalnay, E., Ide, K., Kostelich, E.J., Miyoshi, T., Szunyogh, I., 2010. An ensemble Kalman filter data assimilation system for the martian atmosphere: Implementation and simulation experiments. Icarus 209, 470–481. https://doi.org/10.1016/j.icarus.2010.03.034

Lam, R., Sanchez-Gonzalez, A., Willson, M., Wirnsberger, P., Fortunato, M., Alet, F., Ravuri, S., Ewalds, T., Eaton-Rosen, Z., Hu, W., Merose, A., Hoyer, S., Holland, G., Vinyals, O., Stott, J., Pritzel, A., Mohamed, S., Battaglia, P., 2023. Learning skillful medium-range global weather forecasting. Science 382, 1416–1421. https://doi.org/10.1126/science.adi2336

Lee, C., Lawson, W.G., Richardson, M.I., Anderson, J.L., Collins, N., Hoar, T., Mischna, M., 2011. Demonstration of ensemble data assimilation for Mars using DART, MarsWRF, and radiance observations from MGS TES. J. Geophys. Res. 116, E11011. https://doi.org/10.1029/2011JE003815

Lei, L., Stauffer, D.R., Deng, A., 2012. A hybrid nudging-ensemble Kalman filter approach to data assimilation in WRF/DART. Quarterly Journal of the Royal Meteorological Society 138, 2066–2078. https://doi.org/10.1002/qj.1939

Lewis, S.R., Read, P.L., Conrath, B.J., Pearl, J.C., Smith, M.D., 2007. Assimilation of thermal emission spectrometer atmospheric data during the Mars Global Surveyor aerobraking period. Icarus 192, 327–347. https://doi.org/10.1016/j.icarus.2007.08.009

Montabone, L.; Young, R.M.B.; Millour, E. (2023). SWIMALONG TN1b: Mars Weather Network Configuration-Science Optimisation Report-Orbiter Network Study. ESA Contract ref. ESA 4000138021/22/NL/DB.

Reale, O., Fauchez, T., Teinturier, S., Guzewich, S., Greybush, S., & Wilson, J. (2021). Building a standardized Observing System Simulation Experiment (OSSE) framework for Mars. *Bulletin of the AAS*, *53*(4). https://doi.org/10.3847/25c2cfeb.0483bad0